UNIVERSITEIT VAN PRETORIA
UNIVERSITY OF PRETORIA
YUNIBESITHI YA PRETORIA

AN INVESTIGATION INTO THE USE OF BACKFILL TO REINFORCE PILLARS IN HARD ROCK BORD AND PILLAR LAYOUTS

by

DIVINE-ITO ILE

Presented in fulfilment of the requirements for the degree

M.Eng. (Mining Engineering)

in the Faculty of Engineering, Built Environment, and Information Technology

Department of Mining Engineering

29 August 2023

DECLARATION OF ORIGINALITY

I hereby declare that this project is my own unaided work and I have referenced all the sources I have used. It is being submitted in fulfilment of the requirements for the degree M.Eng. (Mining Engineering) at the University of Pretoria, Pretoria. It has not been submitted before for any degree or examination at any other university. This document represents my own opinion and interpretation of information received from research or / and interviews. I thus accept the rules of assessment of the University and the consequences of transgressing them.

Divine-Ito Ile

16051132

29 August 2023

UNIVERSITY OF PRETORIA

FACULTY OF ENGINEERING, BUILT ENVIRONMENT AND INFORMATION TECHNOLOGY

DEPARTMENT OF MINING ENGINEERING

The Department of Mining Engineering places great emphasis upon integrity and ethical conduct in the preparation of all written work submitted for academic evaluation. While academic staff teach you about systems of referring and how to avoid plagiarism, you too have a responsibility in this regard. If you are at any stage uncertain as to what is required, you should speak to your lecturer before any written work is submitted.

You are guilty of plagiarism if you copy something from a book, article or website without acknowledging the source and pass it off as your own. In effect you are stealing something that belongs to someone else. This is not only the case when you copy work word-by-word (verbatim), but also when you submit someone else's work in a slightly altered form (paraphrase) or use a line of argument without acknowledging it. You are not allowed to use another student's past written work. You are also not allowed to let anybody copy your work with the intention of passing if of as his/her work.

Students who commit plagiarism will lose all credits obtained in the plagiarised work. The matter may also be referred to the Disciplinary Committee (Students) for a ruling. Plagiarism is regarded as a serious contravention of the University's rules and can lead to expulsion from the University. The declaration which follows must be appended to all written work submitted while you are a student of the Department of Mining Engineering. No written work will be accepted unless the declaration has been completed and attached.

I (full names):	Divine-Ito Ile
Student number:	16051132
Topic of work:	An Investigation into the Use of Backfill to Reinforce Pillars in Hard Rock Bord and Pillar Layouts

Declaration

1. I understand what plagiarism is and am aware of the University's policy in this regard.
2. I declare that this dissertation is my own original work. Where other people's work has been used (either from a printed source, internet, or any other source), this has been properly acknowledged and referenced in accordance with departmental requirements.
3. I have not used another student's past written work to hand in as my own.
4. I have not allowed and will not allow anyone to copy my work with the intention of passing it off as his or her own work.

Signature _____

Abstract

An Investigation into the Use of Backfill to Reinforce Pillars in Hard Rock Bord and Pillar Layouts

DIVINE-ITO ILE

Supervisor: Prof Francois Malan

Department: Mining Engineering

University: University of Pretoria

Degree: M.Eng. (Mining Engineering)

The production of tailings is inherent to mining and minerals processing and will remain so for the foreseeable future. Catastrophic tailings dam failures, such as those at Canada's Mount Polley in 2014 and Brazil's Samarco and Brumadinho in 2015 and 2019, are a reminder that more needs to be done to safeguard lives, improve production, and protect the environment. As the global population increases, so does the demand for the metals and minerals required for modern life. With increased demand and supply comes the challenge of extracting greater value from low grade deposits, mining deeper ore bodies, and increased mineralogical complexity, all of which have the potential to lead to a higher production of tailings. This study was an investigation of the potential benefits of using the tailings as backfill in bord and pillar mines with specific emphasis on its use to increase the strength of the pillars and reduce the volume of tailings stored on surface.

The literature indicated that backfill is extensively used in Chinese coal mines in conjunction with high extraction mining methods, mostly for environmental considerations. However, it is not commonly used in hard rock bord and pillar mines. This study explored the use of backfill to increase the extraction ratio in hard rock bord and pillar mines at increasing depths. The typical decrease in extraction ratio with increasing depth is illustrated in the dissertation with the aid of a simple analytical model, which emphasises the need to study backfill as an option to ensure viable mining operations in future. To simulate the effect of backfill confinement on pillar strength, an extension of the TEXAN limit equilibrium model was explored in this study. The model can simulate the failure of the pillars as well as the effect of confinement applied on the edge of the

pillars. A simple plane strain model of the limit equilibrium model, with the confinement component, is derived in this study to study the attributes of the model. This was used to illustrate the effect of the backfill confining stress on the normal pillar stress in the failed zone of the pillar. An increase in confinement results in a substantial increase in stress carried by the failed pillars. This was also illustrated by conducting numerical modelling of an idealised bord and pillar layout with increasing levels of confinement. The intact core of the pillars increased in size for a larger magnitude of confinement and the resulting average pillar stress (APS) of the pillars also increased correspondingly. These preliminary models indicated that the limit equilibrium model with the confinement component behaves as expected.

The magnitude of confinement that will be exerted by backfill on the pillar sidewalls is unknown. This study used a combination of literature sources and earth pressure theory to estimate the level of confinement that can be expected when placing backfill. Lateral earth pressure refers to the pressure that soil exerts in the horizontal direction, and it is an important parameter for the design of geotechnical engineering structures such as retaining walls. The analysis and historic studies indicated that a value of 0.05 MPa is a possible realistic value of confinement that will be exerted by the backfill.

Numerical modelling of an actual platinum mine layout was done to illustrate the beneficial effect of backfill on pillar stability at greater depths. This illustrated that the zone of failure decreases for increasing confinement and there is a substantial reduction for a 2 MPa confinement value. It is nevertheless doubtful whether such a magnitude of stress will be exerted by the backfill unless there is substantial pillar dilation. Calibration of the actual confinement exerted by the backfill needs to be done as future work. Trial backfill sections in mines with sensitive instrumentation in the backfill will, therefore, be required to quantify this effect.

In summary, the confinement limit equilibrium model proved to be a valuable approach to simulate the effect of backfill confinement on pillar strength. Mining areas where the pillar strength is reduced due to the presence of weak layers may benefit significantly from the placement of backfill. Additionally, the use of backfill will also reduce the requirement for tailings storage on surface, thus minimising the risk of environmental damage.

Acknowledgements

I would like to thank the Department of Mining Engineering for its unwavering support over the years. I would particularly like to express my sincere gratitude to my supervisor, Prof Francois Malan, for his guidance, patience, and invaluable contribution to my research and my growth as an individual. I would not have been able to get here without you, Prof.

I would also like to thank African Rainbow Minerals for kindly funding my post-graduate studies and for organising frequent well-being workshops.

I would like to thank my group of supportive friends for humouring me and for having an overwhelming amount of confidence in me and my capabilities. You have kept me sane throughout the last three years.

To my younger brother, Christian, thank you for being you. Thank you for always putting a smile on my face, even on the days where I annoy you the most, and for encouraging and believing in me. You are a true blessing, and I love you.

Lastly, I would like to thank my parents, Angelique and Richard, for their endless love, prayers and support, and for constantly uplifting my spirits. Your hard work and sacrifices have brought me this far and helped shape me into the woman that I am. I will never be able to express just how much I love and appreciate you both.

TABLE OF CONTENTS

LIST OF FIGURES

LIST OF TABLES

LIST OF ABBREVIATIONS

Average pillar stress	APS
Cascading pillar failure	CPF
Cemented rock fills	CRF
Cemented paste backfill	CPB
Energy Release Rate	ERR
Factor of Safety	S_F
Limit equilibrium model	LEM
Platinum-group metals	PGMs
Tabular Excavation Analyser	TEXAN
Tributary area theory	TAT
Uniaxial compressive strength	UCS
Width-to-height ratio	w/h ratio

1. INTRODUCTION

South Africa hosts two of the world's most valuable ore bodies, namely the platinum-bearing pyroxenites and chromitites of the Bushveld Complex and the gold-bearing conglomerates of the Witwatersrand Basin (Durrheim, 2010). The Bushveld Complex is the world's largest layered igneous intrusion, and it comprises approximately 85% of the Earth's known platinum-group metal (PGM) resources. In recent years, the industry has seen a decline in the number of new mines that have been developed and a depletion of mineral resources. To meet the growing demand for minerals, mines are getting deeper, which leads to increasingly capital-intensive operations.

Additionally, there is still uncertainty regarding the strength of the pillars in the shallow tabular excavations of the Bushveld Complex (Malan and Napier, 2011; Couto and Malan, 2023). The Canadian Hedley and Grant (1972) and the Stacey and Page (1986) empirical formulae are typically used to estimate pillar strength. These formulae seem to work well, and a large number of stable layouts have been designed using them. The lack of precise knowledge regarding pillar strength nevertheless causes a conservative approach to be adopted in most cases. For many years, the strength of the pillar material, K, in the Hedley and Grant formula, was typically assumed to be a third of the uniaxial compressive strength (UCS) of laboratory specimens. This, in conjunction with the adoption of the 1.6 factor of safety (S_F) used in the coal mining industry, has resulted in oversized pillars and low extraction ratios in many cases (Ryder and Jager, 2002). As the mining depths increase, the designed pillar sizes will also increase if it is desired to maintain the required S_F. This will affect the extraction ratio negatively, and these mines may not be profitable in future.

When the bord and pillar mining method is used to exploit the orebody, pillars provide the necessary stability and must prevent surface subsidence. Leaving larger pillars in the layout leads to enhanced excavation stability. This, however, reduces the extraction ratio, and mining operations are typically not economically viable with very large pillars. Alternatively, for small pillars, secondary pillar support methods such as mesh, thin spray-on liners, and tendons, are occasionally used if pillar spalling is observed. These methods are, however, not always successful (Malan and Napier, 2011).

Mining operations generate significant quantities of waste tailings and when this material is stored in facilities on surface, ecological concerns arise. The use of tailings as backfill presents an opportunity to minimise the damage that mining causes the environment. The quality of the backfill material affects the overall costs, the required amount of fill, as well as the performance of the equipment (Zhang et al., 2019). Using an appropriate backfilling ratio ensures that the strength of the system meets the support requirements of the layout. An aspect that remains unexplored in

the South African hard rock bord and pillar mines is the possible use of backfill to increase the pillar strength and to reduce the number of tailings dams on surface.

This study explores the effect of backfill on pillar strength and how this may affect the layouts of bord and pillar mines in the Bushveld Complex. Backfill may enable the adoption of smaller pillar sizes, which will result in higher extraction ratios at greater depths.

Tailings refer to the by-products of mining operations resulting from the separation of the minerals from the gangue material. This is a mixture of crushed rock and processing fluids from mills or concentrators that remain after the extraction of valuable minerals or fuels (Kossoff et al., 2014). The volume of tailings, which can be solid, liquid, or slurries of fines, normally exceeds that of the liberated minerals, with the ratio of mineral concentrate to tailings usually being around 1:200. Figure 1-1 illustrates an estimate of global tailings production for various commodities. The generation of tailings is higher for certain commodities because of the quality, quantity, and production rate (International Council on Mining and Metals (ICMM), 2022). The combined tailings production rate increased by 40% between 2010 and 2018, with the copper and gold industries being responsible for most of the tailings generation.

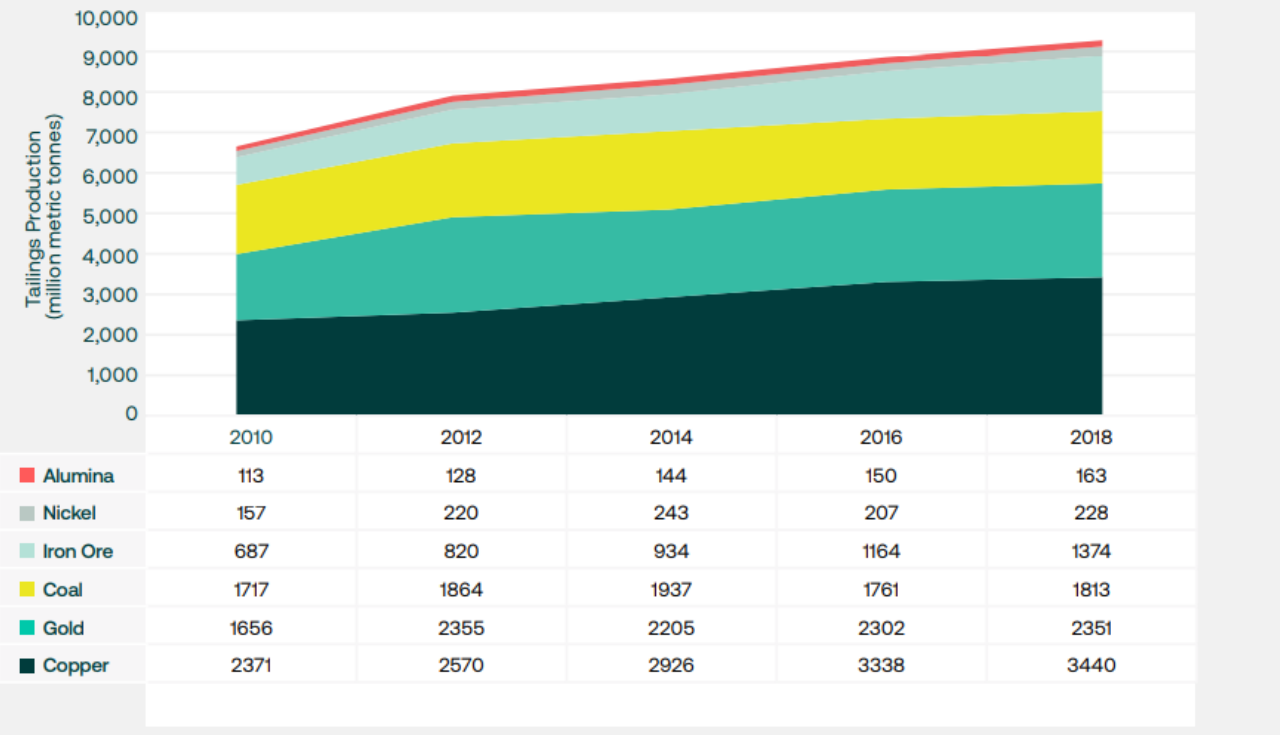

	2010	2012	2014	2016	2018
Alumina	113	128	144	150	163
Nickel	157	220	243	207	228
Iron Ore	687	820	934	1164	1374
Coal	1717	1864	1937	1761	1813
Gold	1656	2355	2205	2302	2351
Copper	2371	2570	2926	3338	3440

Figure 1-1. An estimation of the global annual production of tailings by commodity (after Hatch, 2022).

As the tailings tend to contain potentially hazardous contaminants, all mining operations need to isolate these to prevent them from entering groundwater and other waterbodies (Kossoff et al., 2014). The measures for the handling and storage of tailings include dry stacking, submarine and riverine disposal, wetland retention, backfilling, and storage in isolated tailings dams (Kossoff et al., 2014). According to Owen et al. (2020), the number of disastrous dam failures is rising significantly, with the failure rate increasing to a frequency of five or six significant failures per year since the year 2000. These failures present significant ecological concerns due to the extensive damage that is caused to the local environment. Additionally, tailings dams can be a source of acid drainage, with failures causing damage to aquatic wildlife, and in extreme cases, result in human fatalities.

As mentioned earlier, mines are going deeper to access new resources and some of these orebodies may also decline in grade. The production of tailings is higher in ore bodies with lower grades (International Council on Mining and Metals (ICMM), 2022). Additionally, there have been reports that established a correlation between the mining of lower grades of ore, which produces greater volumes of waste, and the failure rate of tailings dams (Owen et al., 2020). The use of the tailings dams has therefore seen a decline as mining operations seek to find more environmentally friendly means to store the waste.

The investigation aims to study a novel approach for the use of backfill in hard rock bord and pillar operations in South Africa to increase the pillar strength. In these operations, approximately 25% of the reef is typically left behind as pillars to provide stable excavations. In the case of multi-seam mines, percentages of extraction ranging from 75% in shallow operations to as low as 40% in deeper operations are achieved (Blight, 1984). Backfill can provide the beneficial effect of restricting the lateral deformation of the pillars and convergence of the roof (Donovan, 1999). The placement of tailings as backfill in underground stopes presents an opportunity to mine the historical pillars if a practical method can be devised and perhaps even enable the use of smaller pillars, thereby increasing the extraction ratio as well as the life of mine.

1.1. Problem statement

With the depletion of mineral resources, hard rock mining operations should explore the possibility of placing tailings underground for support and to enable the extraction of existing pillars. As no hard rock bord and pillar mine uses backfill in South Africa, this investigation had to be a desktop study and the literature study was therefore important to investigate the adoption of backfilling practices.

The objectives of the study were:

1. To highlight the concerns associated with tailings dams in the global mining industry.
2. To assess the value of backfilling in pillar mining layouts, and in particular the effect of confinement on pillar strength.
3. To identify mining operations that have implemented backfilling practices for the extraction of pillars.
4. To explore a suitable numerical model that could simulate the effect of backfill confinement on pillar strength in the underground workings for both idealised and irregular layouts.

In summary, the key objective was to explore whether the use of backfill will be beneficial to safely increase the extraction ratios in bord and pillar operations in the South African hard rock mining industry, especially at greater depths. The challenge associated with increasing depth is illustrated in the next section.

1.2. The effect of depth on extraction ratio in bord and pillar layouts

As an illustration of the detrimental effect of depth on extraction ratio in bord and pillar layouts, consider the layout shown in Figure 1-2. A similar approach was described by Malan and Esterhuyse (2021), but a more general equation was derived by the author of this dissertation below to highlight the problem. The technical aspects of backfill confinement are discussed in more detail in later chapters, but this section is included in the first chapter as it clearly describes the problem encountered when designing bord and pillar layouts at greater depths.

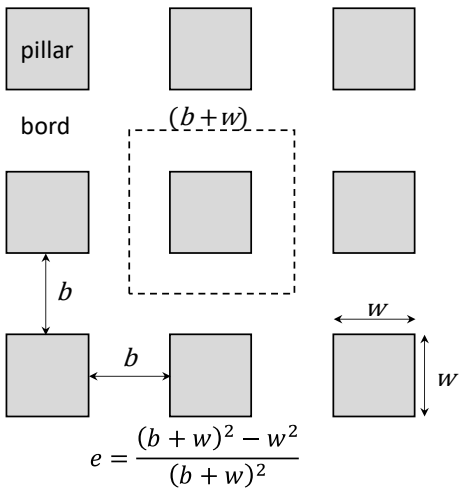

Figure 1-2. A simplified illustration of a regular bord and pillar layout to define the extraction ratio, *e*.

When the reef is mined, some of the reef material supporting the overburden is removed. To ensure that stability is maintained, the weight of the strata must be transferred to the remaining pillars (Ryder and Jager, 2002). The tributary area theory (TAT) is typically used to determine the average pillar stress (APS) on a pillar for a large regular horizontal layout with uniformly sized pillars. The pillar load is influenced by the mining depth, pillar size, and the bord span. Of the three factors, the first parameter is a given and the other two can be controlled (Ryder and Jager, 2002). TAT assumes that each individual pillar supports an evenly distributed load to the surface (Zvarivadza, 2012). However, TAT is not applicable when the pillars vary in size in an irregular mining layout and when there are abutments near the pillars of interest. It should be emphasised that the theory is only useful for regular layouts of large lateral extents (Zvarivadza, 2012).

The dip of the layout in Figure 1-2 is considered to be 0°, and the extent of mining in the two lateral directions is considered to be very large (only 9 pillars of this much larger layout are shown in Figure 1-2). TAT is therefore a good approximation of the stresses acting on the pillars (Ryder and Jager, 2002). The schematic does not account for the abutments that may be present and assumes that the area is mined out for a large distance in both lateral directions.

The APS acting on a pillar can be expressed as a function of the extraction ratio as follows (Ryder and Jager, 2002):

$$APS = \frac{\sigma_V}{1-e} \quad \textbf{[1-1]}$$

where:

$$\sigma_v = \rho g H \quad \textbf{[1-2]}$$

and

σ_v = vertical virgin stress (MPa)

e = extraction ratio

ρ = rock density (kg/m^3)

g = gravitational acceleration (m/s^2)

H = depth below surface (m)

Equation [1-1] can be rearranged, and Equation [1-2] can be inserted to give the extraction ratio as:

$$e = 1 - \frac{\rho g H}{APS} \quad \textbf{[1-3]}$$

To prevent failure of the pillars, a factor of safety S_F is adopted for the design, and this is given by:

$$S_F = \frac{\sigma_s}{APS} \quad \textbf{[1-4]}$$

where:

σ_s = the pillar strength (MPa)

This can be rearranged as:

$$APS = \frac{\sigma_s}{S_F} \quad \textbf{[1-5]}$$

Equation [1-5] can be inserted in Equation [1-3] to give:

$$e = 1 - \frac{\rho g H S_F}{\sigma_s} \quad \textbf{[1-6]}$$

A power-law strength formula is typically used to determine the pillar strength in the South African mines. This empirical relationship is primarily associated with the 1967 reference by Salamon and Munro:

$$\sigma_s = K \frac{w^\alpha}{h^\beta} \quad \textbf{[1-7]}$$

where:

K = in-situ strength of the pillar's rock material (MPa)

w = pillar width (m)

h = pillar height (m)

α and β = constants

This can be inserted into Equation [1-6] to give:

$$e = 1 - \frac{\rho g H S_F h^{\beta}}{K w^{\alpha}} = 1 - \gamma H \qquad \textbf{[1-8]}$$

where:

$$\gamma = \frac{\rho g S_F h^{\beta}}{K w^{\alpha}} \qquad \textbf{[1-9]}$$

From Equation [1-8], the extraction ratio, e, is therefore a simple decreasing linear function of the depth, H, and the rate of decrease is dependent on the parameter, γ. This parameter is a function of the assumed pillar strength, the overburden density and the S_F, and should preferably be as small as possible based on Equation [1-8] to ensure a high extraction ratio at depth. From Equation [1-9], there are not many options to increase the extraction ratio for increasing depths. For example, the mining height can be reduced, but this is not always feasible owing to the reef width or the minimum height limitations of the equipment used in the mines. An additional aspect of these two equations is that the extraction ratio can be increased by increasing the pillar width (increasing the pillar strength). However, the implication of this is that the bord spans will increase to achieve the given extraction ratio, and this is not always feasible based on a consideration of bord stability.

The notion of the pillar S_F was introduced as a measure of pillar stability. Failure of a pillar is therefore expected to occur when the load applied onto the pillar exceeds its load-carrying capacity. In South African coal mines, it was found that a S_F value of 1.6 equates to a probability of failure to 0.001. Values as high as 2 are nevertheless sometimes used as a precaution (Maritz, 2015). In cases where there is critical infrastructure on surface and subsidence must be avoided at all costs, even larger values of S_F are used.

The decrease in extraction ratio predicted by Equation [1-8] is illustrated in Figure 1-3 for a typical hard rock bord and pillar mine. The S_F on the pillars is maintained at a value of 1.6, g = 9.81 m/s^2, the overburden density is 3000 kg/m^3, the mining height is assumed to be 2 m, and the pillar width is maintained at 7 m. The Hedley and Grant pillar strength formula is assumed, and therefore, α = 0.5 and β = 0.75. If the UCS of the laboratory samples is 100 MPa, when adopting the classical rule for the strength of the pillar material, it follows that $K = \frac{1}{3} UCS = 33$ MPa.

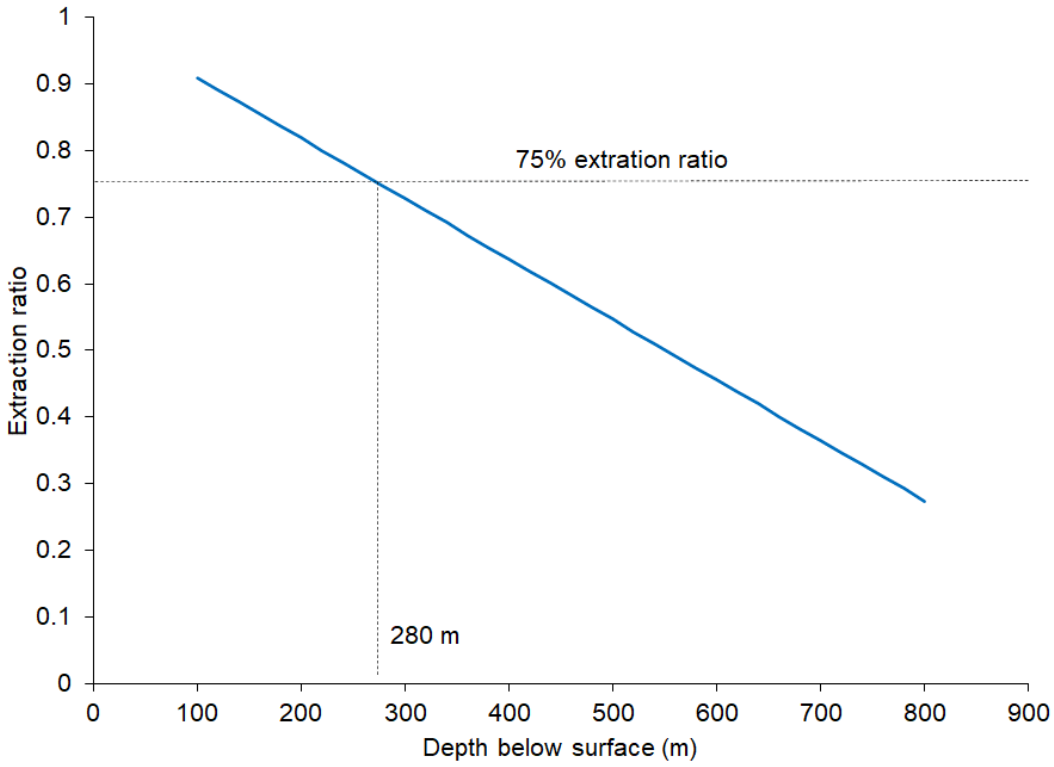

Figure 1-3. Decrease in the extraction ratio for increasing depth.

From Figure 1-3, it is evident that for the assumed parameters and conservative pillar strength, an extraction ratio of 0.75 can only be maintained up to a depth of 280 m. This is clearly a problem for the mines planning to implement mechanised bord and pillar operations at greater depths. Research is currently being conducted to determine better estimates of pillar strength to investigate if higher extraction ratios can be maintained at greater depths and for pillars containing weak material (Watson et al., 2021; Couto and Malan, 2023). An alternative that is not currently being investigated in the industry is to explore methods to artificially increase the pillar strength. This dissertation describes a numerical modelling study of the benefit of using backfill to reinforce pillars. Smaller pillars can possibly be used thereafter at greater depths, and the extraction ratio can be increased.

2. LITERATURE SURVEY

Globally, mining activities have a significant impact on social, environmental, and economic aspects. While millions of tons of rock are mined from the earth's crust to extract a small amount of valuable minerals, the rest of the material needs to be disposed of as waste (Rankine et al., 2007). Typically, the waste is disposed of using the least complicated and most cost-efficient approach with little consideration of the consequences.

The development of many new mines to meet the demand for minerals increases the likelihood of more tailings dam failures occurring (Decipher, 2020). The destruction caused by historic dam failures emphasises the necessity to dispose of mine waste in a safe and secure manner. An alternative that has become increasingly popular for the storage of waste in mining operations, particularly in coal mines, is backfilling. The objective of this dissertation is to investigate whether hard rock pillar strength can be improved by using backfilling.

Pillar design needs to satisfy the requirements of both mine safety and profitability to be considered successful. The ideal pillar is one with the smallest volume that meets the requisite measure of stability (Van der Merwe and Mathey, 2013). The problem of pillar strength will be addressed in this chapter, followed by a discussion on how backfill can be used to safely increase the extraction ratio.

2.1. Tailings dam failures

Tailings production is inherent to minerals processing in the mining industry. Historically, the global mining industry experienced numerous destructive tailings flows because of the breach of tailings dams. In the past five decades, 63 major tailings dam failures have been reported worldwide, with an increasing tendency for these failures since 1990 (Owen et al., 2020). An analysis of European data revealed that 83% of the failures occurred when the dam was active, 15% occurred for inactive and abandoned dams, and 2% occurred in inactive, but maintained dams (Kossoff et al., 2014). This suggests that active tailings dams are the most likely to fail.

The use of tailings dams has seen a decline due to the numerous dam failures that have occurred. The number of failures has doubled over the last two decades with an average of two to four tailings dam failures occurring annually around the world (Armstrong et al., 2019). These failures have economic and environmental consequences and may lead to significant loss of life when the tailings displace over substantial distances with high velocities. This has led to mining companies searching for alternative means to store or use mining waste, with backfill being one of the options.

To illustrate the dangers associated with the use of tailings dams, the following sections briefly describe a few notable dam failures that have occurred in recent years. These examples were arbitrarily selected to highlight the problem and do not form a comprehensive list.

2.1.1. Merriespruit

Merriespruit is located in the mining town of Virginia in the Free State. The tailings dam belonged to Harmony Gold Mine. On February 22nd, 1994, the Merriespruit Number 4 tailings dam failed following heavy rain, leading to a flow of approximately 600 000 m^3 of tailings and water over 4 km and immersing 80 homes in the adjacent suburb (Minerals Council South Africa, 2020). The Merriespruit disaster claimed the lives of 17 people. Figure 2-1 is a photograph that illustrates the breach of the dam and Figure 2-2 shows the extent of the damage to the suburb.

Figure 2-1. Aerial photograph of the Merriespruit tailings dam failure (after Minerals Council South Africa, 2020).

Figure 2-2. The extent of the damage inflicted on the nearby suburb (after Minerals Council South Africa, 2020).

The investigation that followed indicated that poor management of water was the cause of the dam failure. Additionally, the tailings dam did not have the mandated freeboard which is used to control the contents and reduce the likelihood of uncontrolled spilling. The Merriespruit disaster led to the compilation of the mandatory Code of Practice on Mine Residue Deposits for South Africa. The set of standards included the following aspects (Minerals Council South Africa, 2020):

1. The management of excess water.
2. An increase in the height of perimeter walls.
3. The minimum qualification requirements for personnel managing tailings dams.
4. Limits on the permitted proximity of human habitation to tailings dams.

In the years that followed this incident, South Africa was ranked as a leader in the international mining community in terms of tailings dam management standards (Minerals Council South Africa, 2020).

2.1.2. Samarco

The Samarco Mariana Mining Complex is located near the Brazilian town of Mariana. It is a joint venture between BHP Billiton Limited and Vale and produces iron ore. On November 5th, 2015, a disaster occurred when the mine's Fundão dam collapsed entirely, releasing 43 million m^3 of iron ore tailings. This generated mud waves which were up to 10 m high, causing irreversible environmental damage over 668 km of watercourses from the nearby Doce River Basin to the Atlantic Ocean. The damage caused by the collapse was the worst ever recorded in the global mining industry (Do Carmo et al., 2017).

Downstream villages were devastated, causing 19 fatalities and more than 16 injuries. Figure 2-3 shows how buildings in a nearby district were affected by the failure. Scores of people were left without access to clean water.

Figure 2-3. Villages affected by the Fundão tailings dam failure (after Do Carmo et al., 2017).

The investigation that was conducted to identify the cause of failure of the Fundão dam found that three small seismic shocks led to the breach (McCrae, 2016).

2.1.3. Córrego do Feijão

Córrego do Feijão is an iron ore mine owned by Vale. It is in Brumadihno, Brazil, just 120 km from the Samarco operation. The collapse of the tailings dam occurred on January 25th, 2019, unleashing more than 110 000 m^3 of mud. The mining waste flowed through the mine offices and staff canteen where several people were present. It continued to flow 10 km downhill, reaching homes, farms, roads, and the Paraopeba River, a major tributary of the São Francisco River (Rotta et al., 2020).

The volume of tailings that was released is far less than the Samarco disaster; however, as of January 2020, this event had a death toll of 259, while 11 individuals remained missing. Figure 2-4 illustrates how the tailings engulfed the cafeteria, where hundreds of employees were at the time of the dam failure, and Figure 2-5 shows how the mud flow affected the environment.

Figure 2-4. The mine cafeteria destroyed by the dam failure (after Boadle and Nogueira, 2019).

Figure 2-5. Farmland devastated by the mine waste (after Boadle and Nogueira, 2019).

As a result of these mining disasters, the International Council on Mining and Metals recently published a “Tailings Reduction Roadmap” in which technologies that can minimise tailings production were investigated. Their proposals focussed on the following aspects (International Council on Mining and Metals (ICMM), 2022):

1. Precision geology: Geological techniques are needed to better characterise the ore body to maximise ore production and minimise the mining of waste rock. This will reduce the amount of tailings being generated.
2. Precision mining: This also aims to reduce the mining of waste rock and the amount of tailings being generated.
3. Precision segregation: This focuses on better segregation technology to optimise mineral recovery and produce more benign tailings.
4. In-situ recovery: Leaching techniques can possibly be used to optimise mineral recovery and eliminate the production of waste rock.
5. Tailings enhancement: This requires the creation of value from tailings and to minimise the requirements for tailings storage.

The use of tailings to reinforce pillars and reduce pillar sizes is part of the last category and this is explored in this dissertation. The increased profitability of the mine, when using smaller pillars, may be used to offset the additional infrastructure and maintenance to place the backfill underground. The next section gives an overview of pillar strength. This section is included here as the objective is to increase this pillar strength using backfill.

2.2. Pillar strength

Pillar strength has been investigated by researchers for many years and it is an integral part of the study in this dissertation. Pillar behaviour is influenced by the rock type, the confinement of the pillar, and its strength. The latter is the pillar’s maximum resistance to axial compression (Esterhuizen et al., 2008). In bord and pillar layouts, the pillar strength will also be affected by the presence of geological features in the rock mass.

2.2.1. Coal mines

In the coal mining industry, the pillar design must account for the coal’s mechanical and physical properties (Wang et al., 2011). Prior to the 1960s, the pillar dimensions and bord spans in South

African collieries were determined through trial and error. The Coalbrook Colliery disaster led to a systematic research programme to determine pillar strength. On January 21st, 1960, approximately 900 pillars collapsed over an estimated area of 324 hectares in the northern section of the mine. The collapse led to a destructive windblast and increased methane gas concentrations. Unfortunately, many mineworkers were trapped underground (Van der Merwe, 2006). This remains the worst disaster in the local mining industry with a total of 437 fatalities. The figure below shows the area where the collapse occurred.

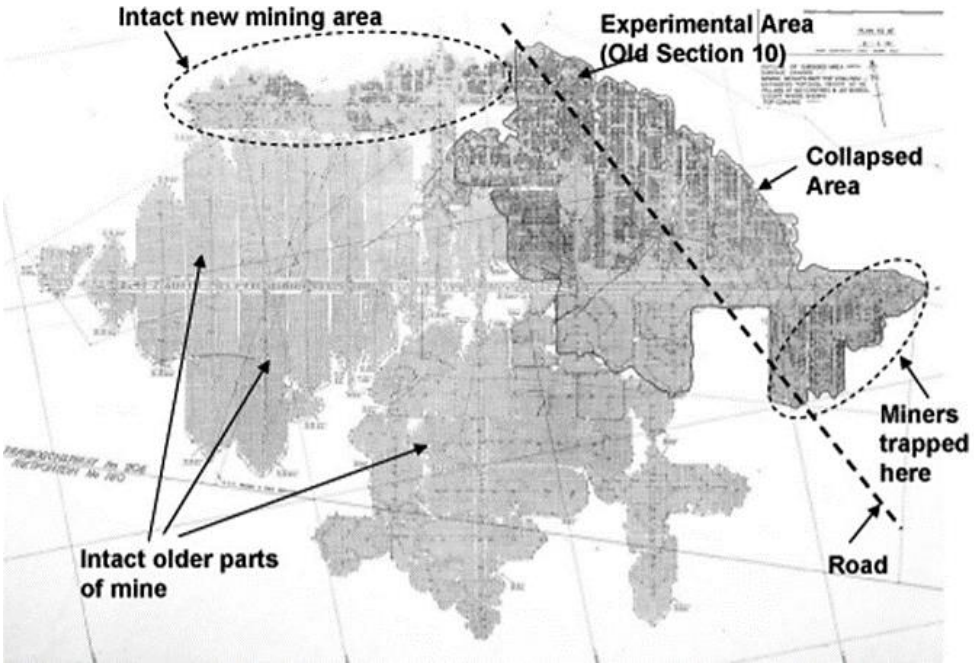

Figure 2-6. A plan of Coalbrook Colliery at the time of the disaster (after Van der Merwe, 2006).

To prevent the recurrence of a similar disaster, research into coal pillar strength and stability gained momentum. The Chamber of Mines established the industry-funded Chamber of Mines Research Organisation, which, together with the Coal Mines Research Controlling Council that was formed by the South African government, conducted research on the strength of pillars (Malan and Napier, 2011). A study was carried out by Salamon and Munro (1967) which led to an empirical strength equation being proposed to estimate pillar strength in South African collieries. The study involved the use of a statistical method, the maximum likelihood method, to determine the parameters for an assumed power-law strength formula. The database used for the calibrations comprises 98 stable and 27 collapsed coal pillar cases (Salamon and Munro, 1967).

The calibrated coal pillar strength equation is given by:

$$\sigma_s = K\frac{w^{0.46}}{h^{0.66}} \quad \textbf{[2-1]}$$

where:

K = 7.2 MPa

It is common to find that the pillars in certain operations are not square, and for such cases, an effective width must be used. It is determined as follows (Wagner, 1974):

$$w_e = \frac{4A}{C} \quad \textbf{[2-2]}$$

where:

A = cross-sectional area (m^2)

C = circumference (m)

Salamon and Munro (1967) noted that pillar strength is also affected by the volume of the rock and its shape, the contact conditions with the roof and floor, and by the load of the overlying strata that it supports up to surface. Equation [2-1] implies that the strength of the pillar will decrease as its volume increases.

A similar database of pillars was compiled from Australian collieries in 1996, and the following pillar strength formula was derived (Galvin et al., 1999):

$$\sigma_s = K\frac{w^{0.51}}{h^{0.84}} \quad \textbf{[2-3]}$$

where:

K = 8.6 MPa

Note that the calibrated values for the exponents in the power-law formula based on the Australian database closely resembled Salamon and Munro's results from thirty years prior. The similarity in the pillar strength formulae that were derived spurred a study based on a combination of both databases in 1999 which resulted in the formula below (Galvin et al., 1999):

$$\sigma_s = K\frac{w^{0.5}}{h^{0.7}} \quad \textbf{[2-4]}$$

where:

K = 6.88 MPa

The introduction of the power-law formula in South Africa did not eliminate the occurrence of pillar failures. In the following years, some of the pillars that were developed prior to the adoption of the formula, as well as the newer pillars, failed. The database of failed pillars therefore increased in size over the years (Van der Merwe and Mathey, 2013). The strength formulae were reassessed using the revised coal pillar databases. These revised formulae are beyond the scope of this study and are not included here.

2.2.2. Hard rock mines

For many years, South African hard rock mines did not have a pillar strength formula that was specifically developed for the local rock conditions. The power-law strength formula's success in the coal industry led to the shallow hard rock mines adopting a similar formulation developed for the Canadian uranium mines (Hedley and Grant, 1972).

Research on pillar strength in hard rock mines was conducted by Hedley and Grant (1972) for the uranium mines in Canada. They used a database of 28 pillars, which is far smaller than the coal database used by Salamon and Munro (1967). Of the 28 pillars in the Canadian database, only three had failed. Hedley and Grant (1972) also adopted the power-law strength formula.

While the original coal power-law equation was developed for square pillars, the uranium mines used long and narrow rib pillars. This was acknowledged by Hedley and Grant (1972), and they assumed that the strength of the rib pillars in their research would not be significantly greater than a square pillar with a width that equals the minimum width of the slender pillar (Malan and Napier, 2011). The pillar database was used to calibrate values for the exponents, α and β (Equation [1-7]). Based on the three sets of values for the failed pillars that were available to the researchers and by assuming a constant value of 0.5 for α, the value of β was calculated. For each of the three pillars, the tributary area stress was assumed to be equal to the strength of the pillar. For each failed pillar, the value of β was subsequently calculated, ranging from 0.736 to 0.768 (Malan and Napier, 2011). The average value of 0.75 was adopted as β. The Hedley and Grant formula is given by:

$$\sigma_s = K \frac{w^{0.5}}{h^{0.75}} \qquad \textbf{[2-5]}$$

Research to develop a strength formula for the South African hard rock environment was never conducted. This has resulted in the Hedley and Grant formula being adopted with a modified K-value to best fit the local rock strengths. Calibration of this K-value is difficult in the absence of large-scale pillar failure and for many years, a third of the UCS of laboratory-tested rock strengths was used as the K-value. The K-value that is used in the South African mines typically ranges from 35 to 60 MPa, as the rock strengths are between 100 and 180 MPa (Maritz, 2015). This may have, however, been a conservative approach, and almost no pillar failures have been reported for the bord and pillar mines.

Many empirical pillar strength formulae for hard rock were developed subsequently (see Martin and Maybee, 2000), but these will not be discussed in this study as the focus is on the strengthening effect of using backfill. It should also be noted that numerical modelling of pillar strength is advocated by some as an alternative to the empirical formulae (see Malan and Napier, 2011 for examples).

A pillar strength formula that is noteworthy to discuss in this dissertation is the "Confinement Formula" developed by Lunder and Pakalnis (1997). It is included here as the term "confinement" may be confused with confinement applied on the skin of the pillar. This is not the case as illustrated below.

The Confinement Formula is a hybrid method based on using the "classic" strength of rock based on failure criteria and empirical methods. To derive the formula, the authors used seven hard rock pillar databases which contain good to very good quality rock masses (Lunder and Pakalnis, 1997). The combined database contains a total of 178 cases, with pillars classified as failed, unstable, or stable. Table 2-1 illustrates the distribution of pillar stability across the databases.

Table 2-1. Distribution of pillar stability for all the databases that constitute the combined database (after Lunder and Pakalnis, 1997).

Pillar stability classification	Combined database	Westmin Resources	Hudyma (1988)	Von Kimmelman et al. (1984)	Hedley and Grant (1972)	Others
Failed	68	18	12	29	3	6
Unstable	52	11	9	11	2	19
Stable	58	2	26	7	23	0

The general form of the Confinement Formula, which employs a "mine pillar friction term", is given by:

$$\sigma_s = (K \times UCS) \times [(C_1 + C_2) \times \kappa] \quad \textbf{[2-6]}$$

where:

K = rock mass strength size factor

C_1 and C_2= empirically-derived constants

κ = mine pillar friction term

Inelastic numerical modelling was conducted and it revealed a relation between the width-to-height ratio (w/h ratio) and "average pillar confinement". This average pillar confinement is defined as the ratio of the average minor and average major principal stress at mid-height of a pillar due to the dilation of pillars typically being the greatest at this height (Lunder and Pakalnis, 1997). The following equation was found to relate the average pillar confinement to the w/h ratio at a modelled extraction ratio of 75%:

$$Cp_{av} = 0.46\left[log(\frac{w}{h} + 0.75)\right]^{\frac{1.4}{w/h}} \quad \textbf{[2-7]}$$

where:

Cp_{av} = average pillar confinement

The mine pillar friction term is obtained from the following equation:

$$\kappa = tan\left[cos^{-1}(\frac{1-Cp_{av}}{1+Cp_{av}})\right] \quad \textbf{[2-8]}$$

The figure below demonstrates the relationship between the average pillar confinement and mine pillar friction factor.

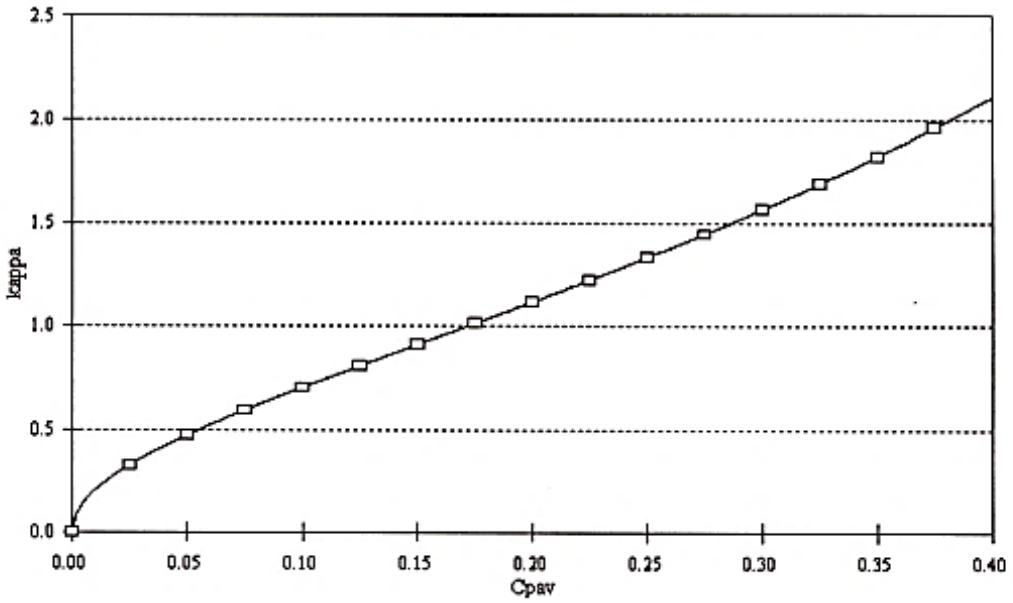

Figure 2-7. Relationship between the average pillar confinement and the mine pillar friction term (after Lunder and Pakalnis, 1997).

Using the information in the databases, Lunder and Pakalnis (1997) arrived at the Confinement Formula for hard rock pillars, and this is given in Equation [2-9].

$$\sigma_s = (0.44UCS) \times (0.68 + 0.52\kappa) \quad \textbf{[2-9]}$$

This formula has not been widely adopted and for the purposes of this study, it should be noted that it does not directly consider the application of confinement on the skin of the pillar, but rather refers to an alternative method to account for the effect of w/h ratio on pillar strength.

2.2.3. Pillar failure

The following section is included to highlight the risk of pillar failures and indicate how backfill may be beneficial to prevent these collapses from occurring. This section also illustrates the risks associated with using empirical strength formulae in geotechnical environments that they were not originally developed for. The concept of “cascading pillar failure” is also useful to highlight under which conditions collapses occur and how backfill can assist.

2.2.3.1. Cascading pillar failure

Cascading pillar failure (CPF) is used to describe the mechanism whereby the strength of a pillar is exceeded, resulting in its failure and load being transferred to adjacent pillars. The added load on these pillars leads to their subsequent failure. This mechanism may lead to the failure of hundreds of pillars, leading to a rapid collapse over large parts of a mine. This kind of failure is referred to as a massive pillar collapse, progressive pillar failure, domino-type failure, or pillar run (Zipf, 2001).

A CPF is a major mining disaster, and it poses a significant risk to safety. The pillar collapse usually causes a powerful airblast created by the rapid displacement of air. The airblast results in flying debris that may cause harm to or kill mining personnel, and it also has the potential to disrupt the ventilation system by destroying ventilation seals, and fan housings (Zipf, 2001). In coal mines, a CPF may also lead to large volumes of rock fracturing, releasing large quantities of methane and this may result in a methane explosion.

Mines that experience CPF tend to exhibit the following characteristics (Zipf, 2001):

1. Extraction ratios usually exceed 60%. A high extraction ratio places the pillar stress near the peak strength and provides a generous amount of room for the expansion of the failed pillar material. This is where backfill can prevent the failures. As the voids between the pillars are filled, the pillars do not have room for expansion.
2. The pillar w/h ratio are always below 3 for failures in coal mines, under 2 for non-metal mine failures, and usually much less than 1 in metal-mine failures. When the w/h ratio is low, this leads to the failed material easily expanding into the neighbouring voids. Again, backfill can be used to prevent this expansion into the voids.
3. Minimum panel widths of 80 m.
4. There are always at least five pillars across the panel width. In some cases, the number of pillars is above ten, which ensures that pillars reach their complete tributary area load.
5. Large barrier pillars with w/h ratio above 10 do not form part of the mine layout.

In South Africa, the Coalbrook Colliery disaster is an example of a CPF. A more recent example is a large collapse that occurred in a bord and pillar base metal mine in Missouri. The failure commenced with four centrally-located pillars and swiftly spread to comprise close to 100 pillars. The pillar width was 8.5 m, and the pillar height was approximately 12 m, resulting in a w/h ratio of 0.7 and an extraction ratio of approximately 78%. The damage caused by the airblast was minor, and fortunately did not cause any injuries (Zipf, 2001). The area of the collapse is illustrated in Figure 2-8.

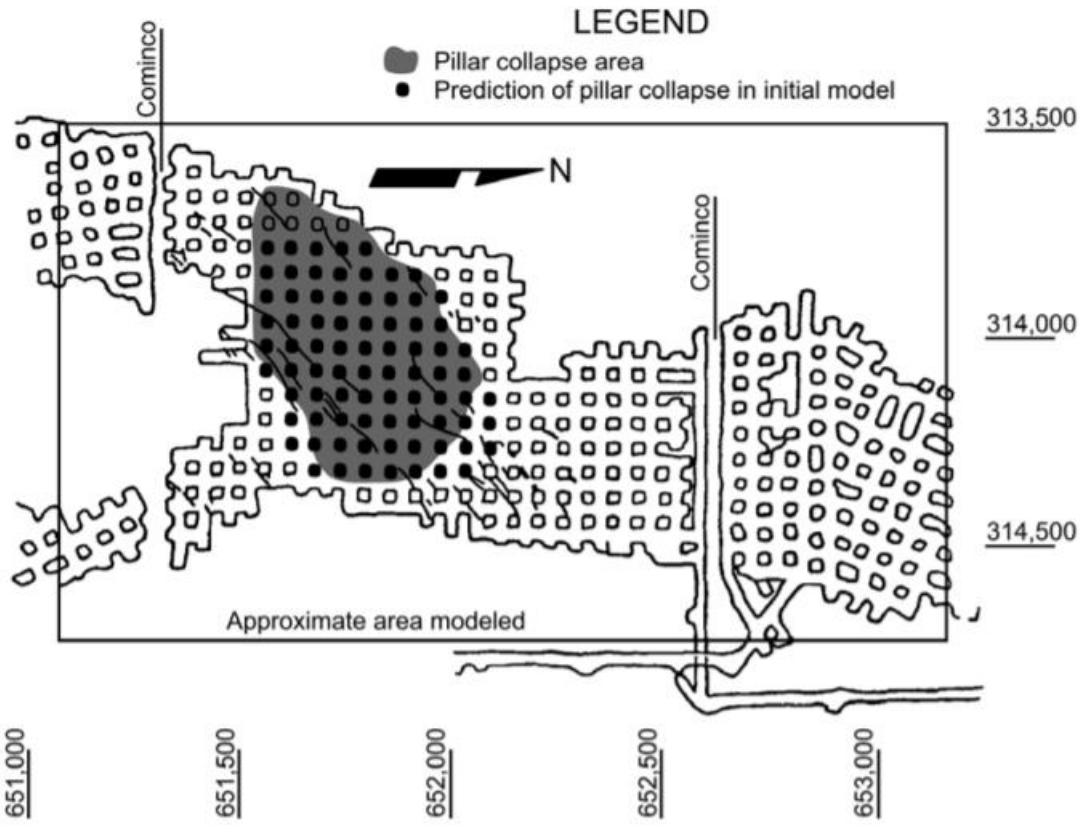

Figure 2-8. Mine layout for the collapsed pillars in a Missouri operation (after Zipf, 2001).

In summary, it should be emphasised that backfill may prevent the occurrence of CPFs by reducing the volume of voids in which pillars can expand and eventually fail.

2.2.3.2. Wonderkop Chrome Mine

This is an example of a mine collapse from South Africa, and it is included to illustrate geotechnical conditions occasionally found in the Bushveld Complex. The placement of backfill may possibly be the only solution to solve the pillar instability problems associated with these geotechnical conditions.

Wonderkop Chrome Mine is situated near Rustenburg and is adjacent to the Spruitfontein dome. Its proximity to this upfold structure influenced the structure of the chromitite reefs. This resulted in thick clay layers being found in the pillars in some areas (Malan and Napier, 2011). The mine's original pillar design was done using the Hedley and Grant strength formula. This resulted in pillar sizes of 12 m × 6 m, an effective width of 8 m, and a mining height of 2 m, resulting in a minimum w/h ratio of 3 when considering the smallest pillar dimension. The K-value was assumed to be a third of the laboratory strength of samples acquired from a neighbouring mine, leading to a value

of 27.3 MPa. The pillar strength was approximated as 45.9 MPa when using the effective width in the strength formula. It should be noted that this value seems conservative, but this did not prevent the mine from collapsing, and the major contributing factor was the presence of weak clay layers in the pillars.

Stoping began in September 1996 and the first underground inspection by the consulting rock engineer was conducted ten months later (Spencer, 1999). It was observed that joints were unravelling at the corners and along the sides of some pillars. Figure 2-9 illustrates the layout of the mine with the positions of the pillars where the observations were made. The failure codes used in the diagram are noted as (Spencer, 1999):

- 0 – No failure.
- 1 – Opening of joints at the corners.
- 2 – Opening of joints at the corners and along the sides.
- 3 – Material spalling off the corners and sides.
- 4 – Horizontal movement occurring along the clay layer.

Measures were put in place to strengthen the pillars, specifically by storing waste material between the pillars, as well as reinforcing the pillars. However, the condition of the pillars continued to worsen and by April 1998, the closure rate had risen to 1.8 mm/day in some areas (Spencer, 1999). Numerous falls of ground occurred, and this led to the subsequent mine closure the following month. This example illustrates the small spans at which failure can occur for these ground conditions. Backfill can arrest this as it will apply confinement to the pillars and prevent the failed material from expanding into the voids.

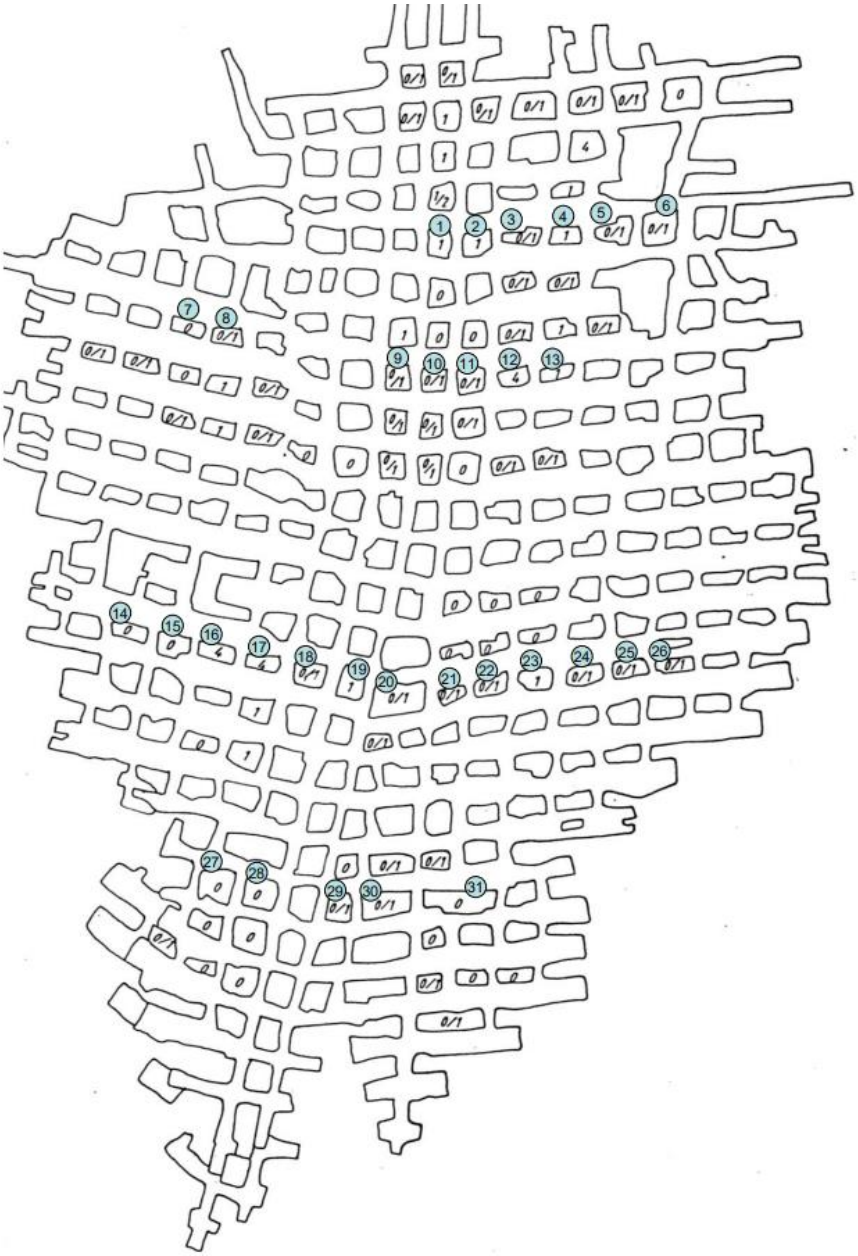

Figure 2-9. Mine layout at Wonderkop Chrome Mine (after Spencer, 1999).

A back-analysis of this failure was conducted by Malan and Napier (2011) using the Tabular EXcavation ANalyser (TEXAN) numerical code. The face positions in July 1997 and July 1998 were simulated, as shown below. This highlights that the stress on the pillars were very low and again indicates that backfill may be the only solution to stabilise this weak pillar material.

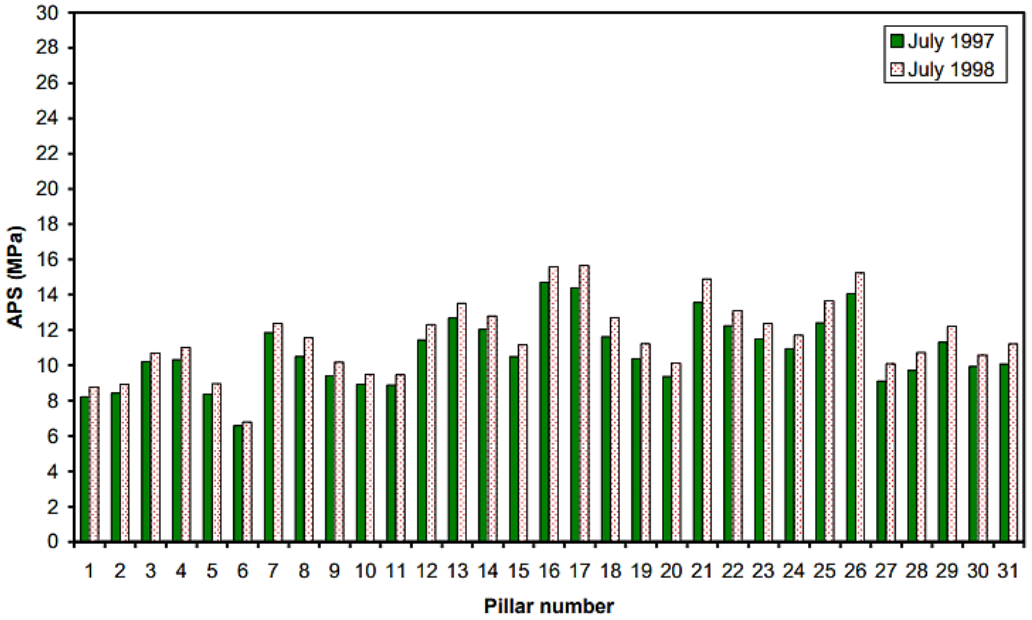

Figure 2-10. Simulated pillar stresses in the Wonderkop Chrome Mine (after Malan and Napier, 2011).

2.2.3.3. Everest Platinum Mine

This example is analogous to the Wonderkop Chrome Mine and a major collapse also occurred at this mine. Everest Platinum Mine exploits UG2 Reef and a major contributor to the collapse was the presence of weak “alteration layers” in the pillars (Couto and Malan, 2023). Figure 2-11 illustrates a weak layer of clay (alteration layer) which is present along the pillar and hangingwall contact.

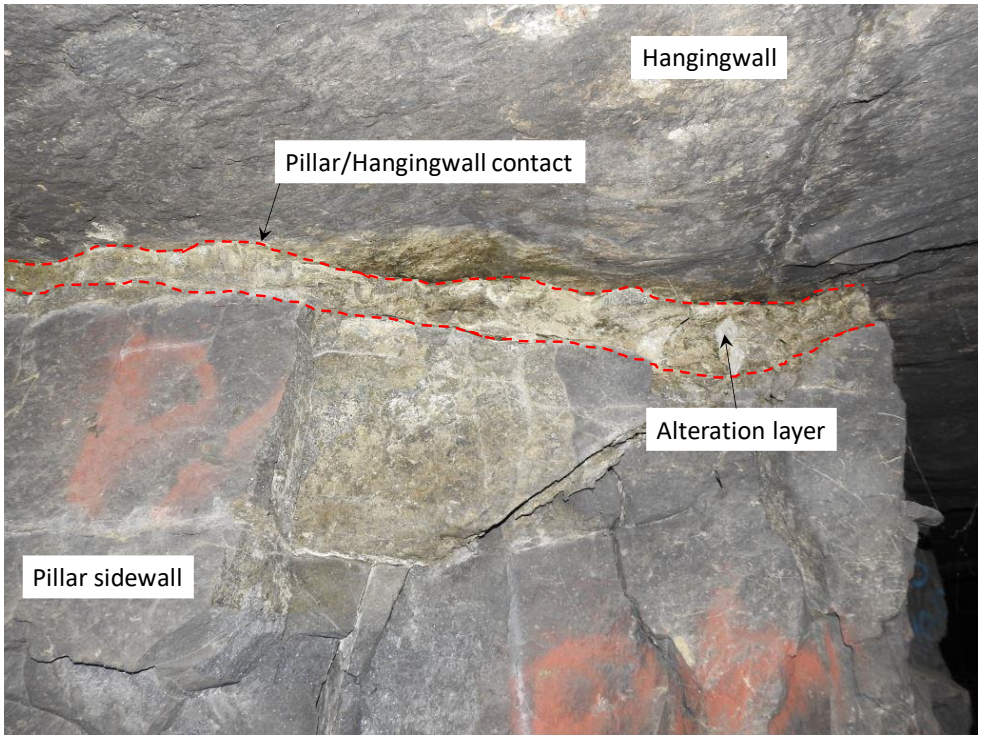

Figure 2-11. The alteration zone at the pillar and hangingwall contact (after Couto and Malan, 2023).

In 2007, pillar spalling was observed in the shallow sections of the mine. An increase in pillar sizes was implemented and closure instrumentation was installed. By November of the following year, the instruments recorded 5 mm of closure in the unstable area. On November 23rd, 2008, the surface mine's water pumps were inundated due to rainfall, and excessive water seepage along the alteration zone occurred. This was a significant contributing factor to the large collapse that occurred soon after on December 8th. Figure 2-12 illustrates the extent of the collapse and the various colours represent the different levels of pillar damage (Couto and Malan, 2023).

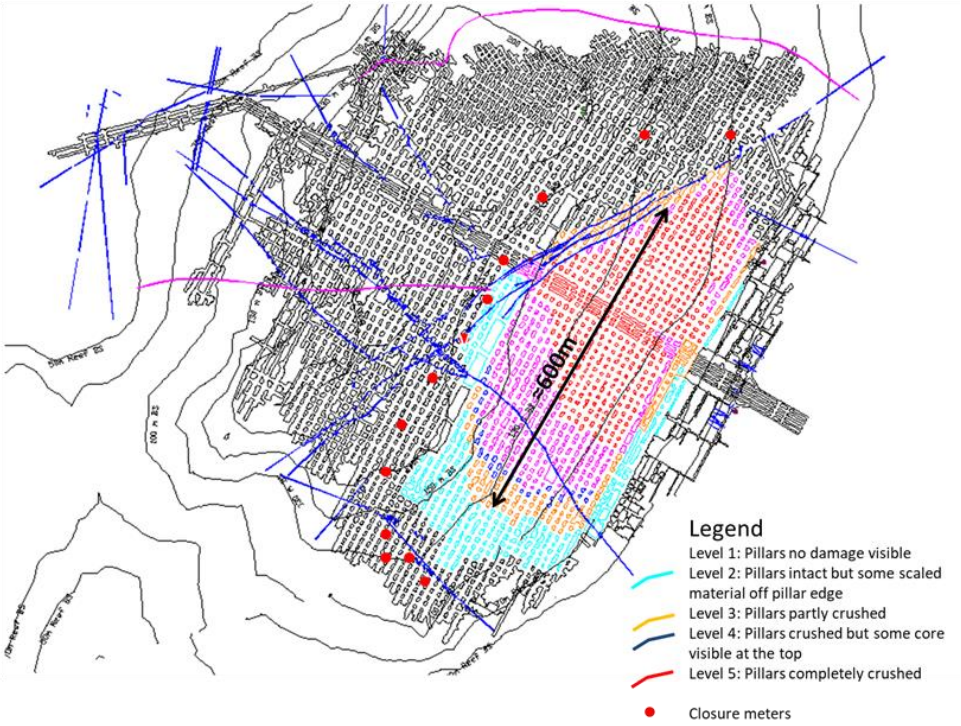

Figure 2-12. The extent of the collapse at Everest Platinum Mine (after Couto and Malan, 2023).

Couto and Malan (2023) recently visited the collapsed area to observe the condition of the failed pillars. Figure 2-13 and Figure 2-14 illustrate the extent of pillar spalling. Note the large amount of pillar dilation that can be arrested by using backfill.

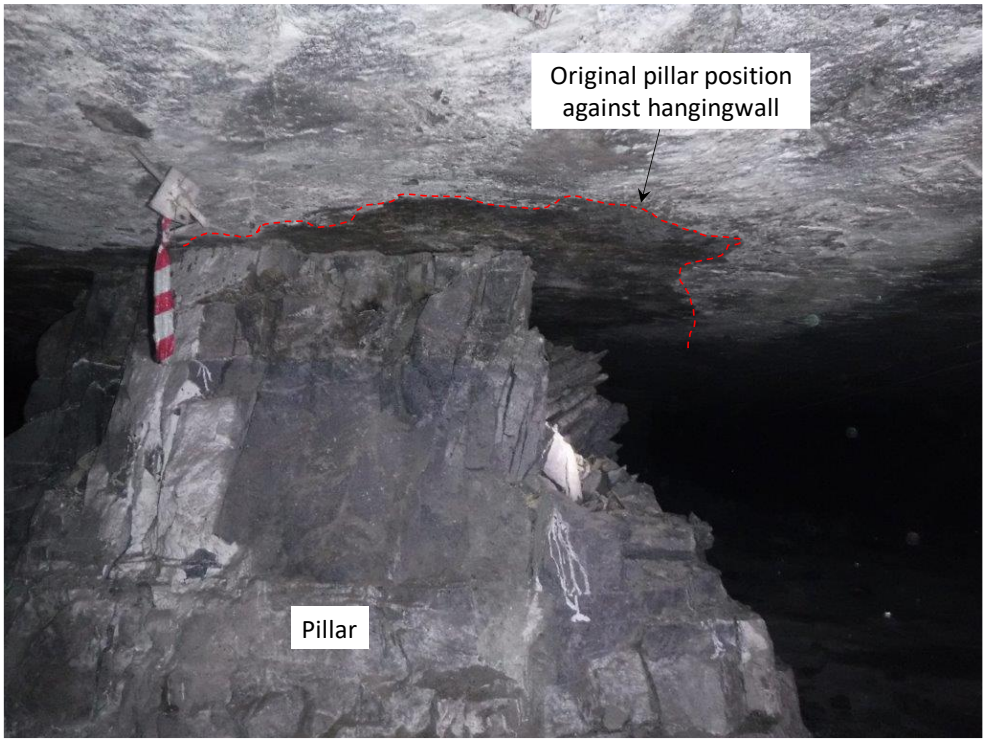

Figure 2-13. The original position of the pillar against the hangingwall (after Couto and Malan, 2023).

Figure 2-14. Some of the pillars were completely crushed during the collapse. This expansion of the pillars could have been arrested by using backfill (after Couto and Malan, 2023).

The original pillar design was conducted using the Hedley and Grant pillar strength formula with a K-value of 35 MPa. In 2008, following a minor collapse, concern was raised regarding the pillar stability. To reinforce the pillars, several of them were supported using fibre-reinforced shotcrete (Couto and Malan, 2023). This, however, did not halt their deterioration and by the end of 2008, the decline became affected by the instability, which led to the operations being suspended.

In summary, the case studies above have shown that empirical pillar formulae may not be applicable to all hard rock mines as these formulae were derived for different rock types and environments. A mechanism of failure discussed above was the presence of clay layers, which substantially weakened the pillars (Malan and Napier, 2011). An alternative approach of using backfill in these areas, where it is known that the pillar strength is very low, should be considered.

2.3. Pillar confinement methods

This section is included to give some background information on methods to achieve pillar confinement other than the use of backfill. In particular, the publications were studied to determine whether the actual increase in pillar strength after the installation of support can be quantified. Backfilling is not included here and is discussed separately in Section 2.4. All these methods attempt to increase the strength of pillars by applying confinement on the skin of the pillar. In underground operations, varying pillar strengths are encountered due to variations in the rock mass strength as well as the pillars not being cut according to the dimensions specified in the layout design. This may lead to instabilities in the mining areas.

An important aspect of the investigation is to reinforce some pillars to facilitate the mining of other pillars. The reinforcement of pillars is achieved by employing rock support systems that maintain the rock's load-bearing capacity and improve its stability (Hoek and Wood, 1987). Pillar confinement provides a means to increase the strength of pillars, which is particularly beneficial for mining operations with complex ground conditions and geological features. There are various methods to confine pillars, and these are discussed below.

A key objective of a support system is to mobilise and conserve the rock mass' inherent strength for it to become self-supporting (Hoek and Wood, 1987). Cables and mesh reinforcement involve the use of wire mesh that is reinforced with cable strapping. Cables and mesh are a passive support system as the rock mass is required to dilate prior to the system becoming active. The effectiveness of this system to maintain rock mass integrity is doubtful since deformation must take place for it to take effect (Jjuuko and Kalumba, 2014).

Regarding pillar support, the wire mesh is wrapped around the pillars to support pieces of loose and broken rock. Studies conducted by Stacey and Ortlepp (2001) and Kuijpers et al. (2002) noted that the addition of rope lacing to mesh elements can substantially enhance the capacity of the support system (Wei et al., 2022). Figure 2-15 depicts examples of the use of mesh to contain broken rock and the application of cable and mesh in a deep mine.

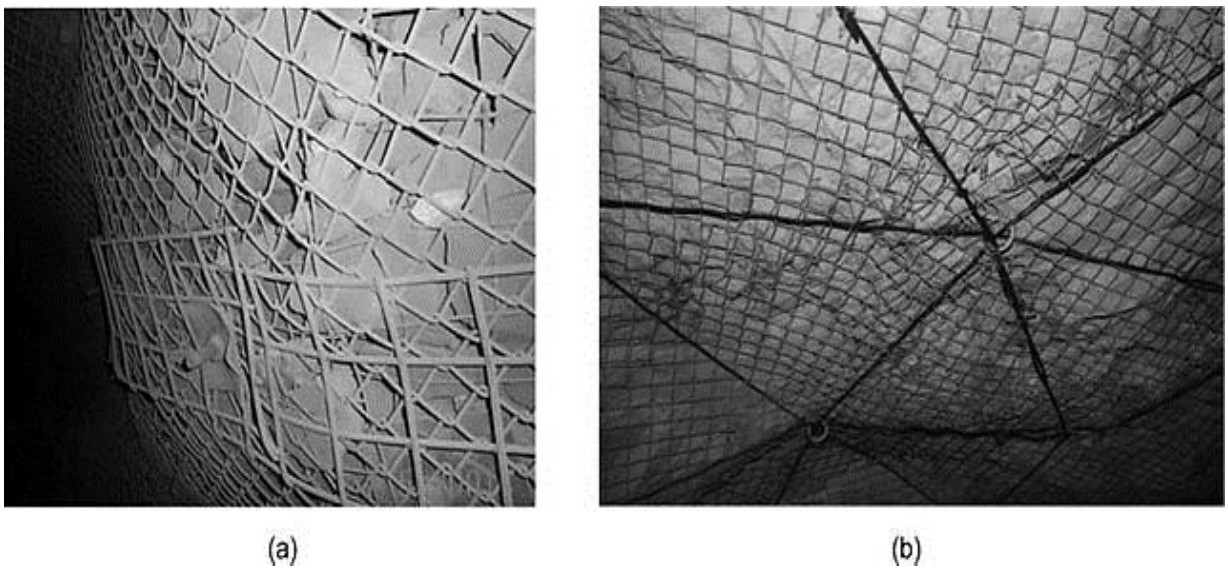

Figure 2-15. (a) An example of mesh and (b) cable and mesh support (after Li, 2011).

The two types of wire mesh that are currently employed underground are weld mesh and chain-link mesh, with the former being the strongest. Both mesh types are economical options for mines, and they can be installed quickly.

Shotcrete was pioneered by the civil engineering industry and was later introduced to underground mining operations in the 1950s as an efficient alternative to the mesh support system (Jjuuko and Kalumba, 2014). Pillar shotcreting refers to the application of a mixture of cement, fine concrete aggregates, sand, and water onto the surface through a hosepipe under high pressure (Haldar, 2018). Shotcrete is typically applied onto surfaces with a thickness ranging from 25 to 100 mm. The two methods of application, namely dry-mix and wet-mix shotcrete, differ by the stage at which water is added to the dry ingredients (Mulenga, 2018). Water is added at the nozzle of the pipe for the former, and during the mixing process for the latter.

Shotcrete develops strength over time, but it is brittle and fails at low rock displacements when employed without any reinforcements (Jager and Ryder, 1999). Weld mesh was traditionally used to improve its ductility, however, the transportation of sizeable quantities of bulk materials to the working areas made it challenging to use. An alternative is steel fibre-reinforced shotcrete (Hoek and Wood, 1987).

Thin spray-on liners, abbreviated as TSLs and commonly referred to as membranes, were introduced to mining to provide support for challenging ground conditions requiring a skin support with a high yielding capability. The membrane is sprayed onto surfaces at a thickness of between 3 and 5 mm and the suppliers claim many advantages, including a fast-curing period, high adhesion properties on rock surfaces, high tensile strength, and the ability to seep into joints and fractures (Kolapo et al., 2021). The latter prevents the rock from unravelling by conserving its natural strength. Additionally, the application of TSLs is rapid, which improves the cycle times. Several papers on the technical characteristics of TSLs as well as their application in underground South African mines have been published.

Steel banding, more commonly known as strapping, is used to contain rock when most of the weakness planes run in one direction. The straps are installed across the weakness planes and for these conditions, they are more effective than mesh (Hoek and Wood, 1987). Figure 2-16 depicts a strap that is installed using rock bolts and it shows that the strap is designed to follow the rock surface.

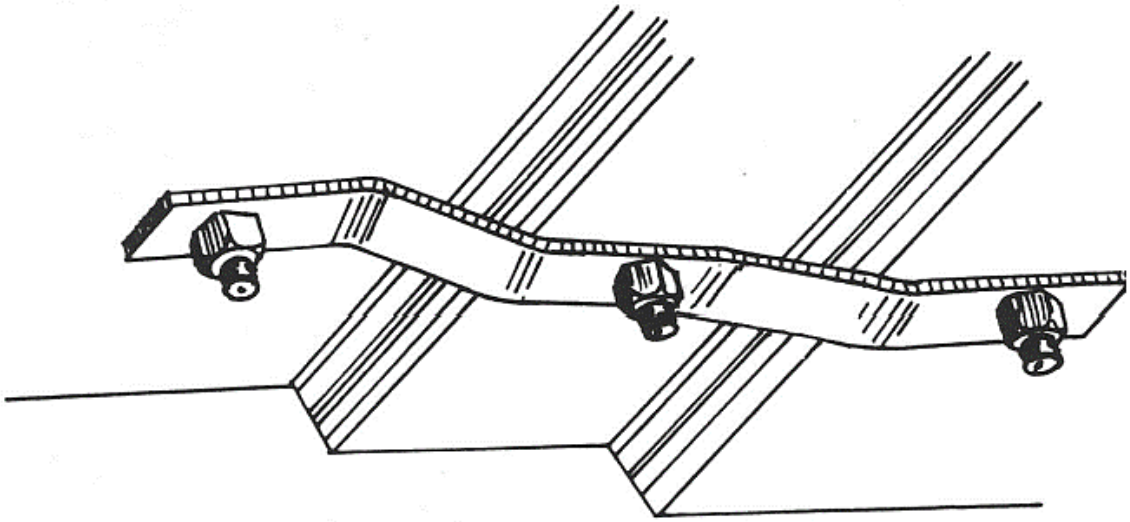

Figure 2-16. A strap installed using rock bolts (after Hoek and Wood, 1987).

Pillar strapping involves using steel cables to enhance the strength of unstable pillars (Alejano et al, 2017). This support system is not useful for pillars where small pieces of loose rock unravel as they tend to fall out between the cables. For these conditions, it is advisable to first wrap the pillars in mesh and then strap them. Strapping for pillar reinforcement is particularly useful to stabilise individual pillars in small mining areas where most pillars are stable (Alejano et al., 2017). Figure 2-17 illustrates the support of a pillar at a Spanish iron ore operation.

Figure 2-17. Pillar strapping at the Santa Rosa Mine (after Alejano et al., 2017).

In summary, some support methods are used underground to increase pillar strength. These methods may or may not work depending on the geotechnical conditions. It is evident from the publications, however, that this is mostly a “trial and error” method and none of the workers provide information on the quantified increase in pillar strength.

2.4. Backfilling in the mining industry

In recent years, some operations have taken interest in adopting backfilling practices to place their tailings underground and to potentially extract some of the pillars. Backfill is placed in voids prior to the extraction of pillars to reduce time-dependent failure by providing confinement to the rock mass (Tesarik et al., 2009).

Backfill is mainly used for regional and local support in deep stopes where rockfall and rockburst problems are encountered. It is also used in shallow operations to enable multi-reef extraction and to provide regional support (Squelch, 1993, cited in Squelch et al., 2001). Backfill does not generate vertical loads until substantial deformation of the roof has occurred. The vertical stresses acting on the fill can be attributed to the overburden pressure (Donovan, 1999). In terms of pillars, the additional support that is provided by backfill is transmitted as a lateral pressure along the sides of the pillars. The confinement that it provides increases the pillar strength (Donovan and Karfakis, 2004). The figure below illustrates the process by which lateral pressure will develop within the backfill.

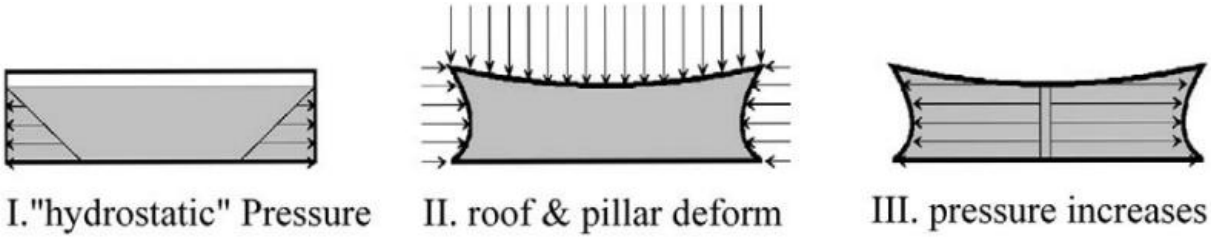

Figure 2-18. Development of pressure within the backfill (after Donovan and Karfakis, 2004).

The types of backfill as well as the use of fill in South Africa's mining industry, which dates to the 19th century in the gold mines, will be discussed in the following section. This review was conducted to determine whether any of this information will be useful to guide the use of backfill in shallow bord and pillar mines.

2.4.1. Types of backfill

Backfilling contributes towards achieving the design objective of a safe and environmentally-sound mine site at the end of life of mine (Rankine, 2004). The backfill material must ensure long-term stability of the excavations and its selection is dependent on the characteristics of the rock mass, the layout, and the loading conditions.

Backfill refers to any waste material that is placed in the mined-out areas underground to perform an engineering function or simply for disposal. The mixture that makes up the backfill material can consist of plant tailings, waste rock, mixing water, and binders for certain backfills. The addition of water to the backfill mixture has three main functions, which are (Cordova et al., 2016):

1. To react with the cement powder and introduce hydration.
2. To act as a lubricant.
3. To secure the required space in the cement paste for hydration products to develop.

Backfill can be separated into two general categories, namely cemented and uncemented fill (Rankine et al., 2007). Uncemented fills do not contain binding agents. These include hydraulic fills, sand fills, rock fills, and aggregate fills. The tailings are typically dewatered to over 65% solids by weight and pumped underground using displacement pumps.

The three main properties that determine the behaviour of an uncemented fill material are shear strength, permeability, and compressibility. The backfill's stability is dependent on shear strength, which is attributed to the following (Cernica, 1995):

1. Interlocking of solid particles to resist deformation.
2. Cohesion and adhesion between the material's particles.
3. Frictional resistance to sliding between the solid particles.
4. Fill density.

A dense fill contains tightly packed solid particles which display greater resistance to shear forces (Donovan, 1999). However, obtaining sufficient uncemented fill material to place in the voids is a challenge. In collieries, for instance, the waste that is produced during the cleaning process is approximately a quarter of the volume of the raw coal removed, which makes it impossible to fill the voids solely with mine waste. Materials such as crushed stone, sand, fly ash, and gravel can provide additional volume, but this results in higher costs.

The benefits of ash, sand, or waste filling in coal mines were described by Salamon and Oravecz (1976). This reference is of value to the study described in this dissertation. Practical experience indicated that filling could arrest the gradual deterioration of unstable pillar areas. As the backfill is typically not in contact with the roof, the fill will not transmit any pressure between the roof and floor. The load on the pillars is, therefore, not reduced by the presence of the fill material (Salamon and Oravecz, 1976). The authors emphasised that the beneficial effect of the fill is that it exerts some pressure on the pillar sidewalls and it can marginally increase the strength of the pillars. The more significant benefit arises when the pillars are failing, and significant lateral expansion of the pillars occurs.

Cemented backfill contains a substantial amount of the waste generated during mining and mineral processing. It also requires a low dosage of pozzolanic binder such as cement, gypsum, or fly ash mixed with water to improve its strength. The cement that is commonly used is the normal or ordinary Portland cement. The cement hydrates with the water in the fill to form a precipitate which clings to the surfaces of the solid particles (Donovan, 1999). This category includes cemented aggregate fills, cemented rock fills (CRF), cemented hydraulic fills, and paste fills. Hydraulic and paste fills are the most common backfills used worldwide (Rankine et al., 2007).

The important properties of cemented fill to consider are (Donovan, 1999):

1. UCS.
2. Deformation behaviour.
3. Cohesion and angle of internal friction.
4. Density and porosity.
5. The mixture's consistency.

The relationship between the type of backfill and its load bearing capabilities is illustrated below for various types of backfill (Jager and Ryder, 1999). All types of backfill require substantial strain before stress is generated. The backfill with the aggregates generate stress more rapidly at lower

strains. These are considerations for gold mines where different amounts of closure will be experienced in the stopes. Uncemented classified tailings (CCT) are the most common in South African gold and platinum operations. Almost no closure occurs in shallow bord and pillar stopes and these are not the properties that will be considered for such operations. The key consideration will be the lateral force exerted by the backfill on the pillar sidewalls. The confinement by backfilling is mainly generated in response to a pillar's lateral expansion (Galvin, 2016).

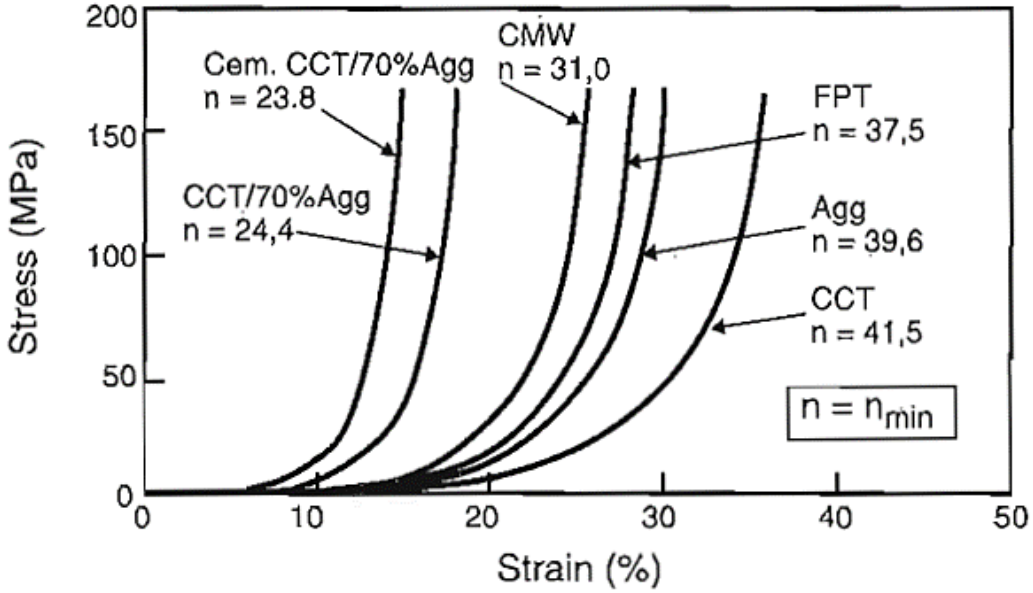

Figure 2-19. Stress – strain curves for different types of backfill (after Jager and Ryder, 1999).

Although the cement content of backfill contributes directly to the fill strength, the final amount of cement that is employed is controlled more by economics than by design strength parameters. The addition of Portland cement represents a significant cost component, particularly in mixes that contain 10% cement by weight (Thomas, 1973). Additionally, the hydration of the cement may cause cracking to occur within the fill when it dries, thus weakening it.

In addition to cohesion, the maximum compressive strength of backfill containing binders is also influenced by the following factors:

1. Particle size and the mineral composition.
2. The distribution and distance between the particles.
3. The water-to-solid ratio.

Squelch (1993) developed a methodology for the selection of backfill for use in the face area. This is shown as the flow chart in Figure 2-20.

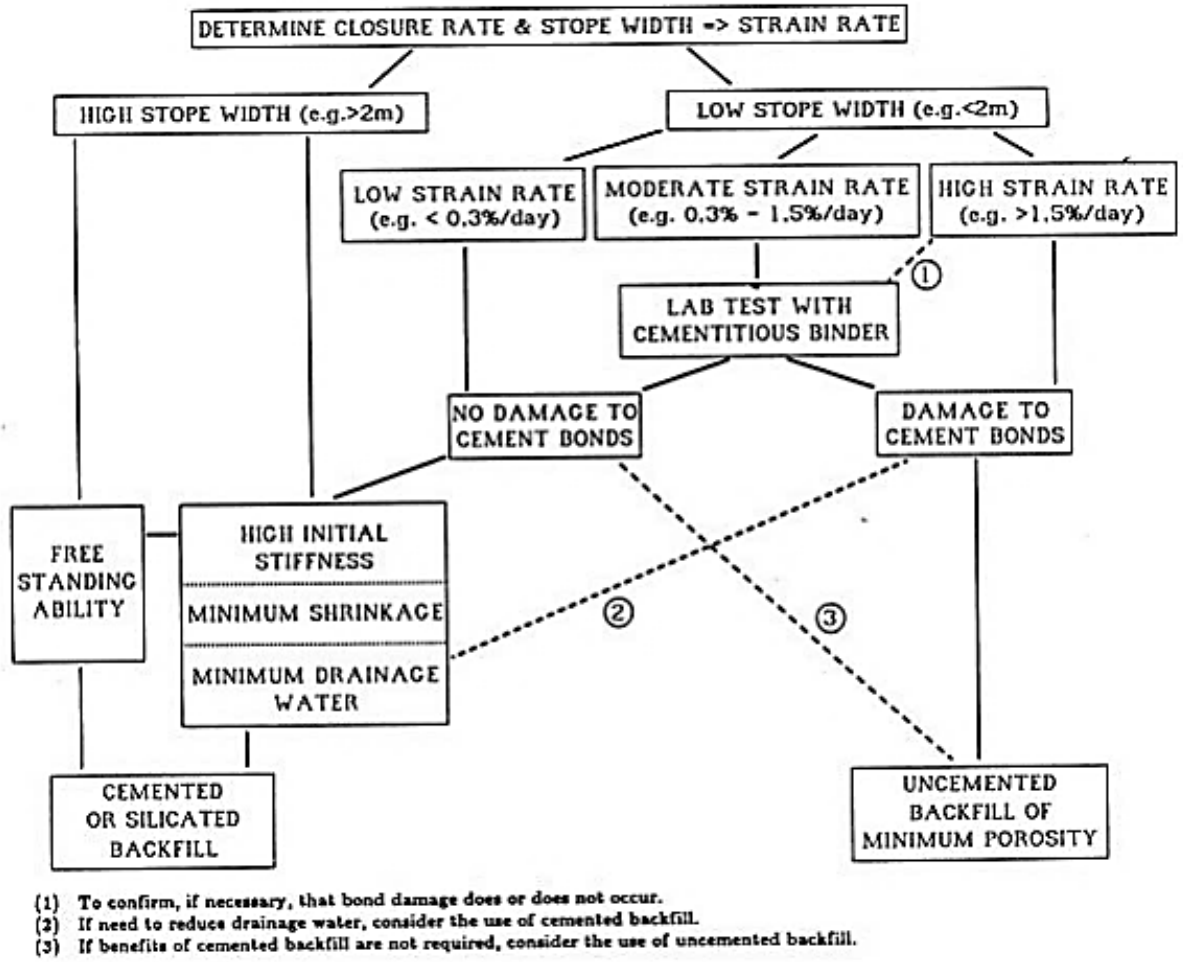

Figure 2-20. Selection criteria of suitable backfill for local support (after Squelch, 1993).

2.4.2. Backfilling procedure

For hard rock bord and pillar layouts, the best sequence of placing backfill is not clear. Backfilling practices differ across the mining industry depending on the commodity that is mined and are affected by the geological features that are present in the rock mass as well as the mining method that is employed. The three steps that are always involved in the backfilling process are (Yu et al., 2021):

1. Producing a slurry by batch processing tailings, cement, and water.
2. Transporting the slurry to the mining areas through a pumping system.
3. Curing the slurry for a pre-determined period to produce the desired backfill strength.

During the third step, the fill develops friction and cohesive properties. Thereafter, the stress conditions near the rock – backfill boundary could cause shear or tensile failure of the boundary, or

create a fracture zone nearby, which may result in safety concerns for any openings near the backfilled stope as well as the creation of new paths for fluids to flow through the rock (Yu et al., 2021). The strength and mechanical behaviour of the rock – backfill interface are influenced by the backfill's viscosity and backfilling rate, excavation surface properties such as strength and roughness, and environmental conditions during curing (Yu et al., 2021).

For a successful backfill system, the working area support that is used in conjunction with backfill must be integrated into the placement cycle requirements. This involves the spacing and timing of installation. Parameters that are vital for the successful integration in the conventional gold mines are (Jager and Ryder, 1999):

1. The minimum and maximum distances between the backfill and the working face. Mining cycles should be designed to ensure that the distance between the backfill and the stope face is below 6 m.
2. The average face advance per blast that is achieved in the area of interest.
3. Deciding whether backfill will be placed after each blast, or after every second blast.

The maximum distance will define the required number of rows of support to be used, and the third parameter, along with the stoping width, determines the size and width of the fill bag. For low to moderately high stoping widths, placing backfill in geotextile bags is preferred. Paddocks are appropriate for high stoping widths, as well as for large areas that need to be backfilled (Jager and Ryder, 1999).

For operations that desire to extract historical pillars, it is critical for the backfill in the extracted stopes to be completely cured to ensure that the rock mass will remain stable with little to no surface subsidence (Yu et al., 2021).

2.4.3. Backfilling in the gold mining industry

South Africa generates roughly 70% of its waste per annum through mining activities, with a large portion being stored in tailings dams. Waste generated by the gold mining industry alone accounts for two-thirds of this waste (Gcasamba et al., 2019). Backfilling practices have a long history in the Witwatersrand Basin, having been applied sporadically from the 1890s to the early 1950s, mainly with hand-packed waste and sand to reduce stope closure, the associated energy release rates (ERR) and to minimise the risk of rockbursts (Jager and Ryder, 1999). Backfill was employed in the gold mining industry for the following reasons (Stradling, 1988):

1. Regional support to reduce the requirements for stabilising pillars.
2. To reduce timber requirements in the stopes.

3. Strata control by reducing accidents and production losses caused by rockbursts.
4. Environmental control by reducing ventilation and refrigeration costs.

During the early decades of the 20th century, mining layouts in the South African gold industry mostly used decline shafts to access the reef, while employing the scattered mining method and the use of pillars and sand fill (Jooste and Malan, 2015). The method was successful in shallow mining areas; however, rockbursts caused by remnants at deeper levels became a major problem during the 1940s.

A typical backfill paddock in one of the deep tabular stopes is illustrated in Figure 2-21. This is illustrated here to highlight the potential difficulties of trying to implement this in bord and pillar operations. The closure compressed the backfill and the outward displacement broke the elongates used to construct the paddock. The aim of the backfill application shown is to reduce the stope closure normal to the plane of the reef and reduce the energy release rates of these stopes. Most historic studies of backfill in the tabular gold mine stopes therefore focussed on the reef normal closure and the stress being generated in this direction. The method of construction of the paddock is shown in Figure 2-22.

Figure 2-21. A backfill paddock in a deep tabular gold mine (courtesy of D. F. Malan).

Figure 2-22. A backfill paddock before it is filled with backfill (courtesy of D. F. Malan).

Interest in the use of backfill in South African gold mines was renewed in the 1970's following the sharp increase in the price of timber and a labour shortage (Stradling, 1988). Mines considered the various advantages that the use of backfill in the Witwatersrand Basin presented. Some of these advantages are (Rankine et al., 2007):

1. Reduced damage caused in stopes by rockbursts as the vertical stress was no longer solely applied onto the pillars.
2. Helped to reduce the effective stoping width and improve the stope face's stability when used along with adequate temporary support.
3. Improved stability of the gullies and travelling ways.
4. Increased the overall extraction by enabling operations to reduce stabilising pillar size.
5. Reduced the labour required to install support.
6. Reduced fire hazards underground by reducing the amount of timber support.
7. Minimised groundwater contamination when binders were used as the backfill was subjected to chemical and physical characteristic changes.
8. Reduced ventilation and cooling costs by limiting the amount of heat entering the workings (less exposed rock surface).

There were, however, disadvantages associated with backfilling practices including (Rankine et al., 2007):

1. High costs, particularly if binders are used.
2. Risk of the tailings liquefying if high saturation levels and a trigger, such as seismic vibration, are present.
3. Possibility of tailings seeping into groundwater and the resulting contamination.
4. Ore dilution from poor backfill placement or extraction management.

Squelch (1990) investigated to assess the potential of backfill to positively impact the stability of stope hangingwalls. This was achieved by obtaining in-situ stress measurements at varying depths into the hangingwall for both unfilled and backfilled stopes (Squelch et al., 2001). The results are shown in Figure 2-23 and Figure 2-24, respectively.

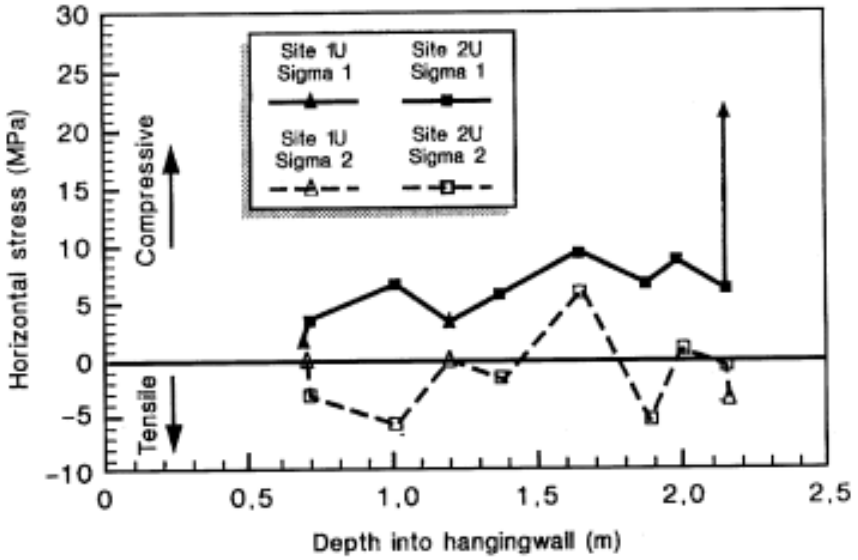

Figure 2-23. Stresses measured in the hangingwall of unfilled stopes (after Squelch et al., 2001).

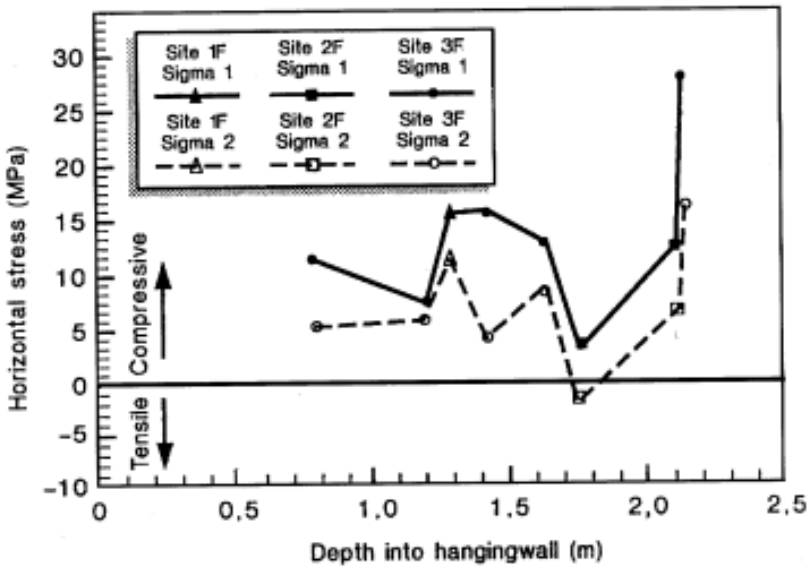

Figure 2-24. Stresses measured in the hangingwall of backfilled stopes (after Squelch et al., 2001).

The concept of ERR was introduced by Cook et al. (1966) in his research regarding rockbursts in South African gold mines. ERR is a measure of stress concentration ahead of a stope face that accounts for the effect of depth and stope geometry, and it is related to the convergence that occurs in the stopes. Studies have indicated that it is best to mine with as small an ERR value as possible and the only way to achieve this is by reducing the stresses or by reducing the closure in the stopes. As reducing stresses underground is not possible without reducing the extraction ratio, the mines implemented backfilling in hopes that it would reduce the magnitude of closure.

Piper and Ryder (1988) studied the effect of backfill as regional support by using numerical modelling. MINSIM-D was used to model an area of 1280 m × 1280 m at depths ranging from 2 to 5 km to determine the ERR values without any backfill. Thereafter, backfill was placed across 20, 40, and 80% of the mined area to determine how the quantity of fill influences the ERR values for each depth (Squelch et al., 2001). Figure 2-25 illustrates the modelling results and indicates that the ERR is greatly reduced with the higher percentage of fill when a good quality fill is used. The a and b parameters define the quality of backfill with typical values of 5 MPa and 0.3, respectively, for a good quality fill material (Squelch et al., 2001).

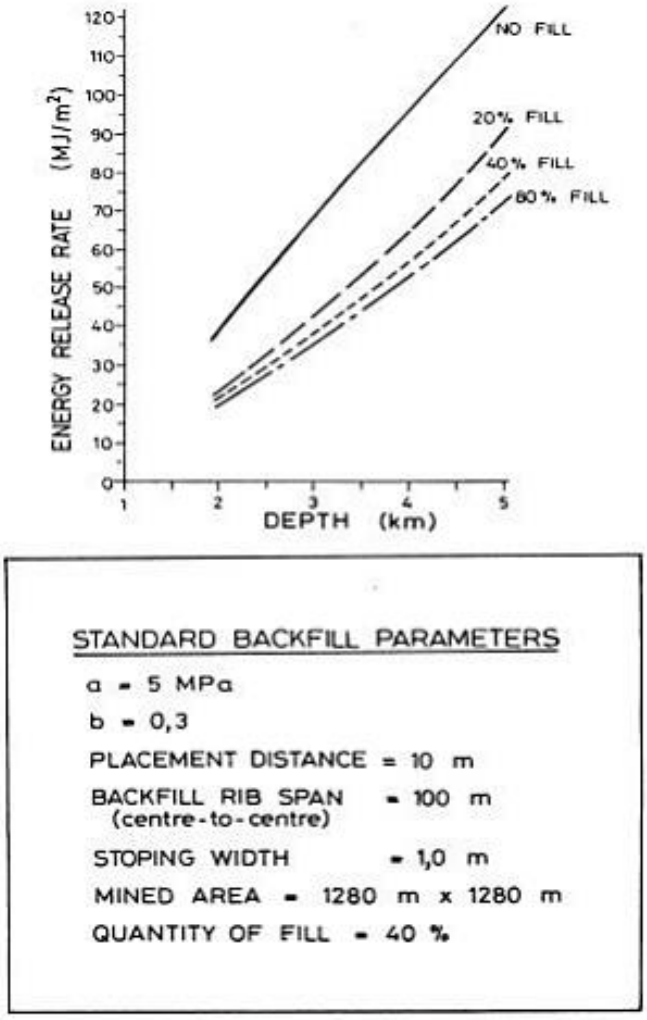

Figure 2-25. Backfill's influence on ERR values (after Piper and Ryder, 1988).

Site investigations were carried out at Tau Tona by Squelch et al. (2001). The mine, which adopted a strike stabilising pillar layout, used pre-stressed elongates, spaced 1.6 m on strike and 1 m on dip, along with backfill placed between the rows of elongates for support. The use of backfill resulted in a reduction of approximately 50% in pillar stress (Squelch et al., 2001). Figure 2-26 summarises the initial and final simulated vertical stress profiles along the stabilising pillar for both filled and unfilled areas. Figure 2-27 shows the simulated vertical stress as a function of face advance at a fixed point with and without backfill.

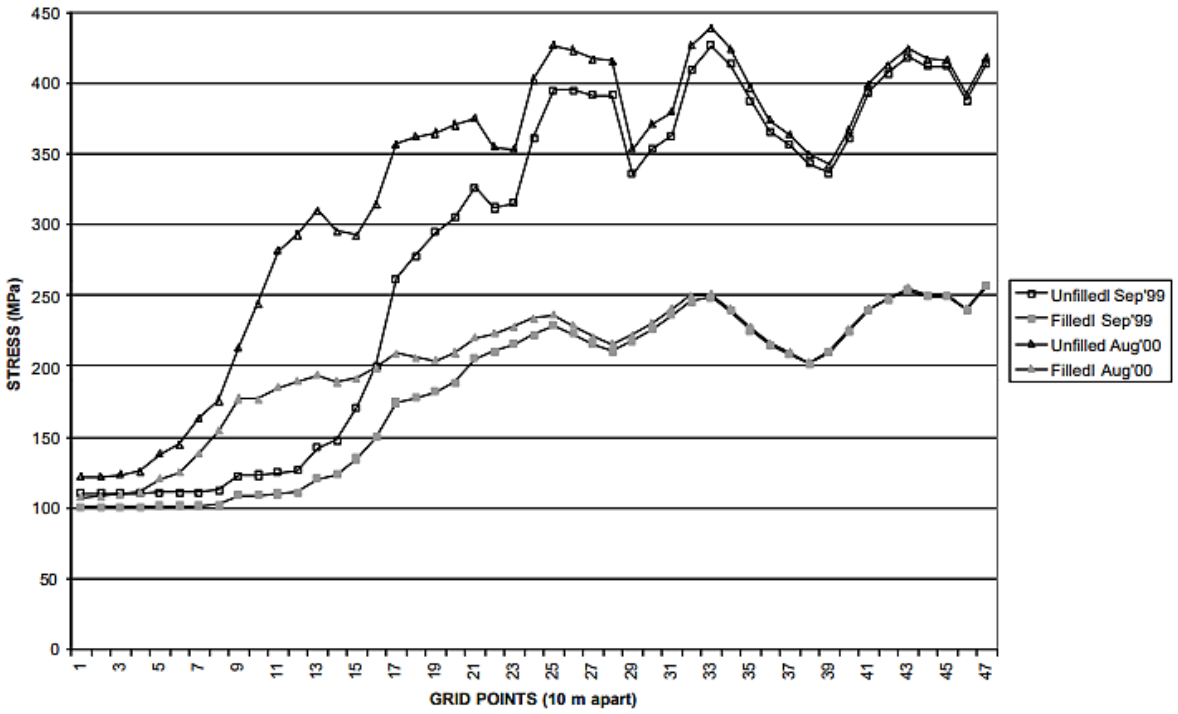

Figure 2-26. Initial and final simulated vertical pillar stress profiles with and without backfill (after Squelch et al., 2001).

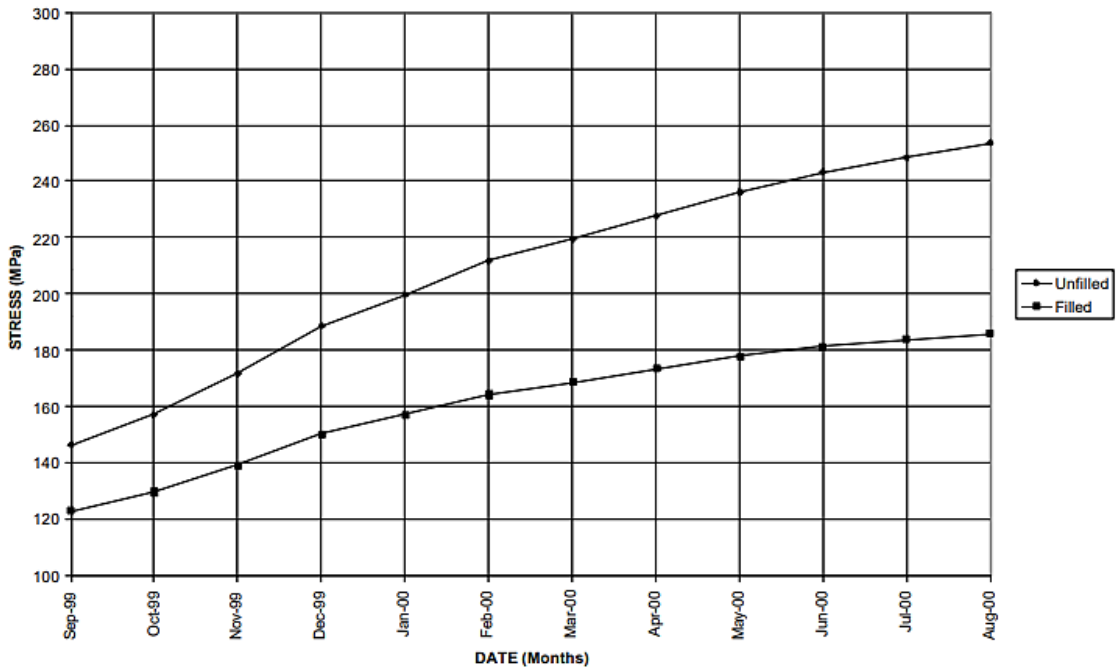

Figure 2-27. Simulated vertical pillar stress at a fixed position with increasing monthly face advance for filled and unfilled cases (after Squelch et al., 2001).

This section discussed the use of backfill material in the South African gold mining industry. Based on these considerations, backfilling was beneficial to the gold mines. None of these benefits are related to the shallow hard rock bord and pillar operations, however, and the potential benefits will need to be studied in a different mining sector. The coal mining industry has used backfill extensively and this is described in below.

2.4.4. Backfilling in coal mines

Coal mines, particularly in China and in Europe, have made use of backfill for several years. This section will highlight how some operations have successfully implemented backfilling as well as how it has affected pillar strength and the stability underground. Figure 2-28 illustrates some of the systems used in coal mines to place the backfill. These methods are beyond the scope of this study, which only focuses on the rock engineering aspects, and specifically the effect of backfill confinement on pillar strength.

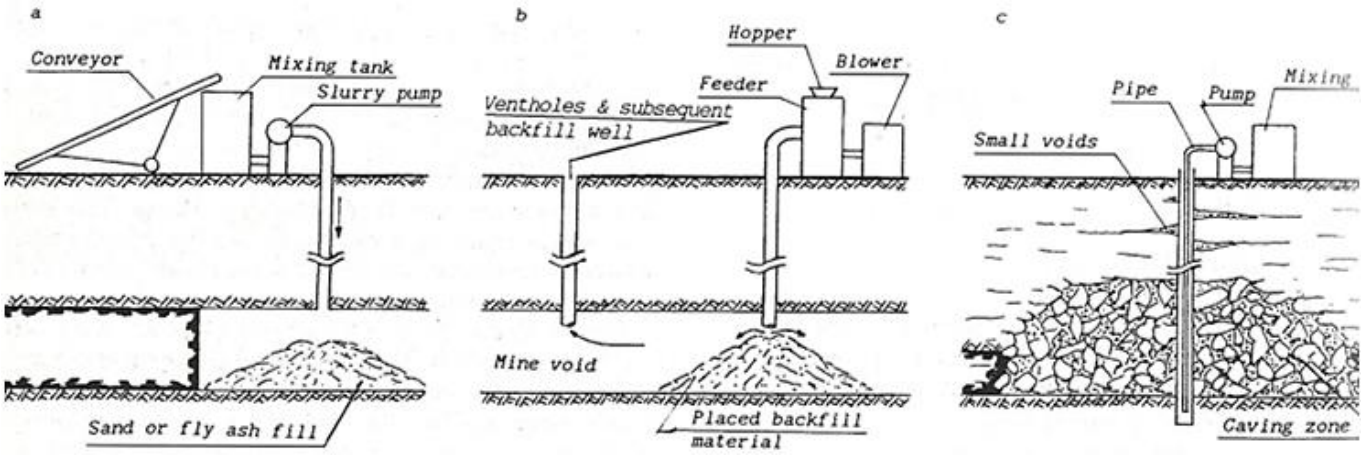

Figure 2-28. Different systems to use backfill in coal mines: a) Pumped slurry; b) Pneumatic filling; c) Grout injection (after Palarski, 1993).

In South African collieries, backfilling practices were considered as a way of stabilising bord and pillar layouts and to achieve higher recovery by increasing pillar height in thick seam conditions (Mo et al., 2018). Mo et al. (2018) used FLAC2D modelling to quantify the effect of backfilling on pillar strength in highwall mining. The simulated behaviour of pillars varies with the type and percentage of backfill placed as well as the pillar width to height ratio. For cohesive backfill, 75% backfilling results in a significant increase in peak pillar strength, especially for the pillars having lower width to height ratios. For non-cohesive backfill, the effect of the backfill is less pronounced.

The Illinois Basin is a major contributor to the coal industry in the United States of America, where close to 100 000 short tons of coal were produced in 2013. The total mineable reserves are estimated at 14.4 billion tons (Kostecki and Spearing, 2015). Most underground operations in the Basin's major mineable coal seams possess a weak immediate floor, called underclay, that is variable in nature and highly friable. Generally, the instability concerns, including pillar punching, loss of entry and pillar sloughing in the short-term and roof subsidence in the long-term, are mitigated by oversized pillars (Kostecki and Spearing, 2015). However, these reduce the extraction ratios in bord and pillar mines significantly, leading to a lower profit.

Currently, the use of backfill is not widely practiced in American coal mines. The low permeability and low water content of paste backfill reduce the likelihood of water egress to the surrounding strata significantly, while its strength makes it possible for it to be used as long-term mine support by reinforcing the mine floor as well as the pillars. The main objective of the investigation conducted by Benton (2013) was to determine the effective usage of paste backfill in a bord and pillar coal mine to determine whether an increase extraction is possible. Data from three bord and pillar collieries in the Illinois Basin were collected. LaModel and Phase2 were used to model conventional mining stresses with additional stresses induced by higher extraction rates.

Two other studies relating directly to the use of backfill to improve extraction in underground coal mines were also conducted. The first, conducted in 1998, revealed that completely backfilling every underground opening was not necessary to achieve a greater coal extraction rate. Partial backfilling was found to be more cost effective, but it could potentially interfere with ventilation (Hume and Searle, 1998). In 2001, an investigation into the ability of backfill to improve recovery in thin-seam collieries was conducted. The study found that increased extraction was possible due to the passive confinement that the fill applies to pillars (Donovan and Karfakis, 2001). The potential of increased extraction was shown to increase with mining depth, with a minimum depth of 650 feet (198 m) required for profitability. Owing to the initial extraction rates being as low as 40%, any improvement was deemed beneficial at this depth.

The performance of pillars is typically estimated by calculating a S_F in mines with rigid floors, however, as mentioned earlier, the mines in the Illinois Basin are underlain by weak strata. The S_F estimations therefore fail because they do not adequately account for the underclay below the pillars. Backfill may be a better alternative to the use of larger pillars as it provides passive resistance and apply confinement to the mine floor while strengthening the pillars by lateral confinement (Hu et al., 2001).

The numerical modelling results obtained by Benton (2013) revealed that the stress changes, as each panel was developed, were smaller than anticipated due to the shallow depths of the mines.

The author therefore concluded that reductions in pillar size are theoretically possible without having to sacrifice mine stability.

Another numerical investigation was conducted by Kotsecki and Spearing (2015) to simulate the effect of high density backfill on pillar and floor stability. In the study, it was found that minimising the distance between neighbouring pillars leads to an improvement in the pillars' ultimate bearing capacity. However, if they are placed too close to one another, the structures may behave as a single pillar and undergo an increase in the settlement of the overburden strata (Kostecki and Spearing, 2015).The study found that a 10 to 40% increase in pillar strength and ultimate bearing capacity is likely when cohesive material is used with between 25 and 75% of the mined height being fill, respectively. The study did not account for non-uniform loading across the pillars to produce a more conservative model. Figure 2-29 shows an example of the simulated pillars at 25% fill where R_w represents half of the total bord width and P_w is the pillar width (Kostecki and Spearing, 2015).

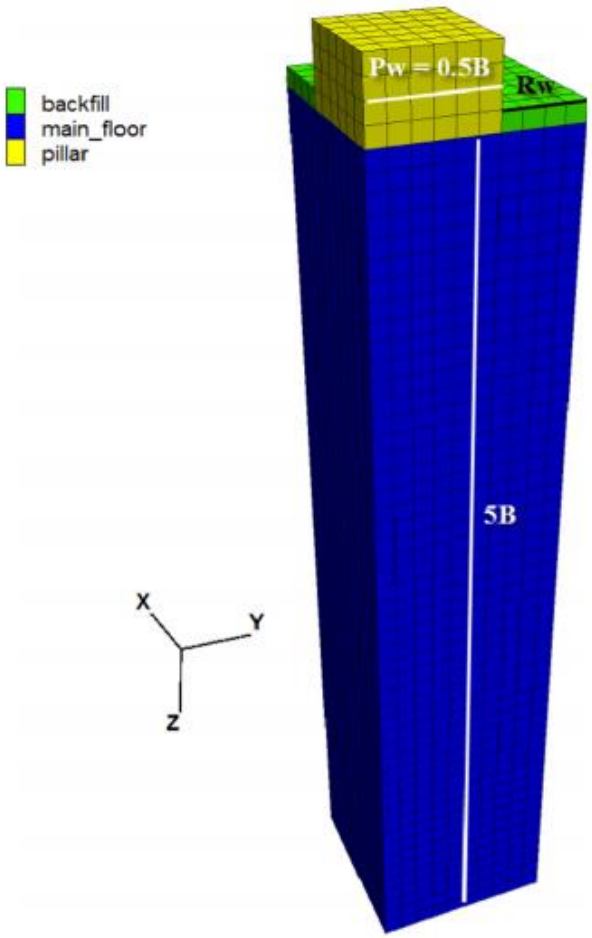

Figure 2-29. An example of the generated grid with 25% fill (after Kostecki and Spearing, 2015).

The simulations were performed using non-cohesive backfill and demonstrated that the backfill had little influence on pillar strength, even with higher fill ratios, since the fill material's tensile strength, shearing resistance and stiffness were low (Kostecki and Spearing, 2015).

During the 19th and 20th centuries, bord and pillar mining was introduced in numerous Australian mines in the Ipswich and Newcastle areas. In recent years, many of these operations have been abandoned due to accelerating urban development and the risk of potential mine collapses and subsidence (Shen et al., 2017). Additionally, several sinkholes have developed in these areas in the last 20 years, leading to economic, social, as well as political concerns among residents and the government. To minimise the possibility of mine subsidence and sinkholes, mine rehabilitation is essential.

With the rehabilitation of abandoned mines, several challenges are encountered. The environmental impact of all the proposed new measures must be considered. When backfilling, the material that is used as the fill will likely interact with groundwater in future, potentially leading to chemical leaching (Shen et al., 2017). A careful assessment of the effects of chemical leaching was conducted to prevent the contamination of groundwater and surface water supplies, particularly in residential areas.

CSIRO conducted a study on backfill technology that uses a mixture of fly ash and mine water as the base backfill material at an 8:10 ratio, without cement or any adhesive agents (Jiang et al., 2017). This technology presents a more economically viable option for backfilling practices in mining operations in comparison to cemented backfill. Additionally, the fly ash technology is easy to operate, environmentally friendly, and provides sufficient strength to support pillars (Shen et al., 2017). A numerical investigation was conducted to explore the effect of backfill on the strength of pillars in a typical bord and pillar mine when using non-cohesive fly ash material. It was expected that it would have the following benefits (Shen et al., 2017):

1. Increase pillar strength and reduce the rate of strength degradation resulting from environmental exposure.
2. Change the post-peak behaviour of pillars from the rapid reduction of strength to hardening so that they will maintain the ability to support substantial loads after yielding has occurred.
3. Reduce roadway void space, thus significantly reducing the magnitude of surface subsidence from potential panel failure.

To approximate pillar strength, the model was configured using FLAC3D to simulate a single pillar using symmetry and monitor the APS (Shen et al., 2017). This is depicted in Figure 2-30.

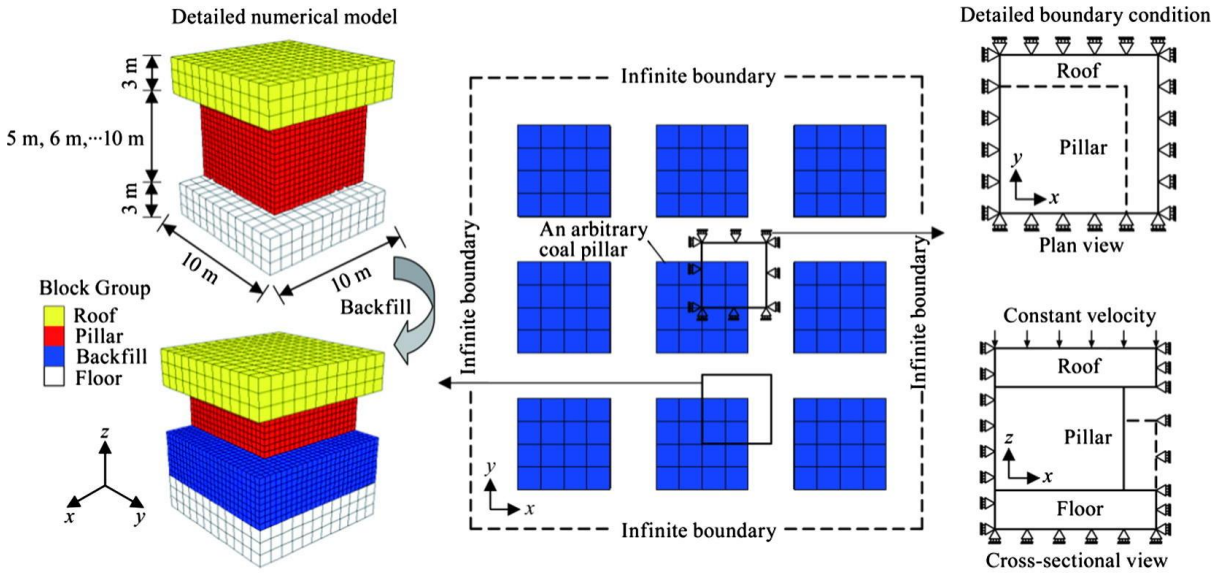

Figure 2-30. A model of a single pillar to examine the improvement of pillar strength when using backfill (after Shen et al., 2017).

To quantify the effect of backfill on pillar strength, 60 models were studied for square pillars with a width of 20 m, mining heights between 5 and 10 m (equivalent to a w/h ratio of 2 to 4), and percentage of backfill ranging between 0 and 100% (Shen et al., 2017). The predicted strength increases for a 7 m high pillar are shown below.

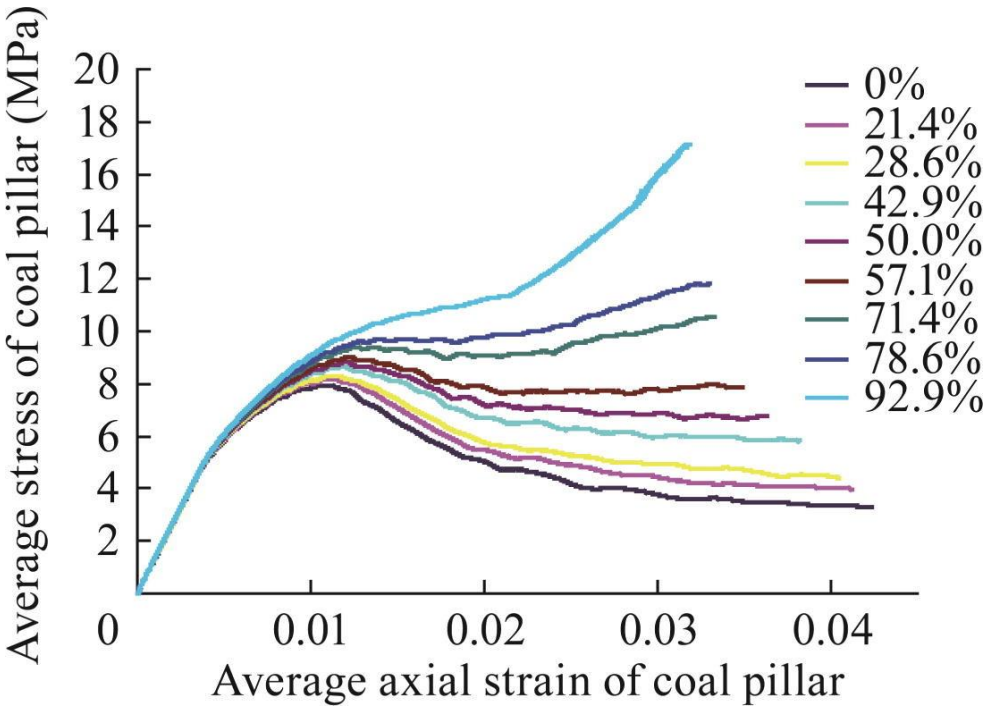

Figure 2-31. Increase in pillar strength for various backfill percentages (after Shen et al., 2017).

For the backfill percentages below 71.4%, the APS reaches a peak and then decreases thereafter until it plateaus. However, when a percentage of 71.4% or higher is used, the pillar strength continues to increase. Particularly, when 90% backfill is used, the pillar strength is predicted to increase by more than 60%.

Wang et al. (2011) studied the influence of roadway backfill on the stability of coal pillars by numerical analysis using the FLAC3D numerical code. A formula resulting from a combination of the South African and Australian databases was employed to calibrate the model and for the analysis of the pillar stability. The relationship between the strength of the coal pillars and the percentage of applied roadway backfill was studied. To quantify the influence of fill on pillar strength, 120 numerical models with varying pillar heights and backfill percentages were analysed. Two different types of backfill were examined, namely a cohesive backfill with a UCS of 1 MPa and a non-cohesive backfill with a friction angle of 42°. Half of the models used cohesive backfill and the remaining 60 were for non-cohesive backfill. The specifications for the models were a 20 m pillar width, a mining height between 5 and 10 m, and the percentage of backfill between 0 to 90%. A pillar with a mining height of 10 m is therefore equivalent to a w/h ratio of 2 and a pillar with a height of 5 m corresponds to a w/h ratio of 4.

The relationship between roadway backfill and pillar strength is presented in Figure 2-32 for both fill types. The results indicate that the strength will increase as the percentage of backfill increases in both cases, with the percentage of increase in pillar strength being higher for the slender pillars. From the figure, with 80% cohesive backfill, the numerical model predicts that a pillar with a w/h ratio of 2 is 97.9%, while a pillar with a w/h ratio of 4 is 45.6% stronger. It is also evident that the effectiveness of the cohesive backfill is greater than the non-cohesive fill (Wang et al., 2011). With the same amount of backfill, a 10 m tall pillar's strength is increased by 27.8% as opposed to 97.9%.

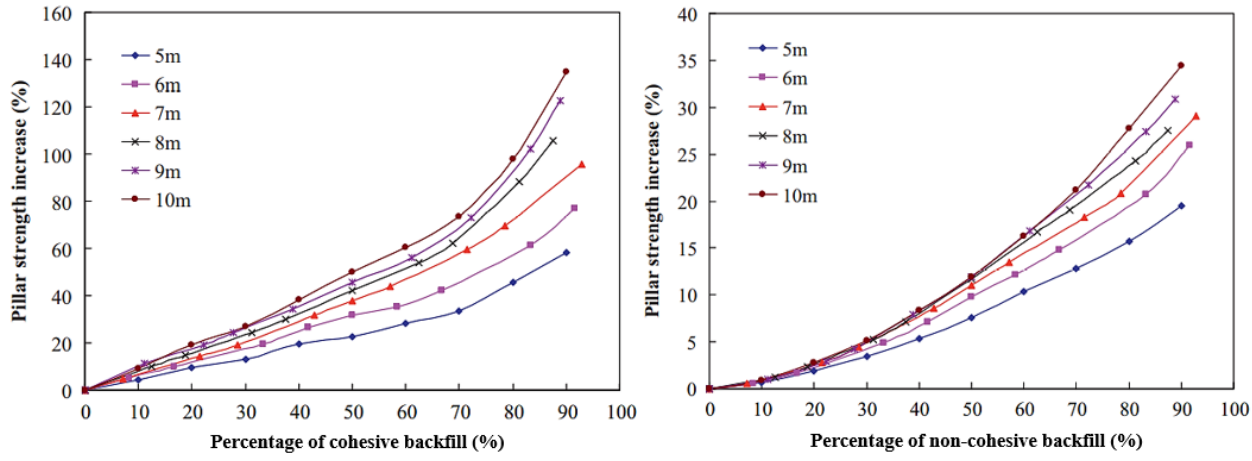

Figure 2-32. Increase in the strength of a pillar against the percentage of cohesive (left) and non-cohesive (right) backfill (%) (after Wang et al., 2011).

From the figure below, it is noted that the pillar strength is less affected by the pillar height when the cohesive backfill is less than 50%. When the fill percentage exceeds 50%, pillar strength increases with pillar height, particularly for the slender pillars. Similarly, when the concentration of non-cohesive backfill is less than between 40 and 50%, the pillar strength increase is constant and increases rapidly once this range is surpassed.

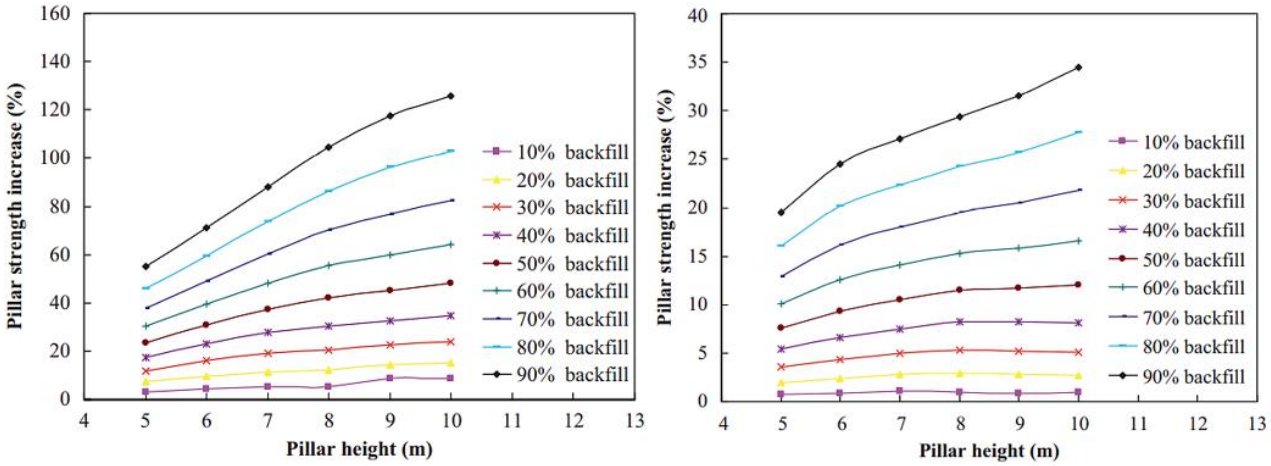

Figure 2-33. Increase in the strength of a pillar as a function of its height for cohesive (left) and non-cohesive (right) backfill (%) (after Wang et al., 2011).

Numerous studies on backfill have been conducted in the ecologically fragile western areas of China, namely Inner Mongolia, Shaanxi, and Ningxia (Sun et al., 2018). The coal resources in these areas are of a high quality and constitute over 85% of the country's total coal deposits. Most coal mines in the western areas employ the bord and pillar mining method and based on recent studies, the pillars that remain subjected to long-term loading are subjected to a reduction in strength (Sun et al., 2018).

Cemented paste backfill (CPB) technology, has been used extensively in Chinese underground operations. It is both economically and environmentally beneficial as it provides support and facilitates waste disposal (Sun et al., 2018). The typical materials that are used as the base for the backfill mixtures, namely tailings and gangue material, are scarce in the western region because of its unique geological conditions. This limits the application of backfill practices because of the related high costs.

Qishan Coal Mine is located between the southern border of Muus Desert and the northern Shaanxi Province, China. Aeolian sand, which is very fine, is widespread on the mine's surface area. Owing to continuous mining in recent years, only the north panel resource had minable coal remaining and the mine had less than 6 million tons of reserves left at the time of this study. Additionally, an in-depth investigation was conducted that revealed that some of the pillars that

were left underground were unstable in the early mining stage and failed when subjected to long-term loading (Sun et al., 2018).

In this study, a CPB mining method was proposed to recover strip coal pillars. Because of its abundance in the local area, aeolian sand was selected as the backfill material for this experiment. For the CPB test samples, fly ash (FA) from a local coal mine in the Shaanxi province, and Portland cement (P.C. 42.5) were used as binders. Nine experiments were conducted with varying aeolian sand, FA, P.C. 42.5, W/C ratio proportions, and curing times (Sun et al., 2018).

With the curing time increasing to the maximum value of 28 days, the UCS, tensile strength, and cohesion increased. The curing conditions had a minimal influence on the backfill's internal friction angle, however (Sun et al., 2018).

For the numerical modelling, FLAC3D was used. The model assumed a length of 125 m, a width of 101 m, and a height of 170 m as shown in Figure 2-34 (a). These values are based on the geological conditions of the mine's panel 73806.

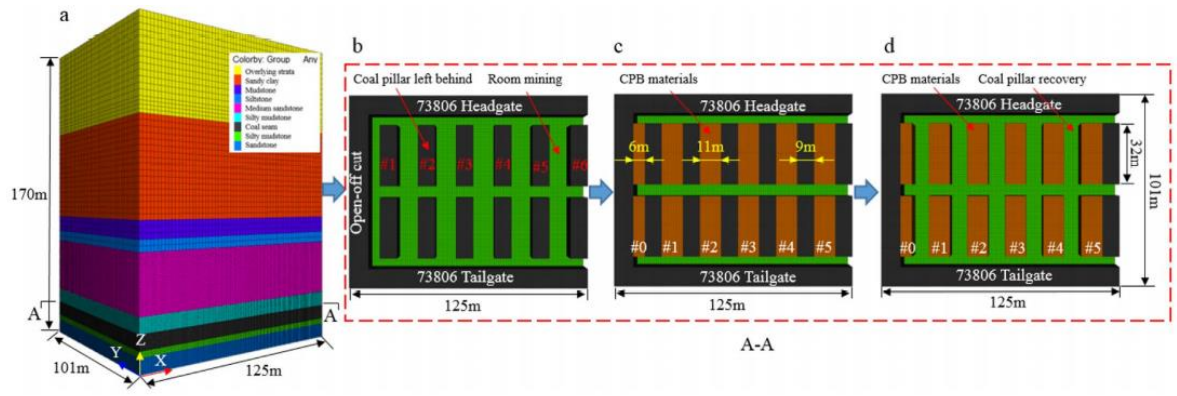

Figure 2-34. Numerical simulation model and modelling process (after Sun et al., 2018).

Figure 2-35 below illustrates the stress field distribution that occurred after extracting the coal pillars. The figure shows that in comparison to #7, the strength of the #2 and #8 CPB materials is small at approximately 2.2 MPa and 2.8 MPa, respectively. The stresses of the surrounding coal and rock are therefore larger at 14.1 MPa and 12.5 MPa, respectively, in the dip direction, and 16.0 MPa and 14.2 MPa in the strike direction, respectively (Sun et al., 2018).

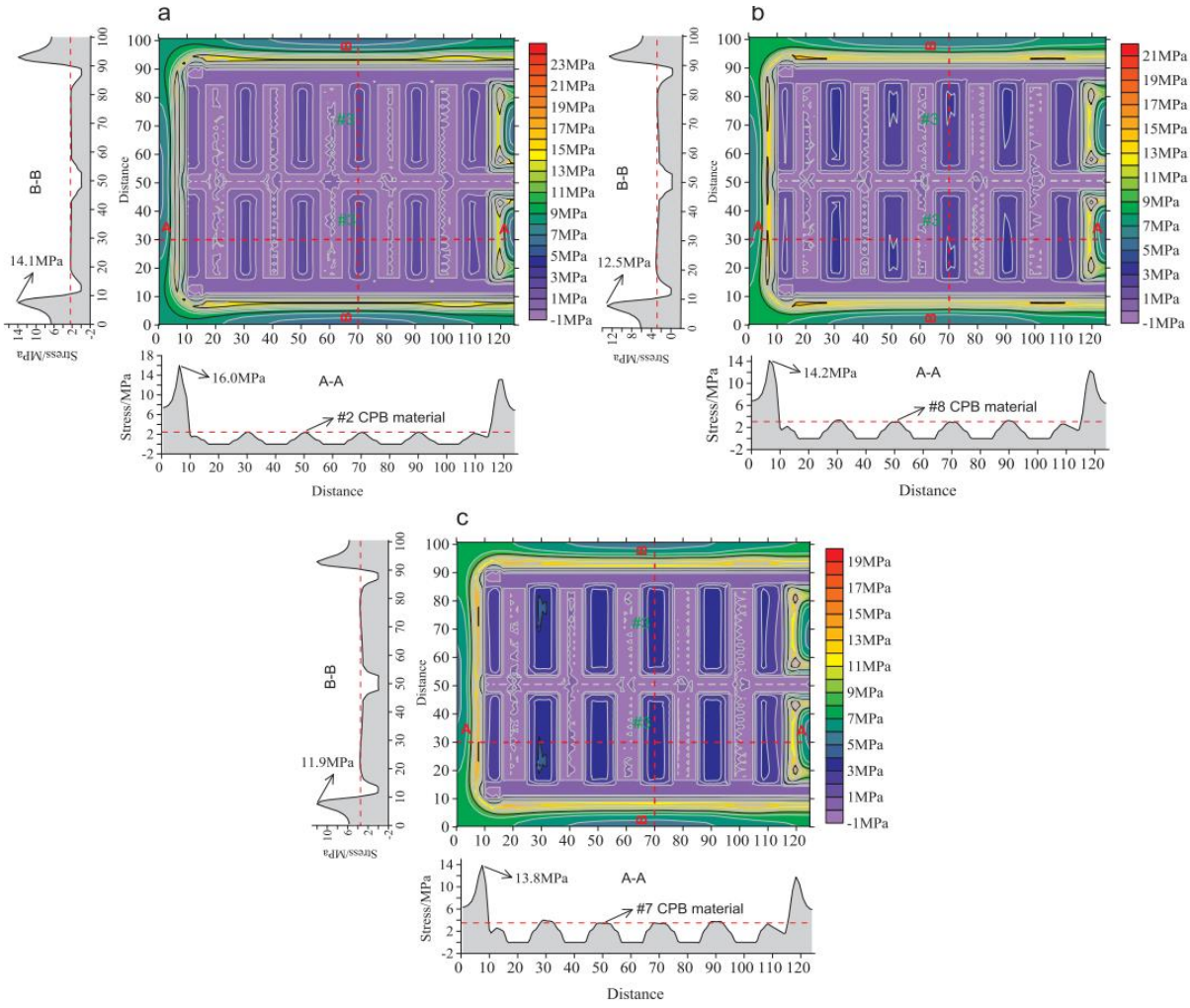

Figure 2-35. Stress distribution following short-strip backfill coal mining (after Sun et al., 2018).

After the mechanical properties of aeolian sand-based cemented fill materials were tested with different proportions, the study revealed that the #7 CPB material can meet the design requirements for the safe recovery of coal pillars while ensuring the protection of water resources.

2.4.5. Backfilling in hard rock bord and pillar layouts

Compared to coal mines, only a few examples are known of the use of backfill in hard rock bord and pillar mines. These examples are included to highlight the potential benefit of backfill in bord and pillar mines and that is pillar reclamation. A well-known example is given below.

Buick Mine is a lead, copper, and zinc bord and pillar mine located 195 km southwest of St. Louis, Missouri. The mine is divided into two sections, namely the North Mine and the South Mine. The former has the highest grade of ore, however, most of the resources exist as support pillars in the

South Mine (Tesarik et al., 1995). A study was conducted in an instrumented portion of the mine to investigate whether the support pillars that remained after primary extraction could be extracted safely. The study began in 1991 and involved the use of CRF as backfill to provide stability and for optimum pillar recovery.

Regardless of the use of CRF, a mine's pillar extraction practices must ensure the following rock mechanics criteria are met (Zur and Apel, 2004):

1. Domino pillar collapse must not occur.
2. The work area must be kept safe for personnel during extraction.
3. Clear back spans resulting from pillar extraction must be less than 46 m – back instability occurs when spans exceed this.
4. The stability of the critical mine areas must not be affected.

A section known as "Area 5" was the first section where backfill was implemented at the operation. The section was selected because of the surrounding barrier pillars that could arrest cascading pillar failure in case it occurred during the trial mining (Tesarik et al., 2009). These pillars measured approximately 8 to 12 m wide per side and 18 m high. The entire backfilled area measured 88 m × 37 m and the bords were approximately 9.8 m wide. Figure 2-36 presents a plan view of Area 5.

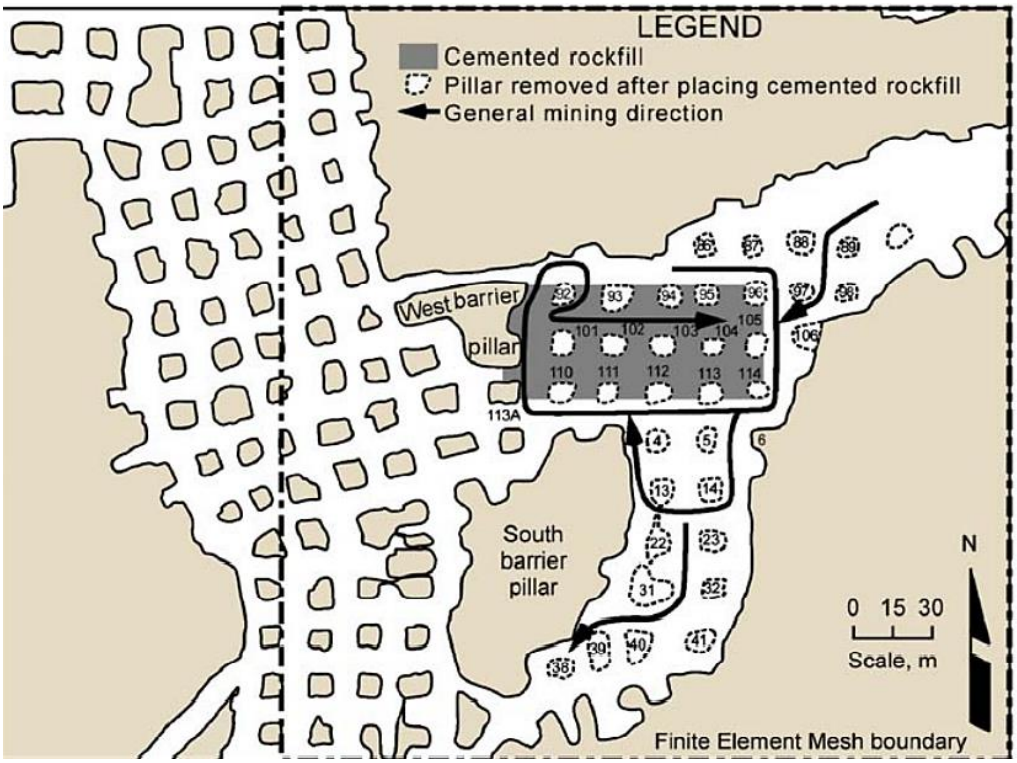

Figure 2-36. A plan view of Area 5 (after Tesarik et al., 2009).

Table 2-2 shows the planned mining sequence. From the table, the duration of the pillar extraction study in Area 5 amounted to just under six years.

Table 2-2. The sequence of pillar extraction (after Tesarik et al., 2009).

Pillar	Day
97, East half	0
96	17
87, South half	17
97, West half	17
95	52
86, South half	52
94	59
105	85
106	85
114	101
5, North half	123
113, Bottom 12.5 m	123
6, West 3.7 m	123
113, Top 4.3 m	127
5, South half	177
14, North half	177
112	192
4, North half	192
4, South half	199
13, North half	199
111	212
110	212
93	221
92	233
101	389
102, 7 Holes	444
102, 20 Holes	451
104	515
103	695
23	1974
22	1984
32	2000
31	2010
41	2048
40	2109
38	2179
39	2181

The CRF was transported to Area 5 using a conveyor and spread in 0.3 m to 0.6 m lifts using wheeled dozers. To contain the backfill as the lifts were placed, a steel-reinforced shotcrete fence was assembled between the perimeter pillars from the floor to the roof of the mine (Tesarik et al., 2009). One of the completed fences is shown in Figure 2-37.

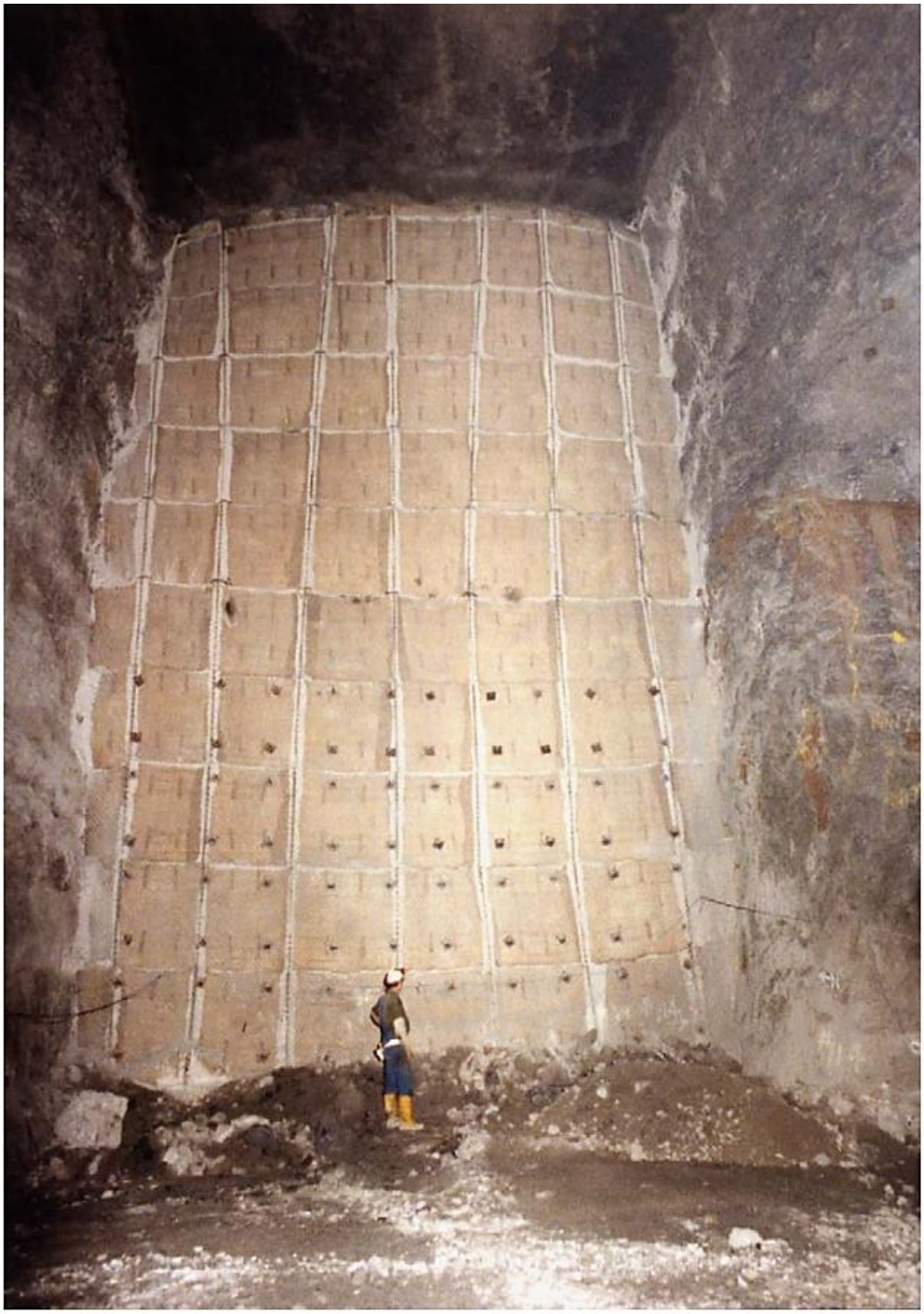

Figure 2-37. A steel-reinforced shotcrete fill fence (after Tesarik et al., 2009).

Geotechnical instruments are required to monitor and quantitatively evaluate the stability of backfilled areas to ensure that the appropriate actions can be taken to address stability concerns (Tesarik et al., 2009). The borehole extensometers that were installed in the test section were used to monitor short- and long-term stability, record the redistribution of stresses to pillars during mining, and to provide input to develop a numerical model. The data from the instruments that

were left in Area 5 after the pillars were mined out provided data for an additional 14 years and was used to record the long-term stability. The backfill remained stable for 16 years after the pillar extraction.

The “trapped pillars” were excavated using an access drift in the footwall. According to Tesarik et al. (2009), since 1991, 12.7 million tons of pillar ore had been mined at Doe Run’s six mines, while 5.4 million tons of CRF were used. The pillar extraction accounted for 26% of the annual rock mining. These mined pillars were large, and the method worked. However, this is not deemed a feasible method for the mines in the Bushveld Complex as the pillar volumes are much smaller and building the fill fence may be problematic for large areas. Additionally, the trapped pillars cannot be accessed via footwall development.

In terms of South African mines, only a few examples of pillar extraction in bord and pillar layouts are known. None of these extractions were done using backfill, but grout packs were used for pillar extraction and is therefore briefly discussed in this section. Although the focus is on grout packs, it is included as it is expected that a similar benefit may be derived from backfilling operations.

The type of grout packs used for support underground depends on numerous factors, including the packs’ required in-situ load bearing characteristics and space constraints (Van der Spuy, 2021). Figure 2-38 and Figure 2-39 illustrate the type of grout packs that can be found underground. Circular grout packs are typically reinforced by being confined in a steel cage with support poles prior to being filled whereas square-shaped packs generally contain a centrally-mounted support pole (Van der Spuy, 2021).

Figure 2-38. Square grout packs (after Van der Spuy, 2021).

Figure 2-39. Circular grout packs (after Van der Spuy, 2021).

Grout packs are spaced at specified intervals to meet the support resistance requirements and to limit the unsupported spans. The spacing is determined by the operation's stoping standard, which is contingent on the pack size, ground conditions, mining method, and required accessibility for effective cleaning operations (Van der Spuy, 2021). Figure 2-40 shows a typical stope standard for a breast mining operation.

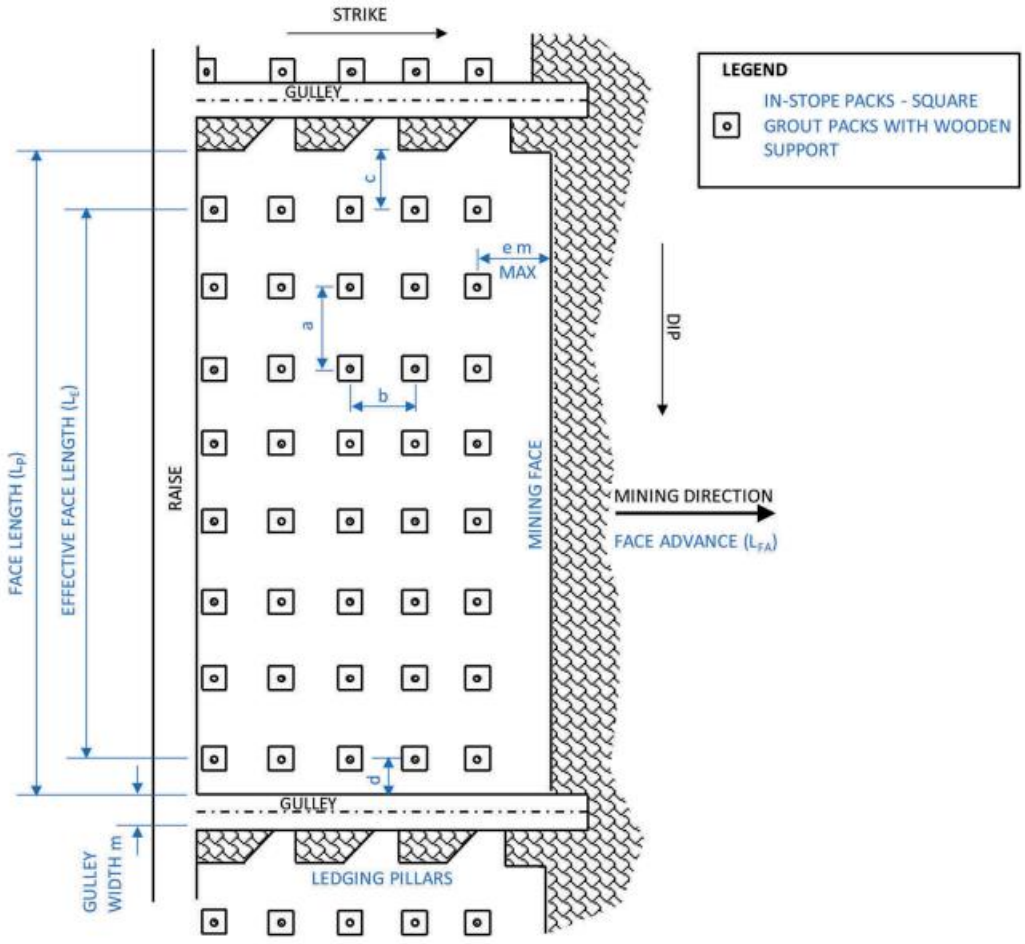

Figure 2-40. A stope standard employed in a breast mining operation (after Van der Spuy, 2021).

One of the gold mining companies in the West Wits Line extracted pillars in a section at one of their operations at a depth of approximately 850 m. A grout plant was not available at the site, resulting in the use of timber or so-called "castle" packs as support in the area of pillar extraction (D. F. Malan 2023, pers. comm.). The load-deformation behaviour of the timber packs resulted in the support system having a low initial stiffness, which led to significant hangingwall deformation.

The support standard for the pillar extraction at this operation is shown in Figure 2-41. There is no information provided regarding the sequence for the installation of support and the pillar extraction thereafter.

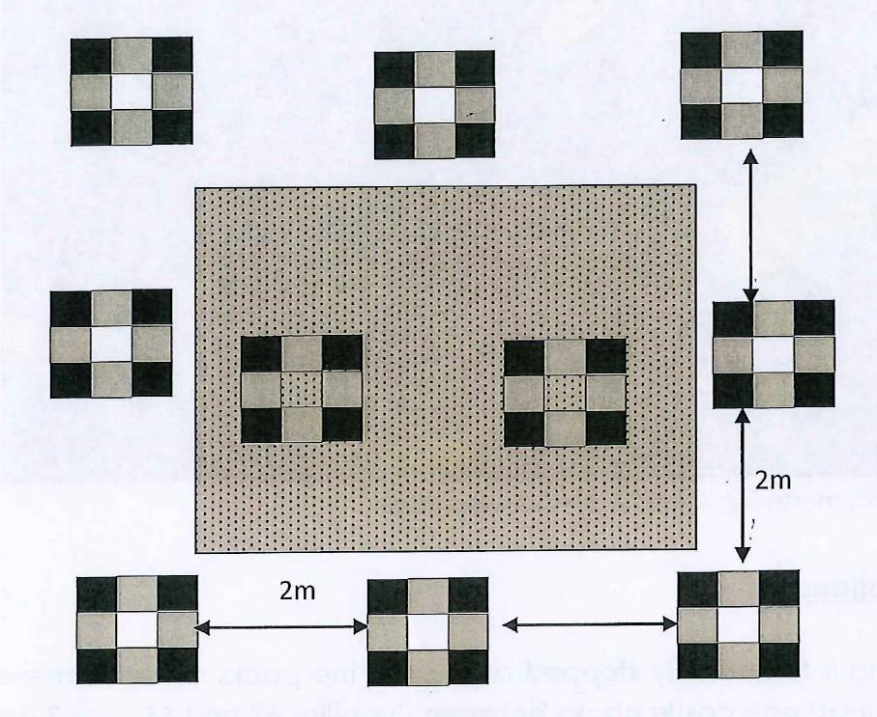

Figure 2-41. Standards applied for the use of castle packs to extract pillars (D. F. Malan 2023, pers. comm.).

The pillars being extracted had to be surrounded by packs as shown in the figure above, but this did not always happen. The photographs below were taken in the section, and a large unsupported span was observed in the area where cleaning operations were carried out. This is concerning from a safety perspective and emphasises the need for a detailed sequence for the placement of the grout packs and the subsequent pillar extraction.

Figure 2-42. Castle packs adjacent to the roadway in the bord and pillar section (D. F. Malan 2023, pers. comm.).

Figure 2-43. Castle packs in the area where pillar extraction is occurring (D. F. Malan 2023, pers. comm.).

Numerical modelling of the area shown in Figure 2-44 was conducted using the TEXAN code.

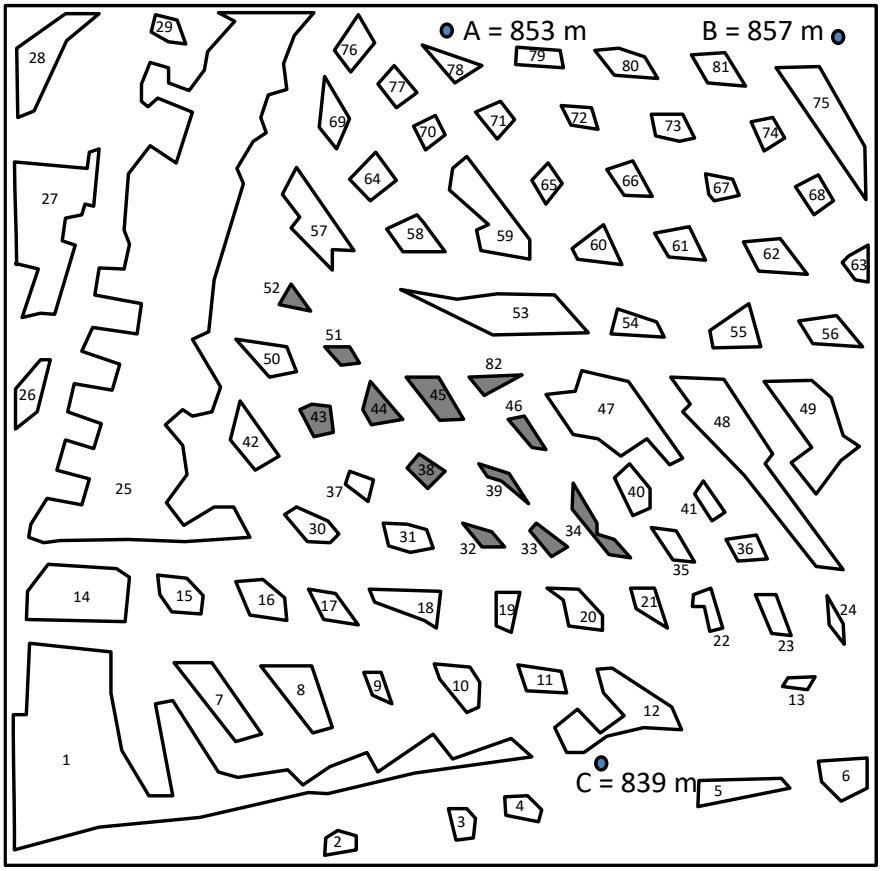

Figure 2-44. Mine layout of the pillar extraction (D. F. Malan 2023, pers. comm.).

The shaded pillars were extracted at the time of the modelling and Figure 2-45 illustrates the simulated APS before and after pillar extraction for some of the pillars surrounding the shaded pillars. The significant increase in APS, ranging between 17 and 43%, indicates that the area where the extraction occurred had to be restricted in size to prevent large-scale instabilities.

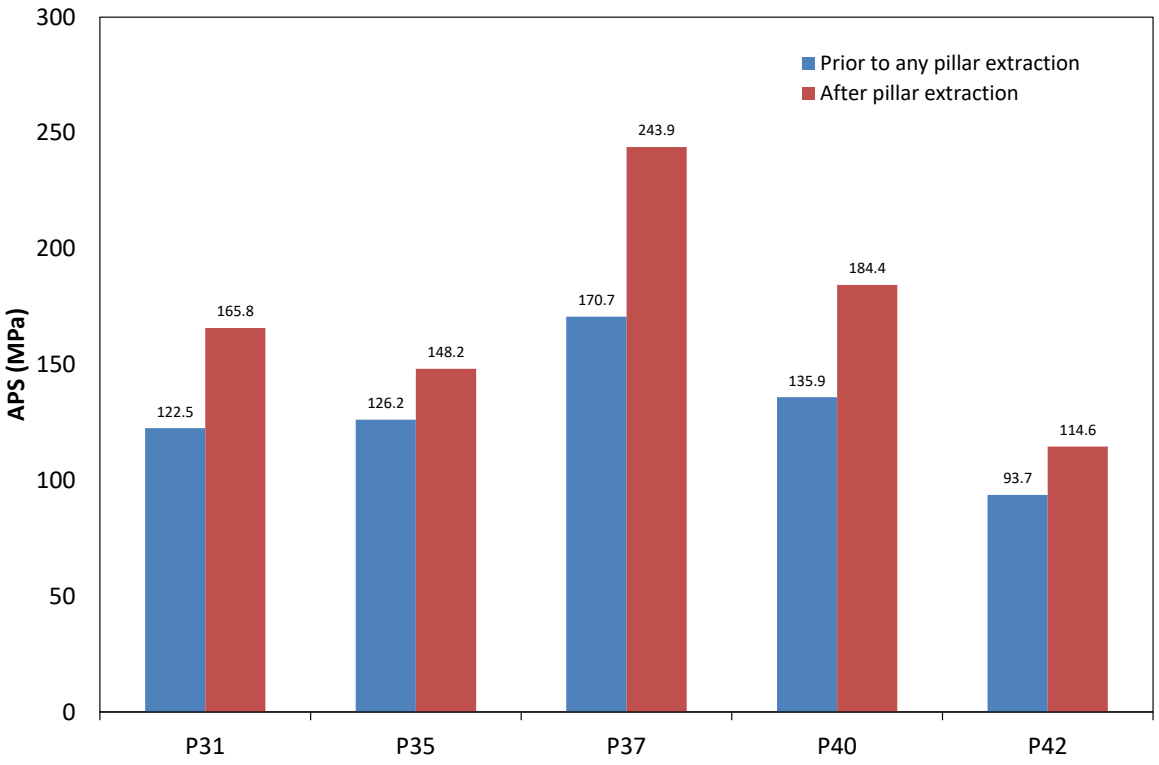

Figure 2-45. Simulated APS before and after the pillar extraction (D. F. Malan 2023, pers. comm.).

Modder East Gold Mine is another South African gold mining operation that has been successful with large-scale pillar mining. The extraction of pillars commenced in 2017, and the first phase of the project was limited extraction of selected pillars with 1.2 m stoping widths. The technique involves the installation of grout packs, as shown in Figure 2-46. Following the success of the first phase, the project was extended to include pillars with stoping widths ranging from 0.9 to 3.0 m (South African National Institute of Rock Engineering (SANIRE), 2021).

Figure 2-46. Grout packs used at Modder East for pillar extraction (D. F. Malan 2023, pers. comm.).

It was observed that only the hard rock pillars near the extracted pillar exhibited stress fracturing. The condition of the grout packs installed adjacent to a mined pillar is shown in Figure 2-47.

Figure 2-47. Condition of the grout packs adjacent to a mined-out pillar (D. F. Malan 2023, pers. comm.).

2.5. Summary

This literature review covered several diverse topics, but all this work is related to the potential benefit of using backfill underground in bord and pillar mines. The tailings dam disasters highlight the potential risk and consequences that are associated with storing mining waste on surface. Backfill derived from tailings is a sustainable alternative to eliminate the hazards associated with storage on surface (Yu et al., 2021). This will reduce the occurrence of dam failures, but will also prevent dust generation and the contamination of surface water resources.

From the literature it was found that backfilling practices to control surface subsidence and for environmental considerations are mostly implemented in the coal mining sector. Extensive use of backfill is made in the Chinese coal mines, as described by Zhang et al. (2019), in conjunction with high extraction mining methods. Backfill can be used to counter subsidence in hard rock mines as the primary long-term ground support provided that its initial design strength accounts for time-dependent loading (Tesarik et al., 2009). In the Buick Mine investigation, the strength of the backfill was adequate to sustain time-dependent loading and remained stable for 16 years following its placement.

Backfill makes it possible to extract reef pillars in a controlled and safe manner. In the South African mining context, however, pillar extraction has not been done by using backfill, but rather with the use of grout packs. The next chapters will highlight the use of backfill as pillar confinement to potentially increase the extraction ratio or extract some of the pillars. Of particular interest is the lateral confinement exerted by the backfill and this is discussed in the next chapter.

3. LATERAL CONFINEMENT

3.1. Introduction

As discussed in the previous chapter, the key objective of using backfill in shallow bord and pillar mining layouts is to apply a lateral stress confinement to the pillars. The magnitude of confinement is unknown, however, as it has never been properly quantified. There is little to no convergence in these hard rock bord and pillar layouts, so no vertical stress will be generated in the backfill. The confinement is, therefore, caused by the weight of the fill material as described below. The distribution of confinement is probably not constant along the edge of the pillar and increases from the hangingwall to the footwall. After placement of backfill, the largest confinement will be at the bottom of the pillar and the least will be at the top.

In contrast, for gold mine applications where there is significant closure, the stress–strain behaviour of backfill can be approximated with a hyperbolic model, as shown in Figure 3-1. For this example, instrumentation placed in the backfill recorded a vertical strain in excess of 20%. The corresponding vertical and lateral stress in the dip and strike directions are shown in the figure. Note that substantial horizontal stress is indeed generated in the dip and strike directions. These magnitudes are nevertheless substantially lower than the stress in the vertical direction. In contrast, in shallow bord and pillar mines, the closure is very small (not more than a few millimetres after an entire area is mined), and these high stresses will therefore never be generated in backfill placed in bord and pillar mines. The small closure and the mechanism of confinement also negates the need for tight filling and backfill contact with the hangingwall is not required. As described by Salamon and Oravecz (1976), the beneficial effect of backfill in bord and pillar layouts is that it exerts pressure on the pillar sidewalls because of its own weight, and it can therefore increase the strength of the pillars.

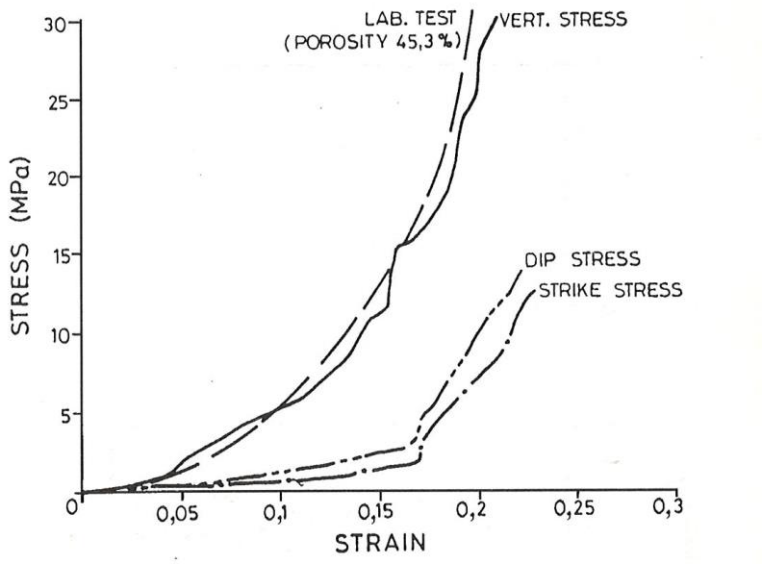

Figure 3-1. In-situ compression behaviour of classified backfill tailings in deep gold mines (after Piper et al., 1993).

Based on Figure 3-1, the stress in the lateral directions (dip and strike) only became meaningful if the strain in the vertical direction exceeded approximately 0.1. This implies that for a bord and pillar layout with a mining height of 2.5 m, at least 250 mm of closure must occur after the backfill is placed. This is never observed for the hard rock bord and pillar layouts in the Bushveld Complex, except for the rare cases where large-scale pillar collapses occurred (Couto and Malan, 2023). A further problem with backfill in flat dipping tabular stopes is that good contact with the hangingwall will never be achieved. Based on these considerations, a different approach will have to be used to estimate the lateral confinement applied by the backfill on the pillars because of its own weight. Rankine's earth pressure theory is useful in this regard.

Blight and Clarke (1983) examined the relationship between vertical and horizontal stress of backfill specimens by casting mixes of various types of fill in steel compaction moulds, and published results on the relationship between the lateral and vertical stress for soft and stiff fills. The ratio of horizontal to vertical stress varies from 0.1 to 0.45 for stiff fills and 0.4 to 0.7 for soft fills. Figure 3-2 illustrates the relationship between the vertical and horizontal stresses for both types of fills when they are subjected to lateral confinement. This again emphasises that substantial vertical stress needs to be generated in the fill before large magnitudes of horizontal stress will be generated. This will not be the case in bord and pillar layouts.

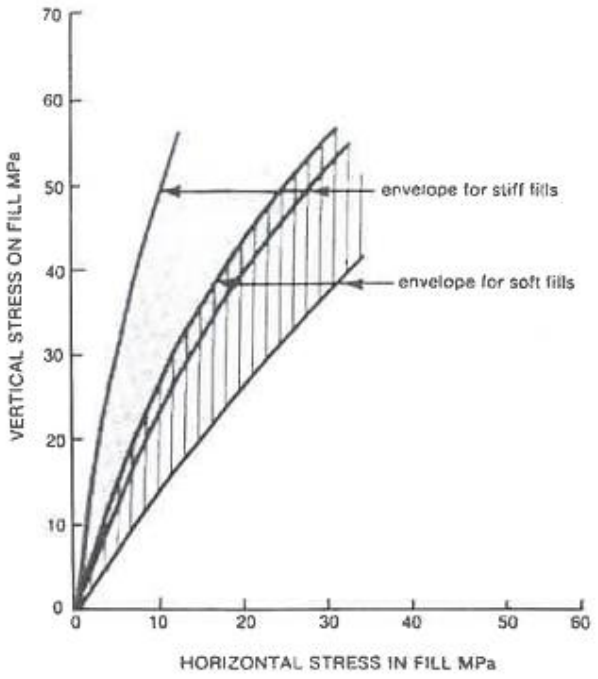

Figure 3-2. Stress envelopes following compression tests on stiff and soft fills (after Blight and Clarke, 1983).

Blight and Clarke (1983) noted that backfill can therefore support pillars but acknowledged that significant vertical strains are necessary to develop the lateral stress. As the vertical strains are very low in shallow bord and pillar operations, a different approach will have to be used to estimate the lateral confinement applied by the backfill on the pillars.

The historic measurements of horizontal stress conducted in backfill in the South African gold mines were not sensitive enough to determine the magnitude of the stress at small strains. Some estimation of the horizontal stress, therefore, needs to be made as this is required for the numerical modelling described in the next section. For coal pillars and ash filling, Buddery (1985) estimated that the strain in the ash fill will be 1.7×10^{-3}, and this translated to a confinement stress of 0.05 MPa when assuming a backfill modulus of 27 MPa and 0.51 MPa for a backfill modulus of 300 MPa. As a crude estimate of the increase in pillar strength, he assumed a “Coulomb failure criterion” for the pillars and illustrated that a 13.6% increase in pillar strength is possible for the higher modulus and confining stress. However, the application of this failure criterion and the associated assumptions is highly uncertain.

Cai (1983) indicated that backfill cannot support the total weight of overburden and acts as a secondary support. When fill is placed in a void, it does not come into immediate contact with the roof of the opening. As the roof begins to deform into the fill and displacements become larger

than the space between them, the fill will begin to provide passive support. The fill also provides lateral passive resistance as the pillars begin to deform.

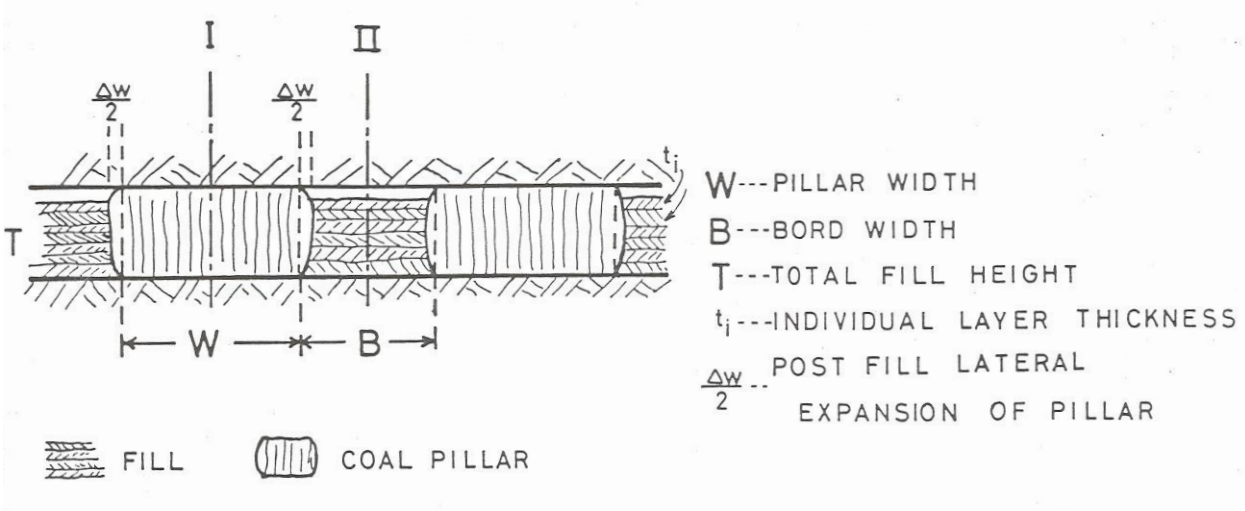

Figure 3-3. Ash filling in a coal mine (after Galvin and Wagner, 1981).

Galvin and Wagner (1981) studied the use of ash filling to improve strata control in coal bord and pillar workings. For the notation shown in Figure 3-3, the fill reaction or pillar confinement stress, σ_F, is given by:

$$\sigma_F = \varepsilon_F E_F = \frac{\Delta w}{B} E_F = k_F \Delta w \qquad \textbf{[3-1]}$$

where:

ε_F = lateral fill strain

E_F = fill modulus

k_F = fill stiffness (MN/m^3), given by:

$$k_F = \frac{E_F}{B} \qquad \textbf{[3-2]}$$

From Equation [3-1], it follows that a large pillar confinement stress can only be achieved if the fill stiffness is high. From Equation [3-2], this stiffness is proportional to the fill modulus, E_F, and inversely proportional to the bord width. Galvin and Wagner (1981) note that dilation of failing pillars is the largest at mid-height and the fill must, therefore, exceed half the pillar height and should preferably be two-thirds of this height.

An alternative estimate of the pillar confinement stress can be made using soil mechanics principles and specifically, calculations of lateral earth pressure. In civil engineering, lateral earth

pressure refers to the stress that is exerted by or onto soil in a horizontal direction when it is placed against structures such as basements and retaining walls. In this chapter, the manner in which the lateral pressure will be exerted on pillars by backfill is explored.

3.2. Earth pressure theory

The presence of lateral stresses in soil is important to civil engineers as it provides confinement. Rankine's earth pressure theory, also known as the classical earth pressure theory, is commonly employed in civil engineering to design retaining walls. The theory, which was proposed in 1857, can provide estimates of the magnitude, and the point of application of earth pressures acting on the wall (Jamal, 2017). The approach is only an approximation in many cases as it assumes that the soil is homogeneous and isotropic, and that the surface upon which the pressure is acting on is frictionless. This approach may be useful to estimate the confining stress acting on pillars after the placement of backfill. Pillar design is typically based on ultimate strength, which implies that pillar failure will occur when the acting load exceeds its strength. A confining pressure, such as the one that is introduced through backfill, increases the pillar strength. A relationship between the initial strength, confining pressure, and the new pillar strength is therefore necessary to incorporate earth pressure theory into pillar design (Donovan and Karfakis, 2004).

Although the pillar support capability of backfill is well known, it remains difficult to quantify. The author of this dissertation explored the use of classical earth pressure theory to estimate the lateral pressure applied by backfill in an underground operation. The backfill was assumed to be homogeneous and isotropic. Figure 3-4 demonstrates that the distribution of the lateral stress, σ_h, increases with depth according to the earth pressure theory. At the surface of the backfill, the stress will be zero and this increases linearly to a maximum value at the bottom of the pillar. If the pillar sidewall retreats from the backfill (not practical, but it occurs in soil mechanics for retaining walls), σ_h decreases until the limiting value of active earth pressure, σ_a, is reached. When the pillar sidewall dilates towards the backfill, σ_h increases until the limiting value of passive earth pressure, σ_p, is reached (as described in Shamsabadi et al., 2017 for retaining walls).

The coefficient of lateral earth pressure, K, is defined as:

$$K = \frac{\sigma_h}{\sigma_v} \qquad \textbf{[3-3]}$$

where:

σ_h = horizontal or lateral stress

σ_v = vertical stress

The symbol for the coefficient of lateral earth pressure should not be confused with K used in pillar strength equations. K is nevertheless used here as it is commonly used in soil mechanics. Equation [3-3] can be rewritten to determine the lateral earth pressure that acts against the pillar as:

$$\sigma_h = \sigma_v K = (\gamma \times h)K \quad \textbf{[3-4]}$$

where:

γ = unit weight of the backfill (N/m^3)

h = height of the backfill (m)

K = coefficient of lateral earth pressure

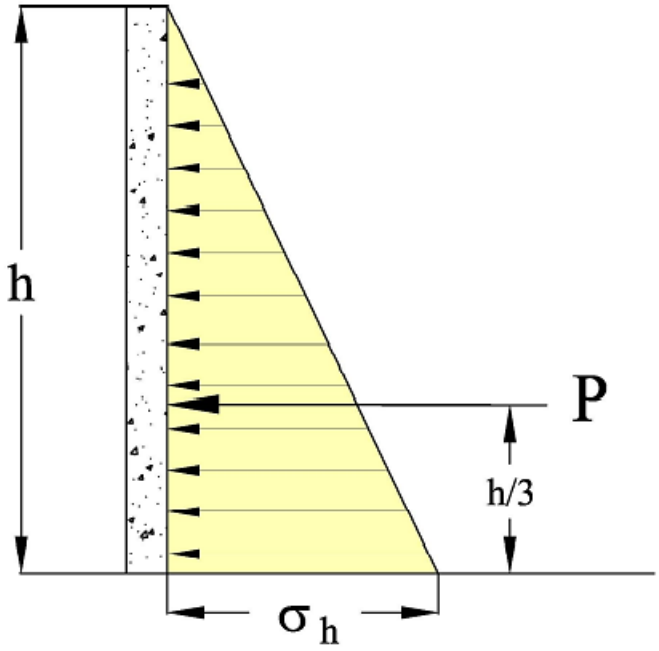

Figure 3-4. Triangular pressure distribution on a retaining wall (after Shamsabadi et al., 2017).

Equation [3-4] does not include any surcharge loading which would be caused by closure acting on the backfill in a mining excavation. The equivalent lateral earth force is shown above as P in

Figure 3-4. It is equal to the area of the pressure distribution and is assumed to act at a third of the retaining wall's height above its base. The resultant force, which causes bending and sliding in the wall, is determined by (Shamsabadi et al., 2017):

$$P = \frac{1}{2}\gamma h^2 K \qquad \textbf{[3-5]}$$

If the force P acts along a pillar of height, h, the average confinement stress along the pillar face is:

$$\sigma_B = \frac{1}{2}\gamma h K \qquad \textbf{[3-6]}$$

In soil mechanics, there are three types of lateral earth pressure that exist based on the movement of the retaining wall. The coefficient of lateral earth pressure in the equation above can be one of the following (Jamal, 2017):

1. Active pressure, K_a, which applies when the retaining wall is moving away from the soil.
2. Passive pressure, K_p, is applicable when the retaining wall is pushing into the soil.
3. At rest pressure, K_0, applies when the wall is at rest and the soil is in its natural state.

Figure 3-5 depicts the motion of soil relative to the retaining wall for the different lateral earth pressure types.

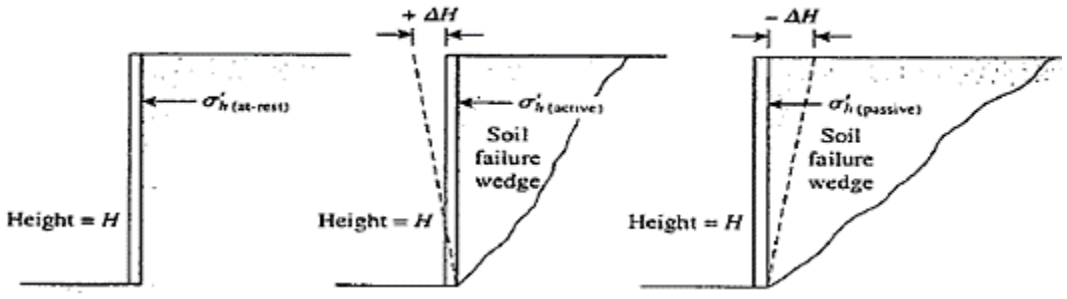

Figure 3-5. The types of lateral earth pressure acting on a retaining wall (after Gurjar, 2018).

In general, for the active condition, K_a is between one and two-fifths of the vertical stress. For the passive condition, K_p is 3 to 10 times the vertical stress. Therefore, inducing passive loading leads to the soil experiencing a higher lateral stress (Franke, 2017). At rest, K_0 is two to three-fifths of the vertical stress. The coefficients of lateral earth pressure can also be determined using Rankine's classical earth pressure theory as follows:

$$K_a = cos\,\beta \frac{cos\,\beta - \sqrt{cos^2\,\beta - cos^2\,\phi}}{cos\,\beta + \sqrt{cos^2\,\beta - cos^2\,\phi}} \quad \textbf{[3-7]}$$

where:

ϕ = backfill's internal angle of friction

β = embankment slope angle

When β is 0, the formula is simplified to:

$$K_a = \frac{\sigma_a}{\sigma_v} = \frac{1 - sin\,\phi}{1 + sin\,\phi} = tan^2\left(45 - \frac{\phi}{2}\right) \quad \textbf{[3-8]}$$

K_p is determined as:

$$K_p = cos\,\beta \frac{cos\,\beta + \sqrt{cos^2\,\beta - cos^2\,\phi}}{cos\,\beta - \sqrt{cos^2\,\beta - cos^2\,\phi}} \quad \textbf{[3-9]}$$

And if β is 0, the coefficient is calculated using the following formula:

$$K_p = \frac{\sigma_p}{\sigma_v} = \frac{1 + sin\,\phi}{1 - sin\,\phi} = tan^2\left(45 + \frac{\phi}{2}\right) \quad \textbf{[3-10]}$$

K_0 is approximated by:

$$K_0 \cong 1 - sin\,\phi \quad \textbf{[3-11]}$$

The application of this theory for backfill against a pillar is not clear and it is hypothesised that the K_0 parameter will be important in cases where there is little or no pillar dilation. For extensive pillar failure and dilation, the K_p parameter may be more important. This is all speculation, however, and underground measurements in backfill will be required to determine the actual lateral confinement applied by the backfill.

A key assumption for the classical earth pressure theory is that the wall is smooth and frictionless. This assumption is inaccurate but simplifies the problem and provides conservative results. The roughness of the pillar would increase the passive earth pressure acting on it (Donovan and Karfakis, 2004).

In cut-and-fill operations, the design of backfill and the amount of support that it provides has been developed from experience. There is not a well-established procedure for pillar design that accounts for the effect of backfill (Donovan and Karfakis, 2004). Incorporating methods to determine the passive earth pressure that backfill exerts on the sides of pillars into the original pillar design makes it possible to determine the widths of backfilled pillars before mining commences.

When a pillar is unsupported, it is designed for a “uniaxial stress state”. When backfill is placed around the pillar, the pillar is in a “triaxial stress state” and has a much higher resistance to compressive stresses (Donovan and Karfakis, 2004). The difference in the design of a backfilled pillar in comparison to an unsupported pillar is that the increase in strength must be accounted for. The strength of a pillar that is confined with backfill is determined by these authors as:

$$\sigma_1{}' = \sigma_1 + K_{pp} \times \sigma_h \qquad \textbf{[3-12]}$$

where:

$\sigma_1{}'$ = backfilled pillar strength (MPa)

σ_1 = original pillar strength (MPa)

K_{pp} = coefficient dependent on coal pillar’s characteristics

The purpose of backfill is to provide additional support in the form of passive resistance. It is difficult to estimate the exact time that passive resistance within a fill is initiated for a failing pillar (Donovan and Karfakis, 2004). Therefore, to determine the passive resistance using Equation [3-12], the pillar must fail before the backfill’s confining pressure is applied.

Unlike civil engineering applications, the incorporation of earth pressure theory into the design of backfilled pillars has its limitations as it has not been done before and cannot be verified through

experience. Soil mechanics principles can nevertheless be applied to address many of the concerns encountered in underground operations such as determining the design and properties of the backfill to support excavations (Blight, 1984). The classical earth pressure theory will therefore be applied to estimate the lateral stress exerted by the placement of backfill.

3.3. Estimating the lateral stress magnitude from backfill placement

The following section will estimate the lateral force acting on pillar by using the earth pressure theory. Some practical values from measurements are also given and from these values, the magnitude of confinement that will be applied to the numerical models in the next chapters was estimated.

For this study, cemented classified tailings was arbitrarily selected as the fill material. The density of the tailings is given as 1.7 kg/m^3 by Squelch (1993, cited in Squelch et al., 2001), and in 2002, Ryder and Jager noted the density as 1.75 kg/m^3. Assuming a friction angle of 30°, the at rest lateral pressure coefficient is determined as:

$$K_0 \cong 1 - \sin 30 = 0.5$$

The relative density of a substance refers to its density relative to the density of water. For classified tailings, its value is 1.75 (Ryder and Jager, 2002). The density of backfill is therefore 1750 kg/m^3 and γ = 17 500 N/m^3. For a hard rock bord and pillar operation with little to no pillar dilation and a stoping height of 2.5 m, using Equation [3-6], σ_B is determined as:

$$\sigma_B = \frac{1}{2}\gamma h K = 11\ kPa = 0.011\ MPa$$

If there is significant pillar dilation after failure, the passive lateral earth pressure coefficient, K_p, must be used. From Equation [3-10], the coefficient is determined as:

$$K_p = \frac{1 + \sin 30}{1 - \sin 30} = 3$$

It then follows from Equation [3-6] that σ_B equates 66 kPa, which is 0.066 MPa. Incidentally, this value is of the same order of the lateral stress value measured by Galvin and Wagner (1981) in the ashfill experiment. In the absence of any better calibrated values, a value of 0.05 MPa is therefore used as a possible realistic value of the confinement that will be exerted by backfill. The obtained confinement value will be applied to the numerical models of the idealised layout from Chapter 4. For the purpose of the study, any additional surcharge load will be excluded from the confinement calculations as the closure is low and it is not expected that the backfill will make good contact with the hangingwall.

4. NUMERICAL MODELLING OF BACKFILL CONFINEMENT

There are two methods that are used to determine pillar strength, namely empirical equations, which have been derived from the back analysis of stable and failed cases, and numerical modelling techniques that use appropriate failure criteria (Malan and Napier, 2011). It is known from the descriptions in Chapter 2 that backfill influences pillar strength, and numerical modelling was therefore conducted by the author to quantify this effect. The magnitude of backfill confinement was estimated in the previous chapter and the author had to find a suitable numerical code and a constitutive model of pillar failure that can include the effect of this backfill confinement.

A model refers to any representation or abstraction of a system or process with a purpose. In engineering, models are used for two different, but interconnected purposes (Jager and Ryder, 1999). These are:

1. Design: for the optimisation of an engineering system based on predetermined conditions.
2. Mechanics: for the development or improved understanding of an engineering system.

When a model is developed correctly, benefits include improved problem definition, understanding of data, communication, and testing of the current state of understanding (Jager and Ryder, 1999). Predictions can be made from the resulting model regarding the behaviour of systems when they are subjected to conditions that have not yet been encountered.

The choice of selecting an appropriate modelling code for this study needs some justification. Simulation of large-scale bord and pillar layouts is a difficult numerical modelling problem, especially if pillar failure needs to be modelled. The finite element method (FEM), finite difference codes or distinct element method (DEM) codes can simulate pillar failure and the effect of pillar confinement if an appropriate constitutive model is used. For example, the FLAC3D code (finite difference code) can simulate pillar failure and support units, such as tendons and liners, can be included in the model. A displacement discontinuity boundary element approach was, however, used for this study owing to the following advantages. For practical mine problems, a large area needs to be simulated to simulate the stresses acting on the pillars. For hard rock mines, these pillars are typically irregular in shape, and it is extremely difficult to build these geometries in finite element or difference codes. In very large models, it may also not be practical to include pillar failure owing to constraints such as the requirement of small element sizes to accurately represent the depth of pillar failure. As a result, three-dimensional finite element or finite difference models are not commonly used to simulate bord and pillar layouts. In contrast, displacement discontinuity models (for example, Brady and Bray, 1978; Crouch and Starfield, 1983) overcome the problem of simulating the large-scale models with many pillars. As a drawback, historically, it was not possible

for most of these codes to simulate the failure of the pillars. This problem can now be circumvented by using the limit equilibrium model in the TEXAN displacement discontinuity code and this model is described below.

4.1. The evolution of numerical modelling codes in the South African industry

In the 1960s, several modelling innovations were made in the South African mining industry. These included several new techniques, based on elastic theory, to simulate the stresses and displacements around tabular excavations (Salamon, 1964; Plewman, et al., 1969; Ryder and Officer, 1964). Examples of the methods include the electrolytic tank and the electric resistance analogue. Following the arrival of digital computers, the simulation of tabular mine layouts has mostly been done using the displacement discontinuity boundary element method. This method was introduced in South Africa by Salamon (1964). The various versions of the BESOL and MINSIM codes used this technique. The optimisation of the mining layouts and sequences, as well as the design of stabilising pillars, were the primary objective during this period to minimise the rockbursts that were being experienced in the deep gold mines. The numerical codes were therefore specifically designed for deep-level layout problems with the “infinite depth” solutions being a good approximation owing to the great depth of the excavations (Malan and Napier, 2006).

The early displacement discontinuity codes, developed for the gold mining industry, were not optimised for use in the Bushveld Complex owing to the significant differences in working depths as well as the different mining layouts. Platinum and chrome mines typically operate at shallower depths ranging from 30 to over a 1000 m, whereas the average working depth in gold mines exceeds 2000 m (Malan and Napier, 2006). The shallow nature of platinum stopes is not compatible with the infinite depth assumption used in the conventional codes. Additionally, the mine layout and pillar designs in the Witwatersrand Basin and Bushveld Complex differ greatly. In deep gold mines, large strike or dip stabilising pillars are designed to limit energy release rates at the stope face whereas in shallow and intermediate depth platinum mines, multiple small in-stope crush pillars as well as bord and pillar layouts are used (Malan and Napier, 2006). Simulating these pillars with the traditional displacement discontinuity codes is not practical. This resulted in a new displacement discontinuity code, TEXAN, being developed by Prof John Napier (Napier and Malan, 2007).

4.2. Overview of the TEXAN code

TEXAN was developed to solve both shallow and deep mining layout problems for excavations in tabular orebodies that may or may not contain many pillars. The code is particularly efficient to solve problems in large-scale layouts with a multitude of small irregular pillars (Malan and Napier, 2006). The code can solve both two- and three-dimensional boundary value problems with several interacting displacement discontinuity elements representing tabular mine excavations and geological features such as faults or slip planes. It can also simulate interacting planar fault planes and tabular reef planes.

Triangular, square, or convex quadrilateral element geometries can be used. This is particularly useful to model unusual pillar geometries that are generally difficult to represent using a square element mesh (used by the older generation of displacement discontinuity codes). The elements can be in an “infinite” or “semi-infinite” environment with a flat, stress-free surface. The host rock is always assumed to be homogeneous, isotropic, and elastic for all the models. An example of a layout that was modelled using triangular displacement discontinuities is shown in Figure 4-1. To assist with the digitising process, the mining outline and pillars on the left were approximated by straight line polygons.

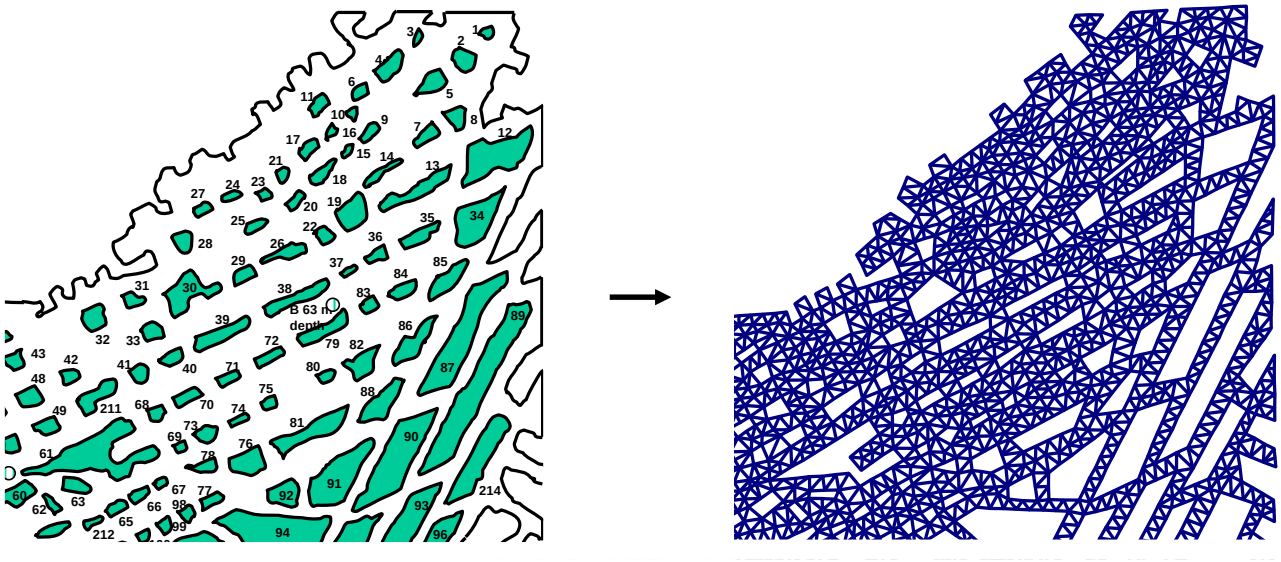

Figure 4-1. The use of triangular elements to simulate a mining layout in TEXAN (after Malan and Napier, 2006).

The advantage of a flexible element geometry is that it allows for the analysis of multiple intersecting reef-fault systems, which is generally not possible when using square element shapes (Malan and Napier, 2006).

For the cases where the pillars that are being simulated are not allowed to fail, the model is referred to as a simple elastic model with “rigid” pillars. For this study, the TEXAN limit equilibrium model (LEM), with confinement, was used to simulate pillar failure. The details of this constitutive model are described in the next section. This is a new model that was implemented in TEXAN and this dissertation is the first study of the behaviour of this model.

4.3. A limit equilibrium model with confinement

The TEXAN code was developed to accurately simulate stresses in hard rock bord and pillar mines. The LEM was added to the code in 2006 to enable the simulation of pillar failure (Malan and Napier, 2006).

The original version of the limit equilibrium model assumed there was no confinement on the pillar edges. A confinement component was recently added to the model to allow for the specification of reef or seam parallel confining stress boundary condition. This can be used to simulate pillar behaviour with the application of pillar reinforcement, such as pillar strapping or backfill.

A simple 2D plane strain version of this model is derived by the author below for this dissertation to illustrate the attributes of the model. Note that the model implemented in TEXAN is more complex as the irregular pillar geometries need to be simulated and special techniques had to be introduced to solve these problems. The simplified 2D model below is nevertheless valuable to understand the attributes of the model for a simple geometry. The more general case of stress variation in complex tabular layout geometries is given in Napier and Malan (2021) if the reader requires additional information. TEXAN uses a special fast marching solution technique to determine the seam-parallel gradient direction in the case of general layout shapes.

The force equilibrium of a thin slice of rock in the failed edge of the pillar is shown in Figure 4-2. This illustrates the mined bord on the left, which was subsequently filled with backfill, and part of the pillar on the right. The fractured pillar material on the edges of the pillar is assumed to be confined between the excavation hangingwall and footwall. The portion of the fractured reef in the diagram has a mining height H at a distance x from the stope face and is acted on by the reef-parallel and reef-normal stress components, namely σ_s and σ_n (Malan and Napier, 2006).

Additionally, there is a shear stress, τ, acting on the parting planes that separates the pillar from the hangingwall and footwall. The edge of the pillar will fail if the applied stress exceeds the strength, and the remainder of the pillar may remain intact depending on the selection of parameters. If weak material properties and high stress are simulated, the entire pillar can fail.

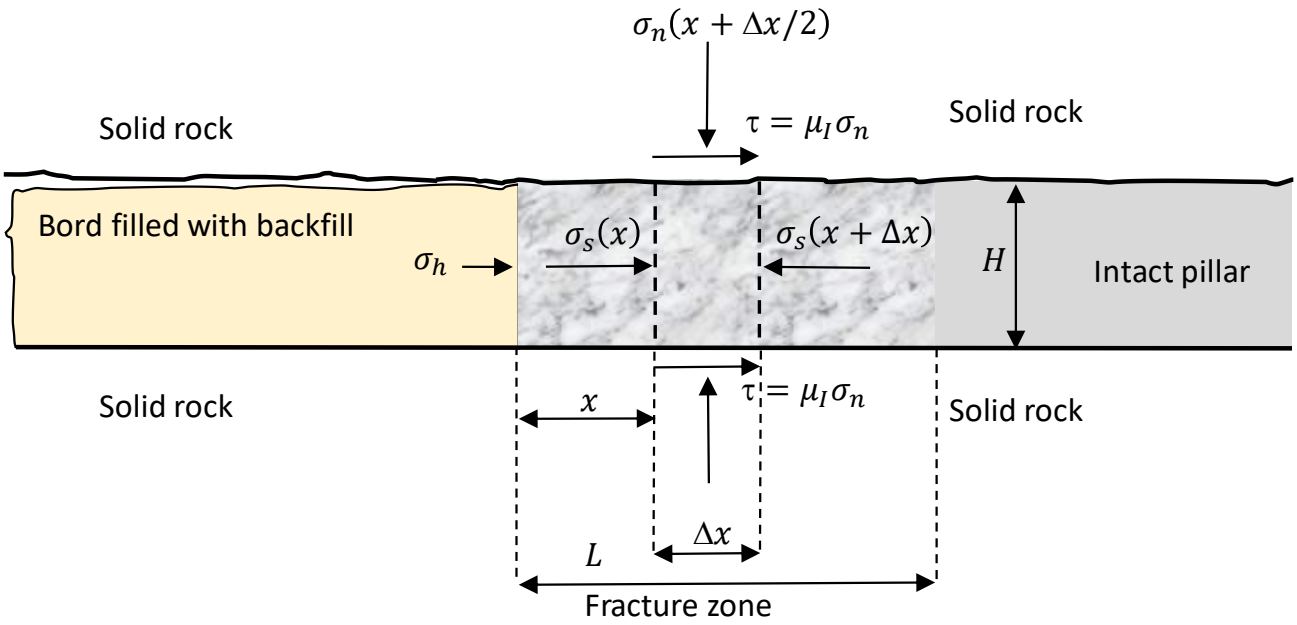

Figure 4-2. A limit equilibrium model, with backfill, illustrating the force equilibrium of a slice of pillar material in the failed zone (D. F. Malan 2022, pers. comm.).

At x = 0, the edge of the pillar, a confining stress, σ_h, is applied because of the backfill placement. It can be assumed that this horizontal stress is given by the lateral earth pressure in Equation [3-4]. This model is a simplification, however, as it is assumed that a constant confinement is applied by the backfill from the top to the bottom of the pillar edge. This assumption needs to be tested using measurements in actual backfill placements underground. The seam-parallel stress component, σ_s, increases as x increases. The thin slice of rock (between the dotted lines in Figure 4-2) is in equilibrium. For this equilibrium condition, it is required that:

$$H\sigma_s(x) + 2\tau\Delta x = H\sigma_s(x + \Delta x) \quad \textbf{[4-1]}$$

Equation [4-1] can be written in the form of a differential equation if the width of the slice tends to zero:

$$\frac{d\sigma_s}{dx} = \frac{2\tau}{H} \quad \textbf{[4-2]}$$

To solve Equation [4-2], assume there is a relationship between τ and σ_s. Assuming that there is friction on the interfaces between the pillar, hangingwall, and footwall, τ is therefore related to the pillar-normal stress, σ_n, by the following condition:

$$\tau = \mu_I \sigma_n = tan\phi(\sigma_n) \quad \textbf{[4-3]}$$

where:

μ_I = coefficient of friction coefficient at the interface of the pillar contacts

ϕ = friction angle on the interfaces

Also assume that σ_n is related to the seam-parallel stress component σ_s by a failure relationship of the form:

$$\sigma_n = m\sigma_s + \sigma_c \quad \textbf{[4-4]}$$

where:

σ_c and m = specified constants

Once failure occurs, σ_c can be considered as the strength of the failed pillar material and m is a slope parameter. Substituting Equations [4-3] and [4-4] into Equation [4-2] gives the following differential equation:

$$\frac{d(\sigma_s)}{dx} = \frac{2tan\phi}{H}[m\sigma_s + \sigma_c] \quad \textbf{[4-5]}$$

Equation [4-5] can be integrated by separation of the variables:

$$\int \frac{d\sigma_s}{m\sigma_s+\sigma_c} = \int \frac{2\tan\phi}{\mathrm{H}} dx \quad \textbf{[4-6]}$$

This equation has the following solution with the integration constant A:

$$\frac{ln[m\sigma_s+\sigma_c]}{m} = \frac{2tan\phi x}{H} + A \quad \textbf{[4-7]}$$

To include the effect of the backfill confinement, constant A is obtained from Equation [4-7] by applying the boundary condition $\sigma_s = \sigma_h$ when $x = 0$. This gives the value of A as:

$$A = \frac{ln(m\sigma_h+\sigma_c)}{m} \quad \textbf{[4-8]}$$

This can be inserted into Equation [4-7] to give:

$$\frac{ln[m\sigma_s+\sigma_c]}{m} = \frac{2tan\phi x}{H} + \frac{ln(m\sigma_h+\sigma_c)}{m} \quad \textbf{[4-9]}$$

This can be simplified as:

$$\frac{1}{m} ln\left(\frac{m\sigma_s+\sigma_c}{m\sigma_h+\sigma_c}\right) = \frac{2tan\phi x}{H} \quad \textbf{[4-10]}$$

and

$$\frac{m\sigma_s+\sigma_c}{m\sigma_h+\sigma_c} = e^{2tan\phi mx/H} \quad \textbf{[4-11]}$$

The solution of the seam-parallel stress is therefore given by:

$$\sigma_s = \frac{1}{m}\left[(m\sigma_h + \sigma_c)e^{2tan\phi mx/H} - \sigma_c\right] \quad \textbf{[4-12]}$$

From Equations [4-12] and [4-4], an expression for σ_n can be derived:

$$\sigma_n = (\sigma_c + m\sigma_h)e^{2\mathrm{tan}\phi mx/\mathrm{H}} \quad \textbf{[4-13]}$$

Equation [4-4] defines the pillar material strength. In the TEXAN code, an extended model is implemented where the failure relationship for the *intact pillar material* is given by:

$$\sigma_n = m^i \sigma_s + \sigma_c^i \quad \textbf{[4-14]}$$

For the *failed pillar material*, the following parameters are adopted:

$$\sigma_n = m^f \sigma_s + \sigma_c^f \quad \textbf{[4-15]}$$

The requirements of $m^i \geq m^f$ and $\sigma_c^i \geq \sigma_c^f$ must be met when selecting these parameters. To illustrate the behaviour of the model, Equation [4-13] is plotted in Figure 4-3 for different values of confining stress. The graph was plotted using the following parameters: m = 2, σ_c = 1 MPa, ϕ = 25°, and H = 2 m. Note how the normal stress in the failed zone of the pillar increases substantially for an increase in confining stress. This is a significant result as it illustrates a substantial increase in the strength of the failed cores of pillars when even small amounts of confinement are applied to the pillar edge.

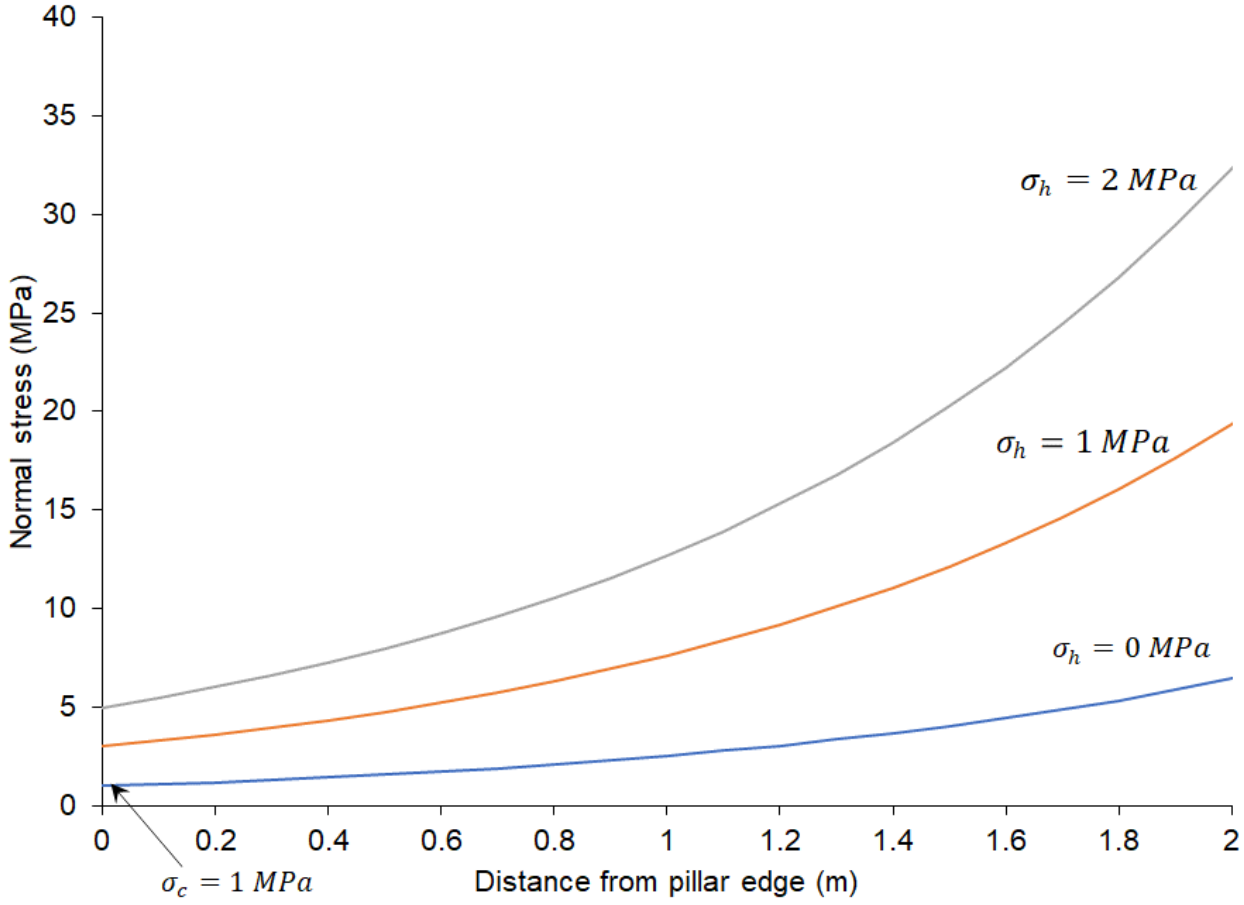

Figure 4-3. An illustration of the effect of the backfill confining stress on the normal pillar stress predicted by the limit equilibrium model in the failed zone of the pillar.

The author also derived a solution of pillar APS using the model above to illustrate the effect of confinement. Note that this solution is only valid for a pillar that is completely failed. Equation [4-13] predicts an exponential increase in the pillar stress away from the edge and towards the centre of the pillar. This can be seen in Figure 4-3. If the pillar width is w and the pillar is completely failed, the stress profile will be symmetric about the centre of the pillar (only half of the profile is shown in Figure 4-3). The average stress in the pillar is then given by the integral equation:

$$APS = \frac{2\int_0^{\frac{w}{2}} \sigma_n dx}{w} \quad \textbf{[4-16]}$$

By substituting Equation [4-13] into [4-16], it follows that:

$$APS = \frac{2(\sigma_c + m\sigma_h)\int_0^{\frac{w}{2}} e^{2\tan\phi mx/\mathrm{H}} dx}{w} \quad \textbf{[4-17]}$$

Solving Equation [4-17] gives:

$$APS = \frac{(\sigma_c + m\sigma_h)H}{\tan\phi mw}\left[e^{\tan\phi mw/\mathrm{H}} - 1\right] \quad \textbf{[4-18]}$$

To illustrate the behaviour of the model, Equation [4-18] is plotted in Figure 4-4 for different values of confining stress. The graph was plotted using the following arbitrary parameters: m = 3, σ_c = 20 MPa, ϕ = 30°, and H = 2 m. Note how the APS of the failed pillar increases substantially for an increase in confining stress.

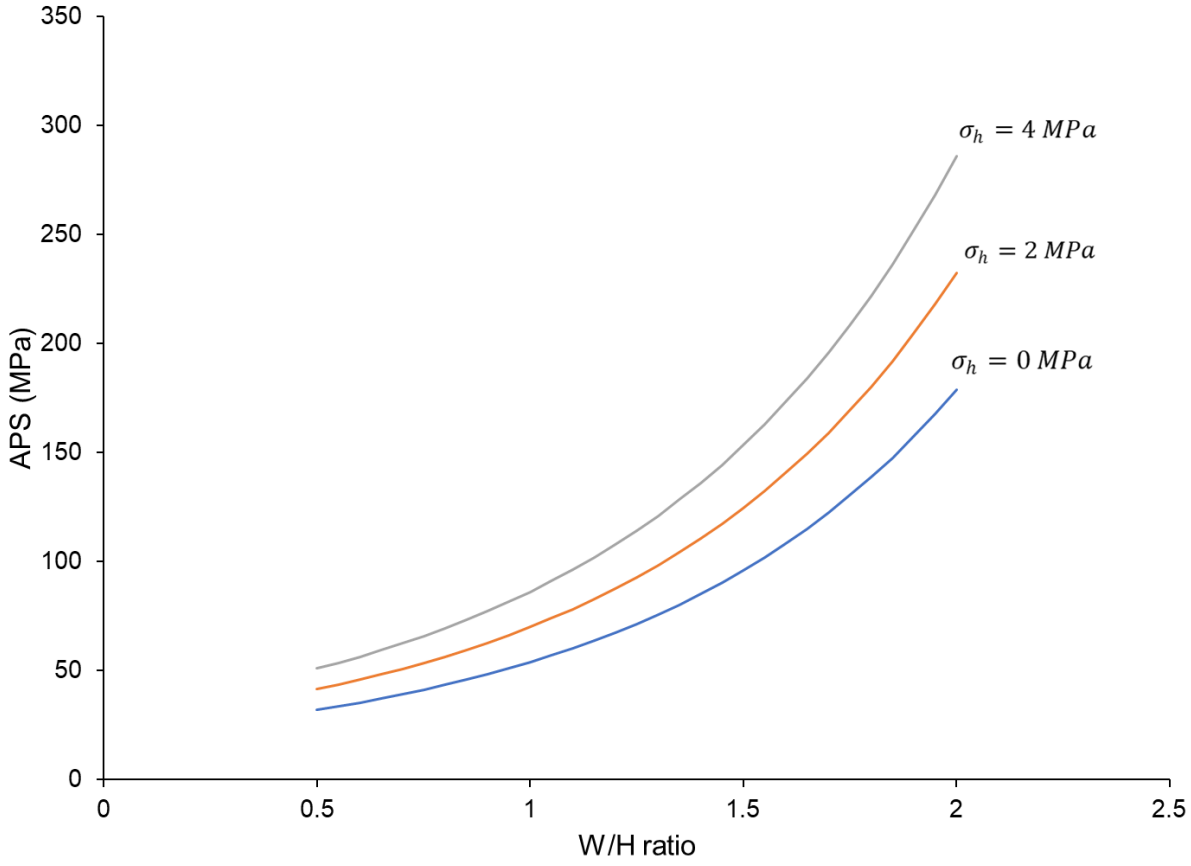

Figure 4-4. Effect of confinement on the APS for a completely failed pillar.

4.4. Numerical modelling using the confinement model

As a first numerical modelling test, the confinement model in TEXAN was applied to a geometry with a single pillar to investigate how the failure is affected by different levels of confinement. The overall dimensions of the geometry were 50 m × 50 m with a perfectly square pillar in the centre, shown in Figure 4-5. It was simulated at a depth of 300 m. The pillar width was 10 m, and this produced a high extraction ratio of 96%, but this was arbitrarily selected to ensure a sufficiently high load acts on the pillar.

The models were simulated using both triangular and square elements to observe how different element sizes would affect the resulting APS values.

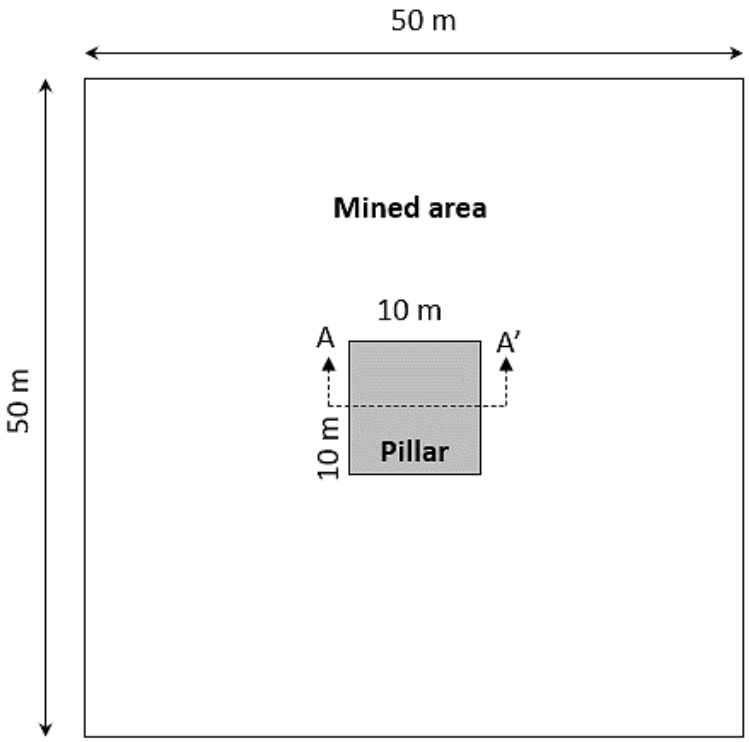

Figure 4-5. Geometry of the single pillar layout simulated.

4.4.1. Triangular element simulation

The geometry was first simulated using rigid pillars, which implies that the pillars cannot deform or fail. Figure 4-6 illustrates the mesh used for the geometry. The simulated APS was 38.1 MPa. The LEM was then used to simulate the pillar with the application of different values of edge confinement. Poisson's ratio, Young's Modulus, the overburden density and the LEM parameters are listed in Table 4-1. These values were arbitrarily selected to illustrate the behaviour of the model. An improved calibration is given in Chapter 5. The pillar size was 100 m^2 and 284 elements were used to represent this pillar. This gives an average element size of ≈ 0.35 m^2.

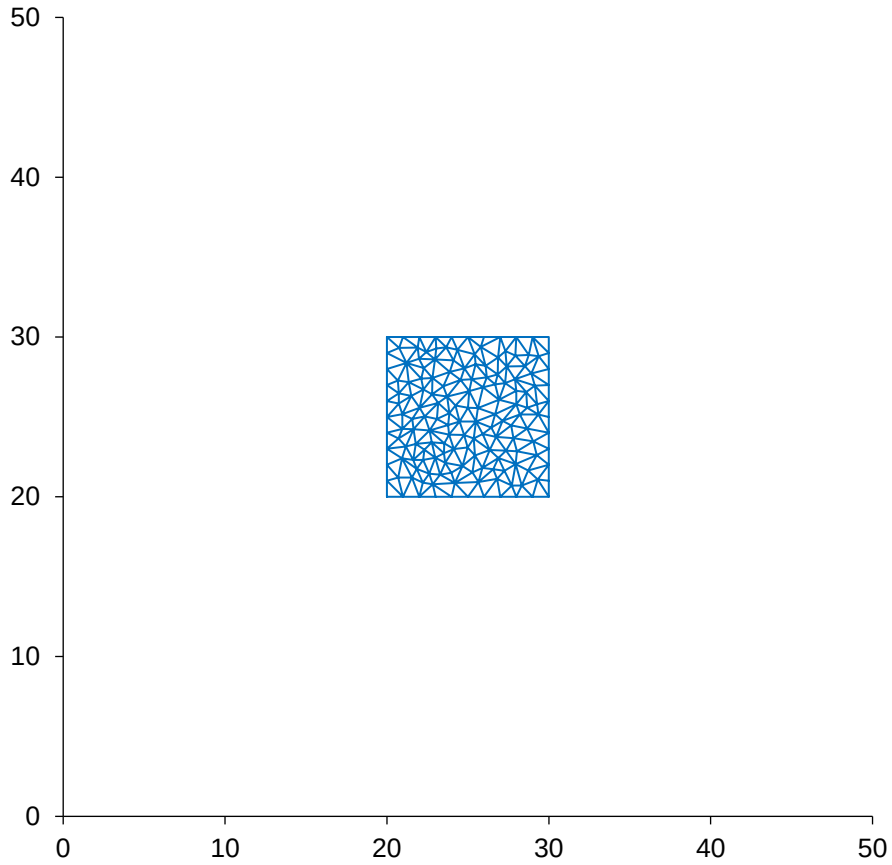

Figure 4-6. Triangular element mesh for the single pillar geometry.

Table 4-1. Parameters values used for the limit equilibrium model.

Parameter	Value
Intact strength intercept, σ_c^i (MPa)	15
Intact strength slope, m^i	4
Initial residual strength intercept, σ_c^f (MPa)	5
Initial residual strength slope, m^f	4
Seam height, H (m)	5.5
Intact rock Young's Modulus, E (GPa)	70
Intact rock Poisson's ratio, v	0.25
Overburden density, ρ (kg/m^3)	3 000
Intact seam stiffness modulus, k_s (MPa/m)	12 727
Fracture zone interface friction angle (°)	30

Table 4-2 illustrates the results that were obtained for the LEM numerical models with confinement values ranging from 0 to 2 MPa. Note how the APS values and strength of the pillar increase for increasing confinement. The model therefore correctly predicts the behaviour expected from the model as illustrated in Section 4.3 above.

Table 4-2. The simulated pillar stresses and pillar failure for different levels of confinement for a triangular mesh. The failed elements refer to the ratio of failed to total elements in the centre pillar.

Magnitude of confinement	Percentage of failed elements (%)	APS (MPa)
0 MPa	66	19.9
0.1 MPa	64	20.4
0.2 MPa	61	21.0
0.5 MPa	53	22.4
1 MPa	45	24.1
2 MPa	30	26.4

Confining the pillar makes it stronger, resulting in a reduced amount of failure. This is illustrated by a reduction in the percentage of failure in Table 4-2.

Figure 4-7 is a plot of the vertical stress in the pillar along Section A-A' (see Figure 4-5) for different levels of confinement. The pillar is located between x = 20 m and x = 30 m on the x-axis of the graph. In all cases, the centre core of the pillar is still intact and the failure on the edges of the pillars can be seen by the decreasing stress values towards the edges of the pillar at x = 20 m and x = 30 m. A stress peak for each pillar is seen at the boundary between the failed edge and the intact core. Of importance is that the size of the intact core increases as the confinement increases and it reaches a maximum value for a confinement of 2 MPa in the figure.

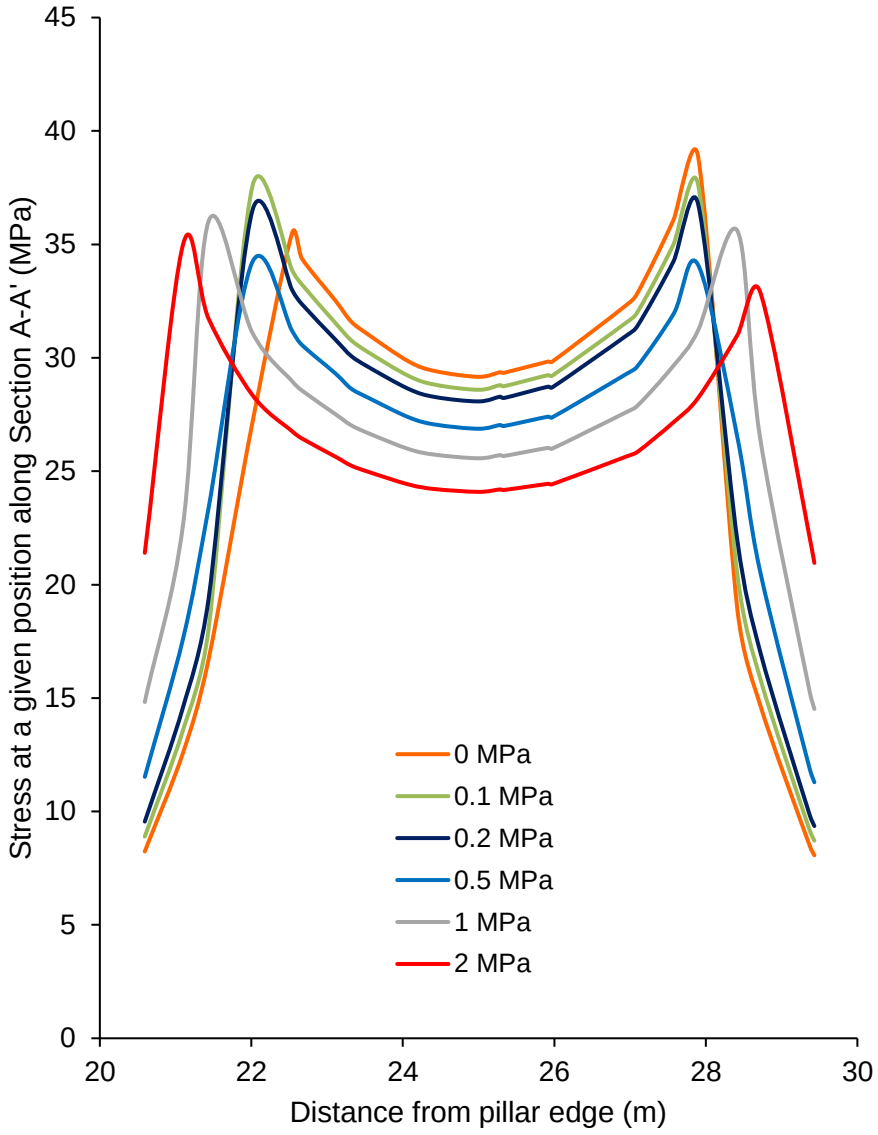

Figure 4-7. A plot of the simulated stresses for Section A-A' across the pillar. This was for a triangular element mesh.

Figure 4-8 depicts the failure of the pillar as the confinement increases. The dots indicate the "collocation points" where the code calculates the stress and displacements at the centres of the triangular elements. Triangular elements were used for these runs and that is why the extent of the failed edge region is somewhat irregular. The intact core of the pillar is visible, and this core gets larger with an increase in confinement. This is in agreement with the stress plots illustrated in Figure 4-7.

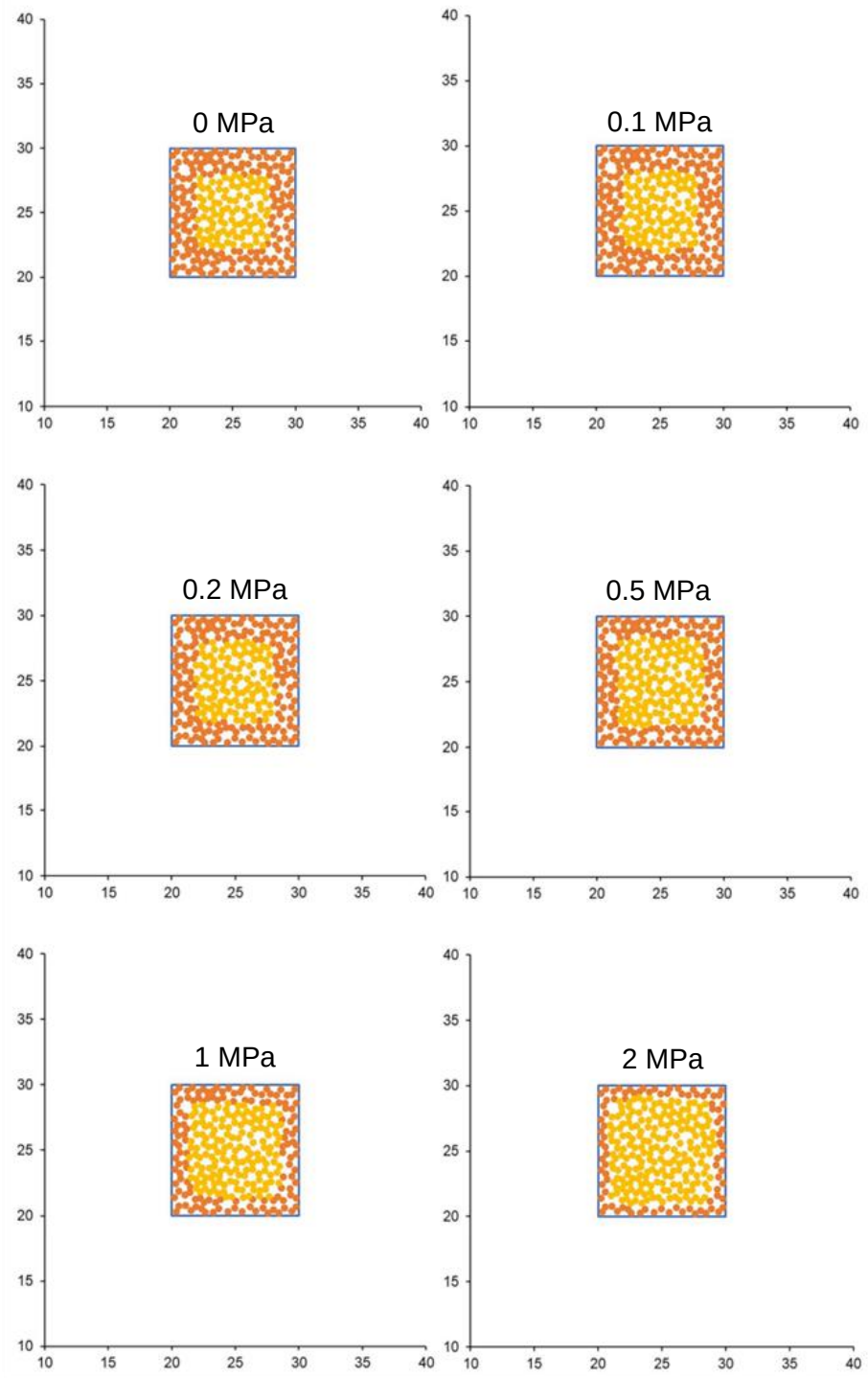

Figure 4-8. Pillar failure plots for a triangular mesh with varying amounts of edge confinement. The yellow dots are elements that are still intact, and the orange dots are failed elements.

Based on the data in Table 4-2, Figure 4-9 below was plotted to examine how the failure and the intact core are affected by the level of confinement. Note that an exponential function gives a remarkably good fit to the data. This is nevertheless only for the range of values given in the graph as the exponential function will only reach a value of 0% failed elements when $x \rightarrow \infty$, and this will be achieved much sooner for the numerical model.

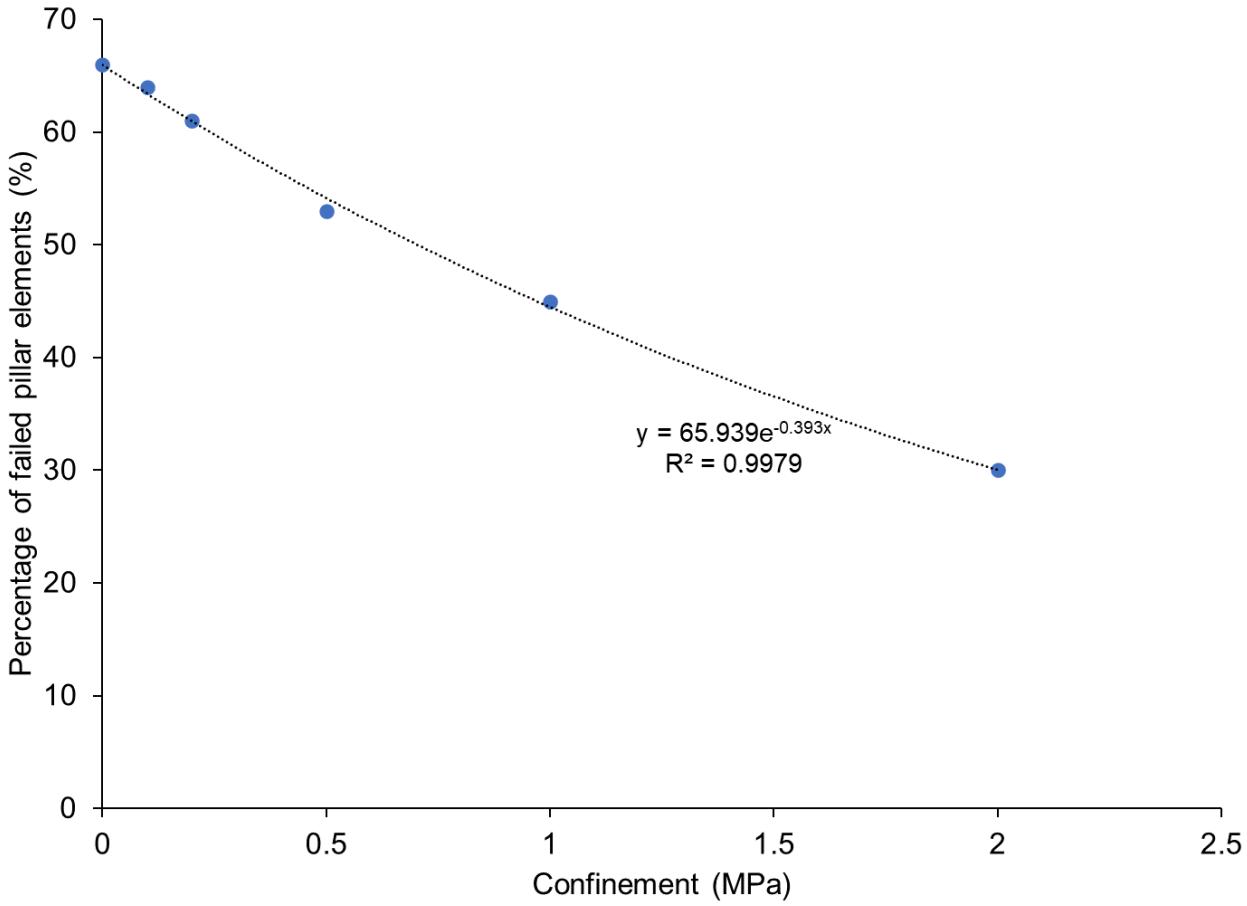

Figure 4-9. Percentage of failed pillar elements as a function of edge confinement.

4.4.2. Square element simulation

The simulations were also repeated using a square mesh to investigate if the shape of the mesh elements affect the extent of failure simulated in the pillar. An element size of 1 m^2 was arbitrarily selected, and it was therefore larger than that of the triangular element mesh. The APS that was obtained from the TEXAN model using rigid pillars was 37.2 MPa, which is slightly lower than the one obtained from the latter's simulation. This smaller value is attributed to the larger element sizes. Napier and Malan (2011) illustrated the effect of decreasing element sizes on APS values. The mesh generated for the single pillar layout is shown below.

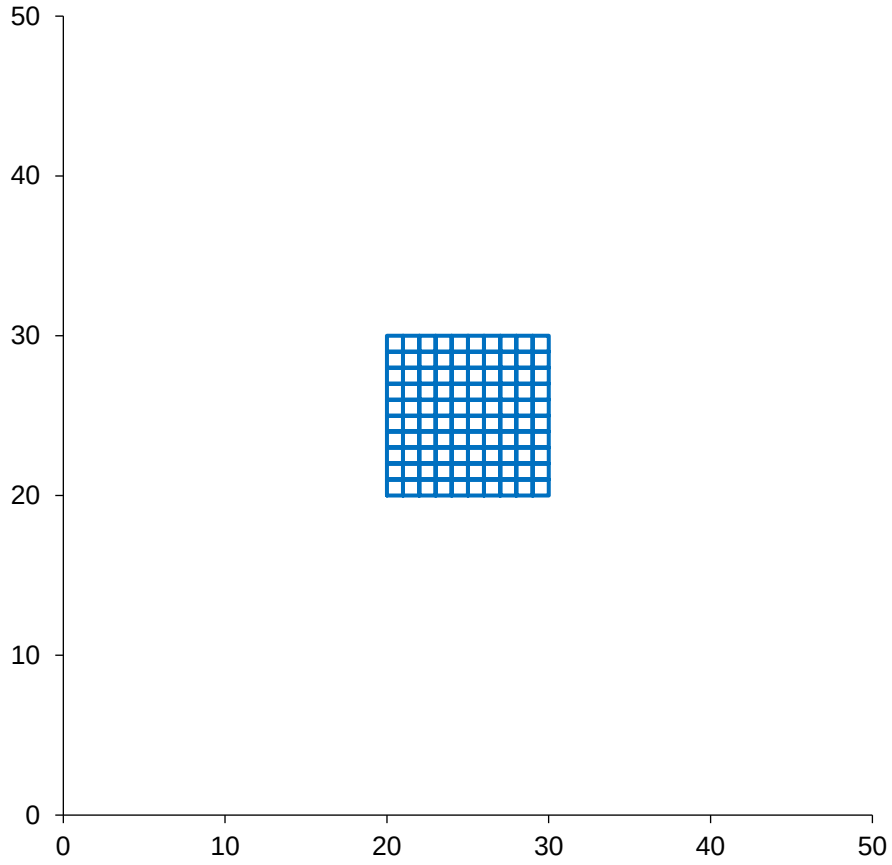

Figure 4-10. Square element mesh for the single pillar geometry.

Table 4-3 summarises the APS values and number of failed elements that were obtained from the LEM models with varying levels of confinement.

Table 4-3. The simulated pillar stresses and failure for different levels of confinement for a square mesh.

Magnitude of confinement	Percentage of failed elements (%)	APS (MPa)
0 MPa	64	19.7
0.1 MPa	64	20.1
0.2 MPa	64	20.6
0.5 MPa	64	21.8
1 MPa	40	24.3
2 MPa	36	25.9

The simulated stresses are approximately similar to those obtained using the triangular mesh. The percentage of failed elements is, however, similar for the smaller confinement values of 0 MPa to 0.5 MPa and only decreases for a value of 1 MPa. This square mesh is clearly less sensitive to the level of confinement, and this is caused by the element shapes. An important conclusion is therefore that if square elements are preferred, small element sizes need to be used. Figure 4-11 is the plot of the pillar stress along Section A-A' (see Figure 4-5). This plot is subtly different compared to Figure 4-7 and it illustrates that the stress profiles are essentially similar for the 0 MPa to 0.2 MPa levels of confinement. The mesh elements are therefore not small enough for these small amounts of confinement. Smaller elements need to be used and a triangular mesh may be preferable. This effect of square element size for a different application was also noted by Malan and Napier (2018) and care should be exercised with the square elements. The failed zones on the edges of the pillars and the decrease in the length of this failed zone are nevertheless still visible for this square mesh.

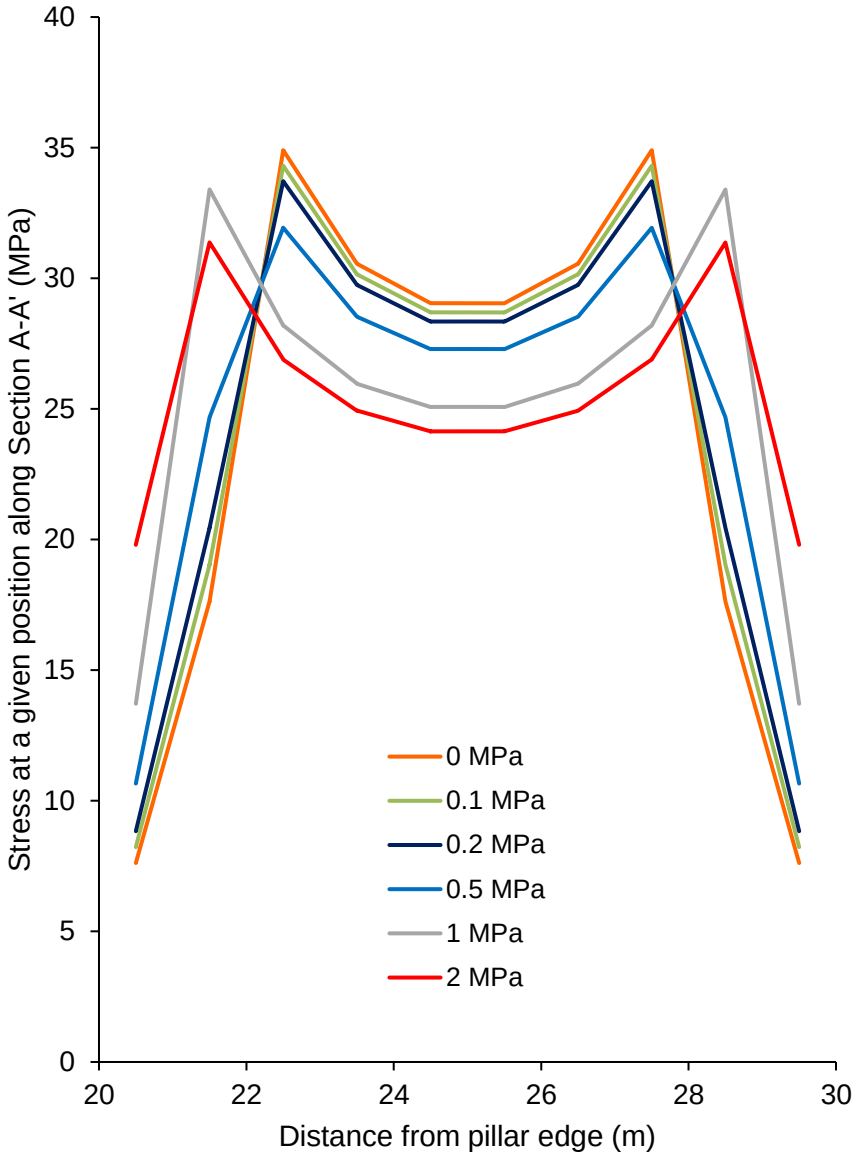

Figure 4-11. A plot of the simulated stresses for Section A-A' across the pillar. This was for a square element mesh.

The plots of the failed portions and intact cores for the pillars of the various simulations are given in Figure 4-12. These plots again highlight that the larger square elements are less sensitive to the level of confinement and values of 0 MPa, 0.1 MPa, 0.2 MPa and 0.5 MPa gave the same number of failed elements and size of intact core.

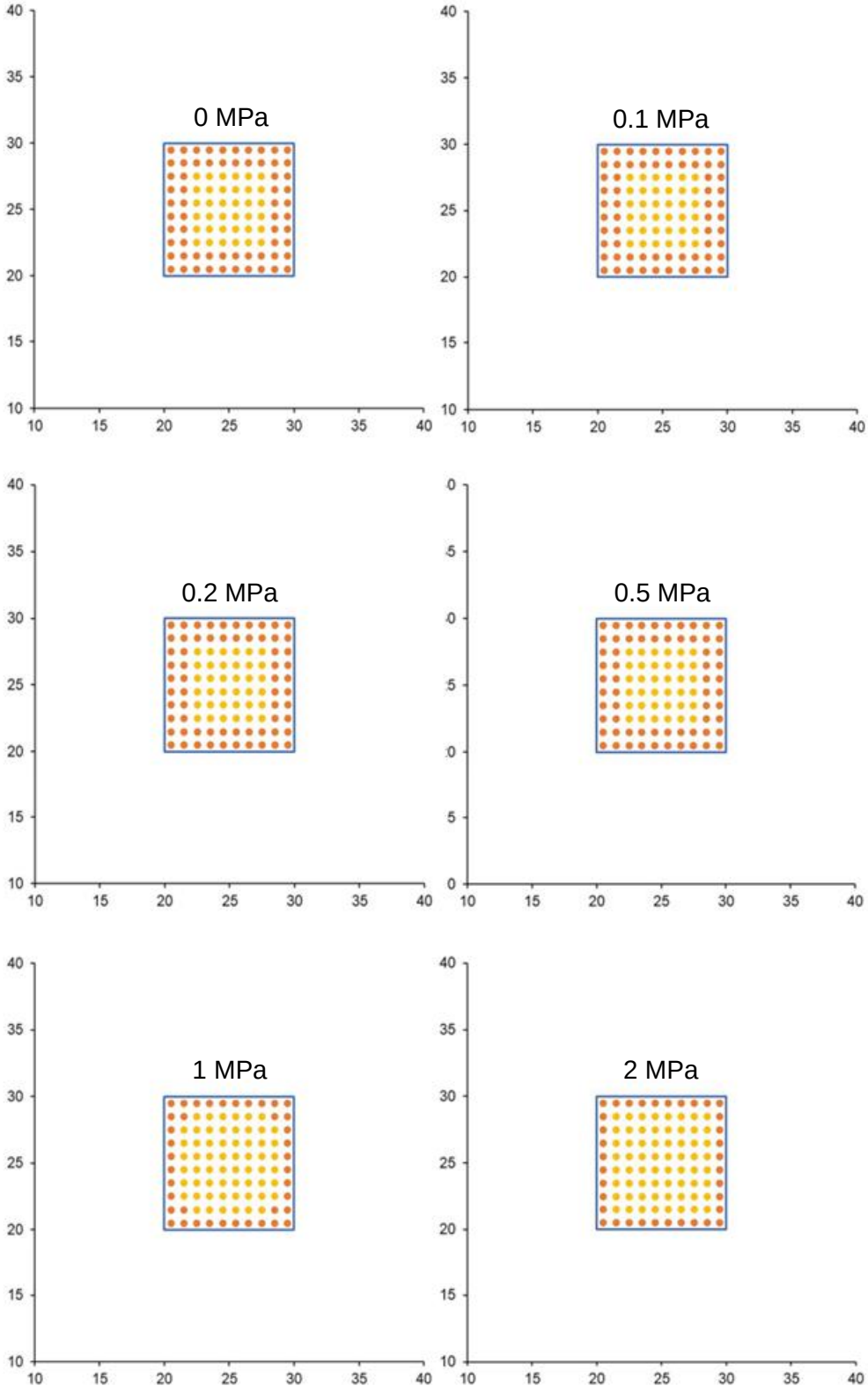

Figure 4-12. Pillar failure plots for a square mesh with varying amounts of confinement. The yellow dots are elements that are still intact, and the orange dots are failed elements.

4.5. Numerical modelling of a regular bord and pillar layout

Additional modelling was conducted using a regular bord and pillar layout consisting of 100 pillars (10 rows and 10 columns) to gain further insight into the behaviour of the confinement model. The pillars were first simulated as rigid pillars, followed by LEM simulations where the pillars could fail.

4.5.1. Geometry and simulations using rigid pillars

The pillar layout, shown in Figure 4-13, was simulated using a pillar size of 7 m × 7 m and a bord width of 8 m. These dimensions are typical of that used in the Bushveld Complex (see Chapter 5) and it gives an extraction ratio of 78%. The diagram is not drawn to scale and the layout was simulated at an arbitrary depth of a 1000 m. As mentioned above, the element size that is used affects the simulated APS and as small as possible elements need to be used. Napier and Malan (2011) have shown that the simulated APS approximates the analytical values more closely if the element size tends to zero. Small element sizes are therefore preferred for the numerical models. The effect of element size was also studied in this chapter.

Figure 4-13. A regular 100-pillar layout.

The initial simulations of the regular layout were modelled using both triangular and square elements to investigate the APS values predicted by the different element types and sizes. Two different triangular element sizes and two square element sizes were simulated. Table 4-4 gives the general model parameters.

The APS value as predicted by TAT for this pillar size and bord width is given by:

$$APS_{TAT} = \frac{3000 \times 10 \times 1000}{1 - 0.782} = 137.6\ MPa \qquad \textbf{[4-18]}$$

Note that this study focussed on the APS values for the pillars within the red outline in Figure 4-13. The outer pillars were not considered due to their proximity to the simulated abutments. It was also

tedious to mesh all 100 pillars using triangular elements as the mesh generator available to the author requires that each pillar be meshed individually.

Table 4-4. Parameters used for the numerical models.

Parameter	Value
Young's Modulus, E (GPa)	70
k-ratio	1
Average overburden density, ρ (kg/m^3)	3 000
Poisson's ratio, v	0.25

4.5.1.1. Triangular element simulations

For the triangular element model, average element sizes of ≈ 0.3 m^2 and ≈ 0.8 m^2 were selected. One of the meshes that was generated is shown in the figure below. The pillars of interest also had to be meshed to compute the APS values, but these meshes are not shown in the figure.

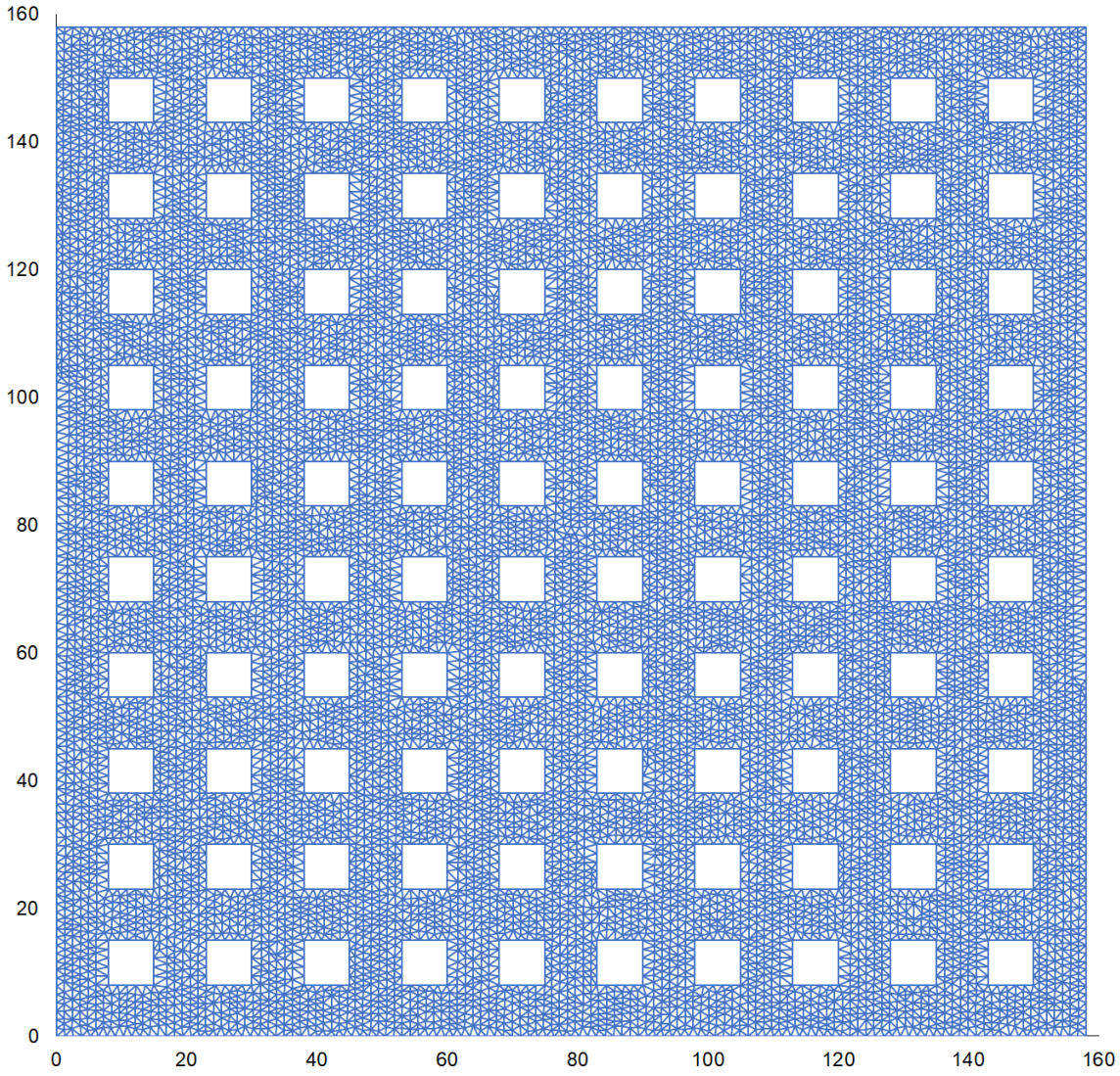

Figure 4-14. Triangular element mesh for the 100-pillar layout with the ≈ 0.8 m^2 element size.

Figure 4-15 below illustrates the different simulated APS values for a row of pillars (see Figure 4-13 for the pillar numbers) for the triangular mesh numerical models. This is compared to the TAT value. The table containing the values is given in APPENDIX A.

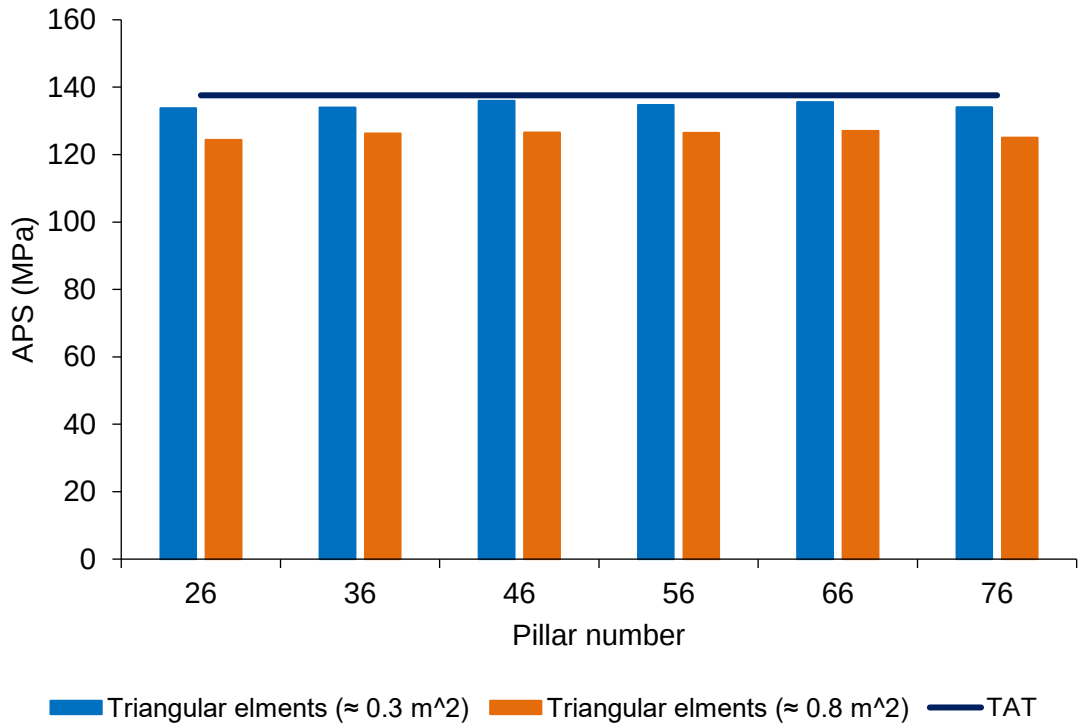

Figure 4-15. Simulated APS values obtained from the triangular meshes relative to the TAT calculated APS.

From the chart, the APS values are the lowest for the outermost pillars, which share their loads with the abutments, for both meshes and increase towards the centre of the layout. Pillars 46 and 56, which are in the centre of the layout, possess similar APS values.

4.5.1.2. Square element simulations

Numerical models were also generated using square elements, and element sizes of 0.25 m^2 and 1 m^2 were selected. The mesh shown in Figure 4-16 has an element size of 1 m^2.

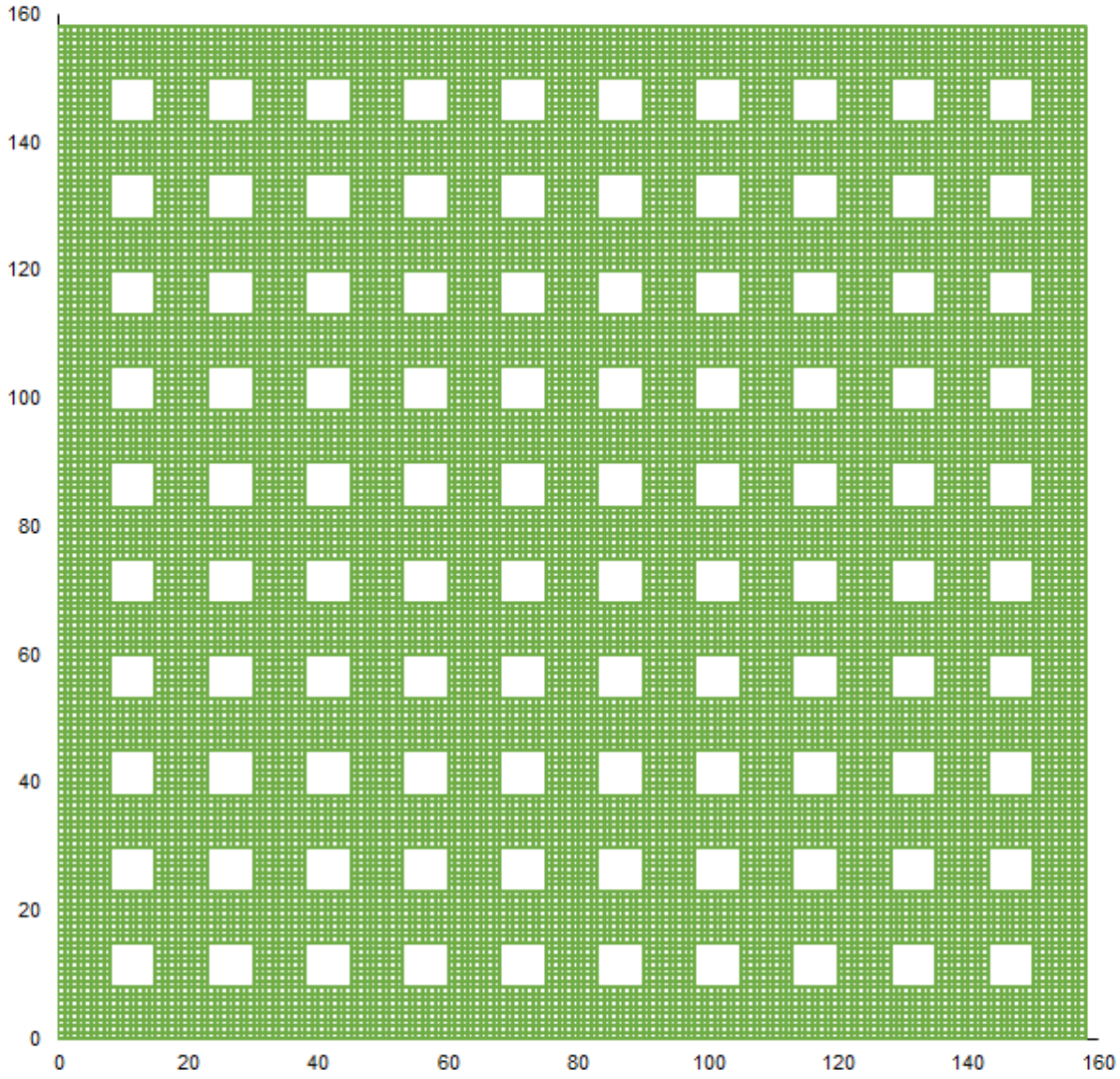

Figure 4-16. Square element mesh for the 100-pillar layout using an element size of 1 m^2.

Figure 4-17 illustrates the simulated APS values across a row for the square element models compared to TAT. Similar to the results of the triangular elements, the APS values are the lowest for the outermost pillars close to the abutments and increase towards the centre of the layout. As expected, the simulated values are lower than the TAT APS for both models. The results also confirm that a more accurate APS solution is obtained for smaller element sizes.

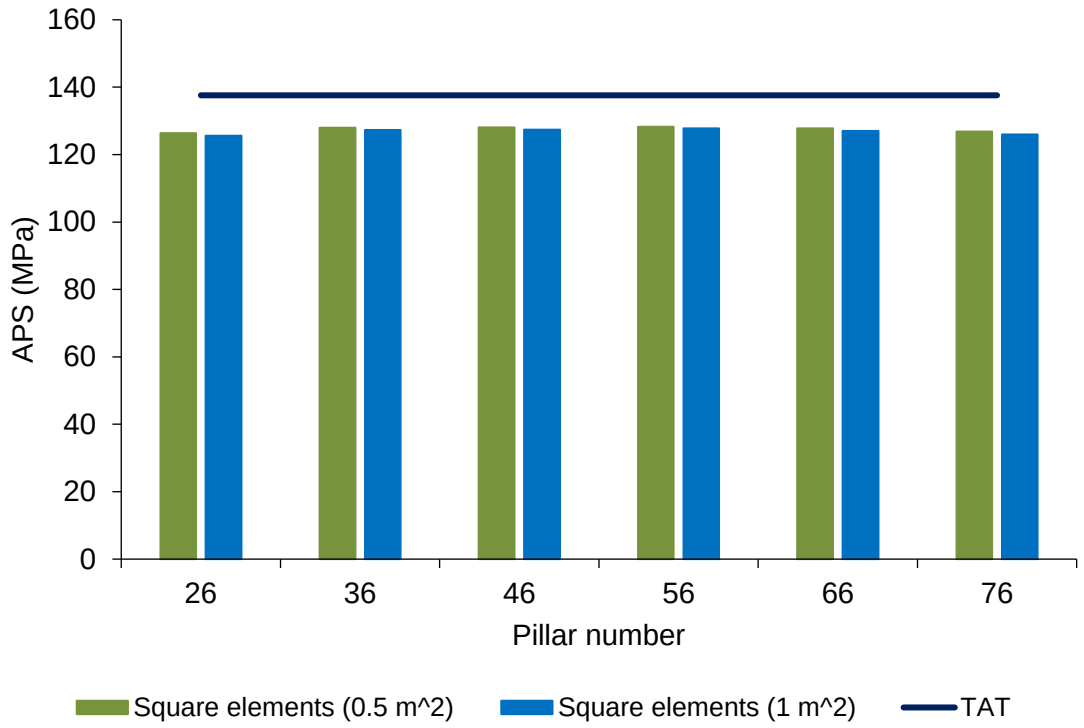

Figure 4-17. Simulated APS values obtained from the square meshes relative to the TAT calculated APS.

In summary, it was found from the models that the largest simulated APS values are in the middle of the excavation. As expected, the pillars closer to the abutments have lower values. The simulated values are lower than the TAT APS value. This is also correct as TAT assumes an infinitely large excavation in both directions. Similar to Napier and Malan (2018), it was found that smaller element sizes result in larger simulated APS values. The bar charts for both the square and triangular meshes illustrate this clearly. For these displacement discontinuity simulations, the smallest possible element sizes should therefore be used.

4.5.2. Limit equilibrium model

The objective of simulating the larger model was to study the effect of using backfill on pillar extraction. This is described in Section 4.6 below. As a first step, the 100-pillar layout was therefore also simulated at a depth of a 1000 m using the LEM constitutive model to study the failure of the pillars for different magnitudes of applied confinement. The parameters in Table 4-5 were used for the model. Note that these were again arbitrary parameters to ensure that the pillars fail and to investigate the effect of different levels of backfill confinement.

Table 4-5. Parameters used for the limit equilibrium model.

Parameter	Value
Intact strength intercept, σ_c^i (MPa)	50
Intact strength slope, m^i	7
Initial residual strength intercept, σ_c^f (MPa)	5
Initial residual strength slope, m^f	7
Seam height, H (m)	5.5
Overburden density, ρ (kg/m^3)	3 000
Intact rock Young's Modulus, E (GPa)	70
Intact rock Poisson's ratio, v	0.25
Intact seam stiffness modulus, k_s (MPa/m)	12 727
Fracture zone interface friction angle (°)	30

4.5.2.1. Pillar failure for a triangular element simulation

Figure 4-18 illustrates the pillar failure when there is no confinement. The ≈ 0.8 m^2 mesh size was used for these simulations. Figure 4-19 to Figure 4-22 illustrate the effect of increasing confinement. The intact core increases in size as the confinement increases. Note that only the sixteen pillars in the centre of the large 100-pillar model are plotted here, and not all the pillars shown in Figure 4-13.

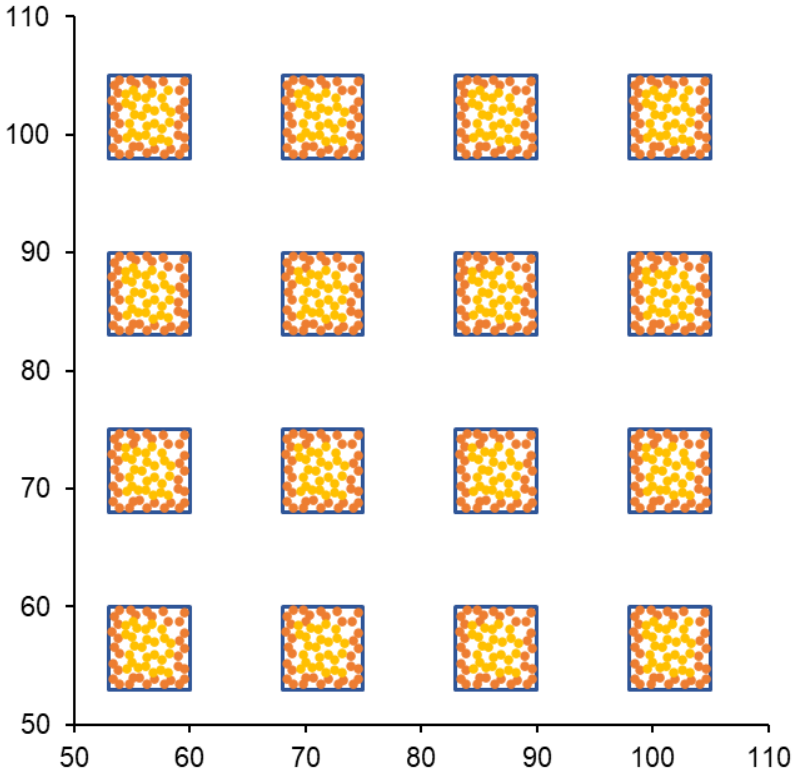

Figure 4-18. LEM plot for ≈ 0.8 m^2 triangular mesh without confinement.

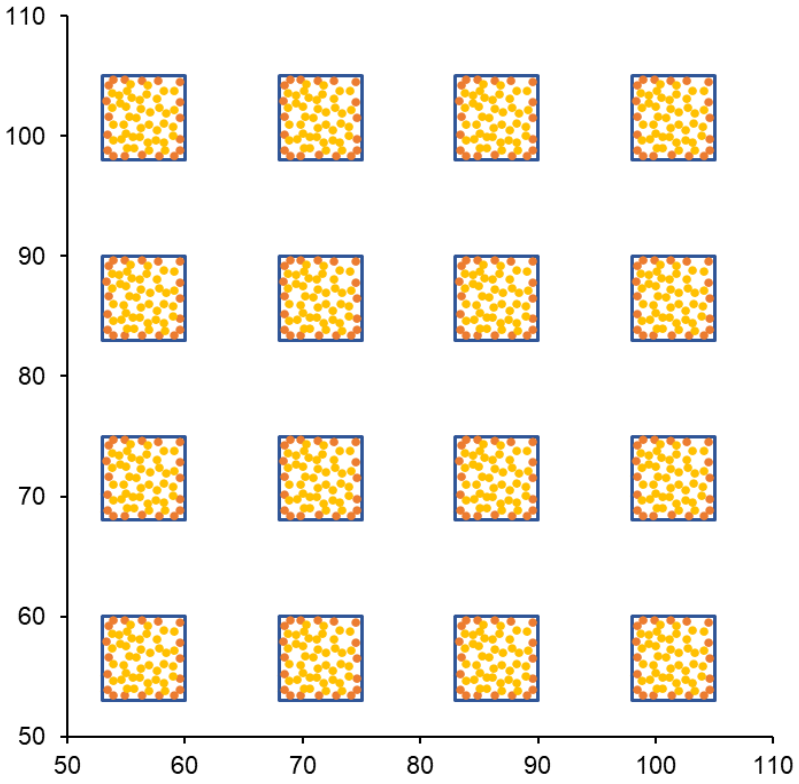

Figure 4-19. LEM plot for ≈ 0.8 m^2 triangular mesh with 0.5 MPa confinement.

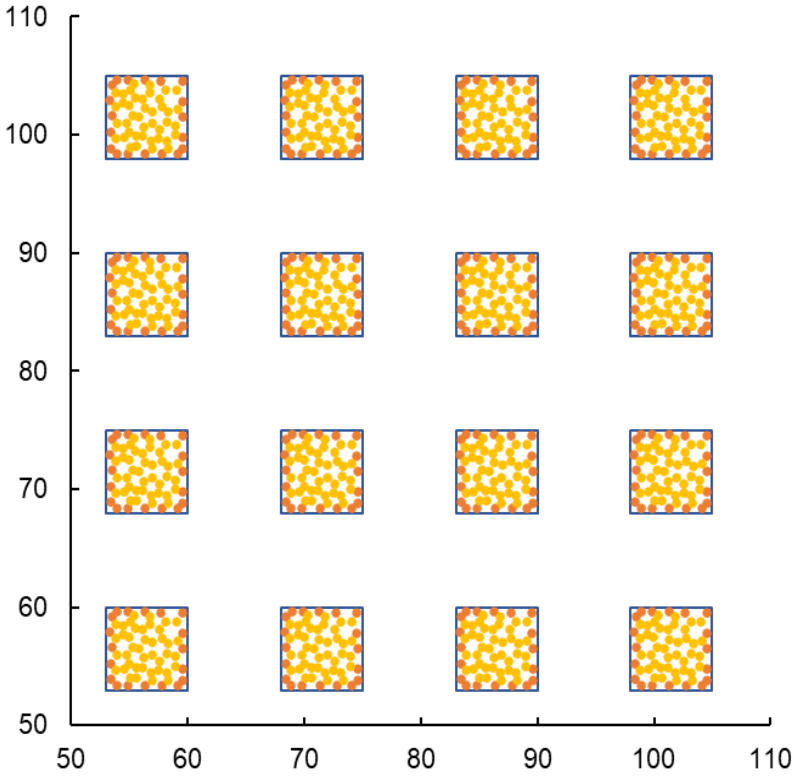

Figure 4-20. LEM plot for ≈ 0.8 m^2 triangular mesh with 1 MPa confinement.

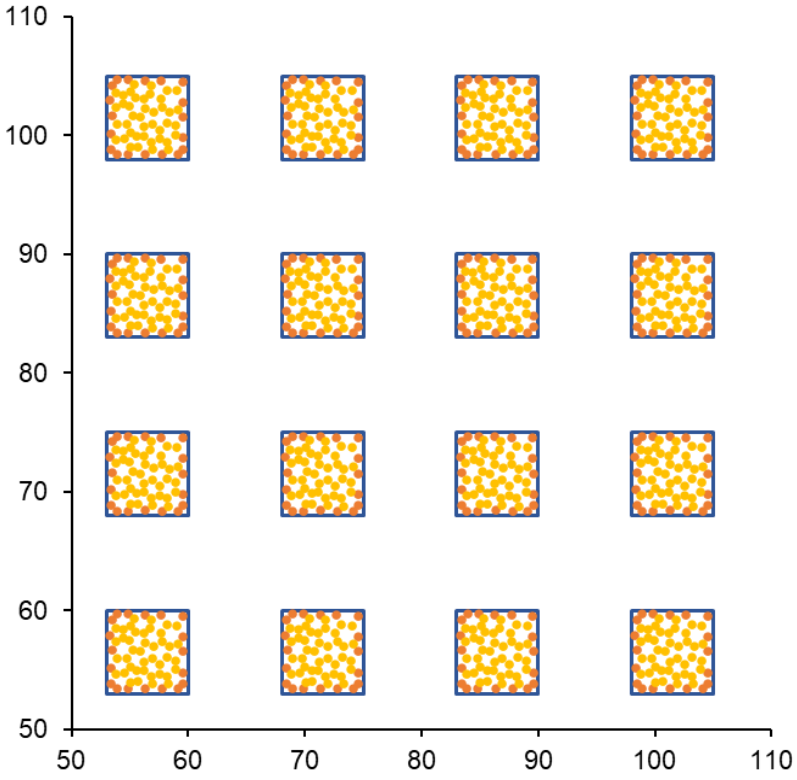

Figure 4-21. LEM plot for ≈ 0.8 m^2 triangular mesh with 1.5 MPa confinement.

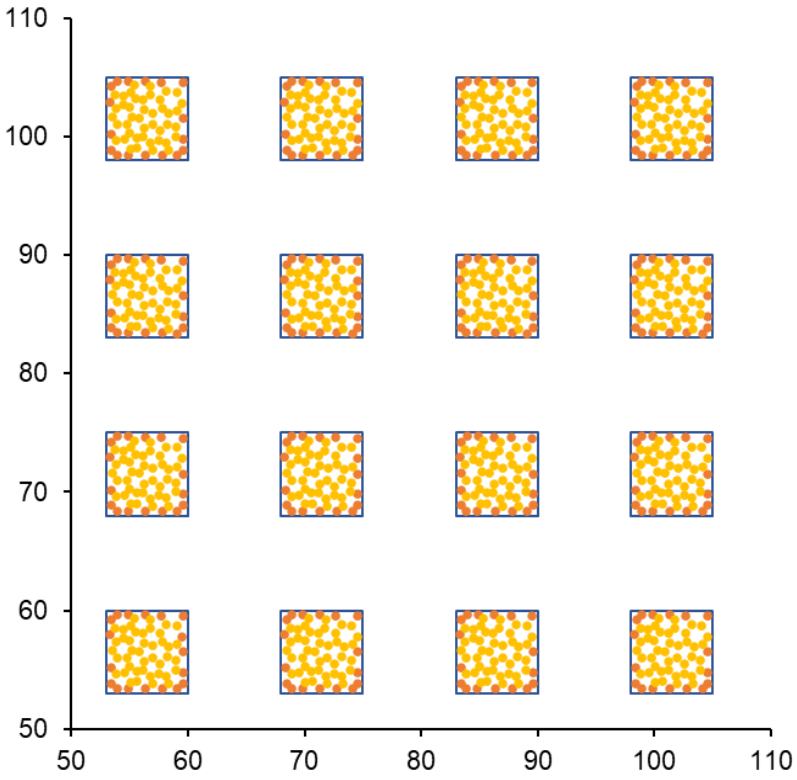

Figure 4-22. LEM plot for ≈ 0.8 m^2 triangular mesh with 2 MPa confinement.

Table 8-6 in APPENDIX B contains the APS values that were simulated using the LEM confinement model. As expected, the trend is that the APS increases for each pillar with an increase in confinement. Figure 4-23 illustrates the APS values obtained by using the LEM model for a row in the centre.

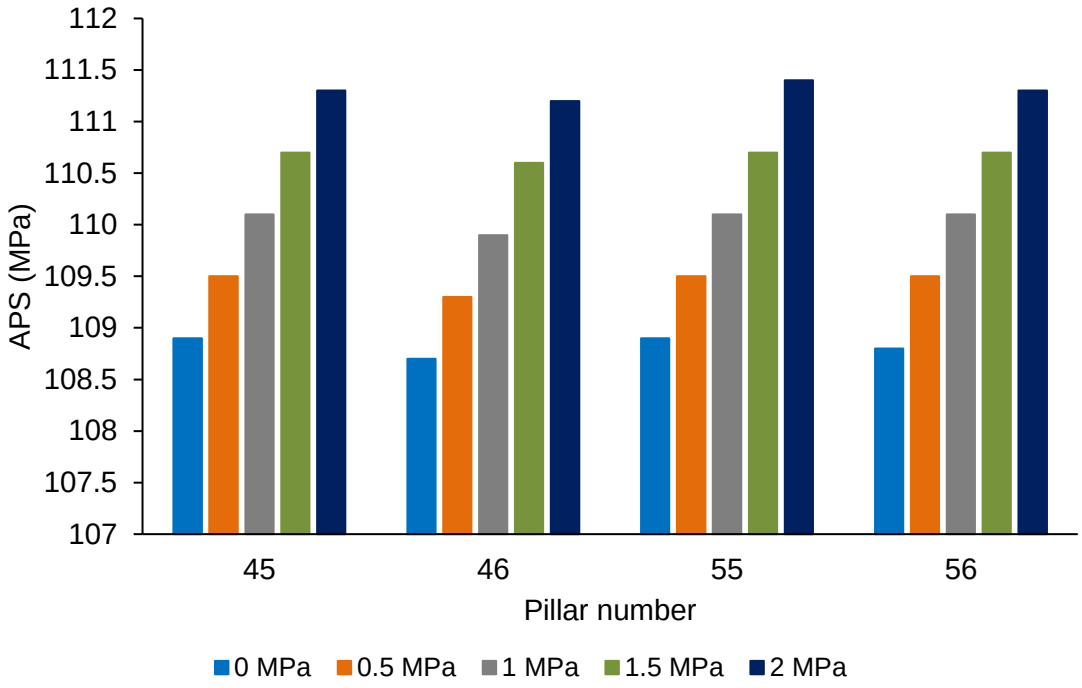

Figure 4-23. Simulated APS values by using a LEM failure model for the triangular mesh.

Figure 4-24 shows how the APS values increased for Pillar 46 as the level of confinement increased for the two triangular meshes. This pillar was selected due to its central position in the regular layout.

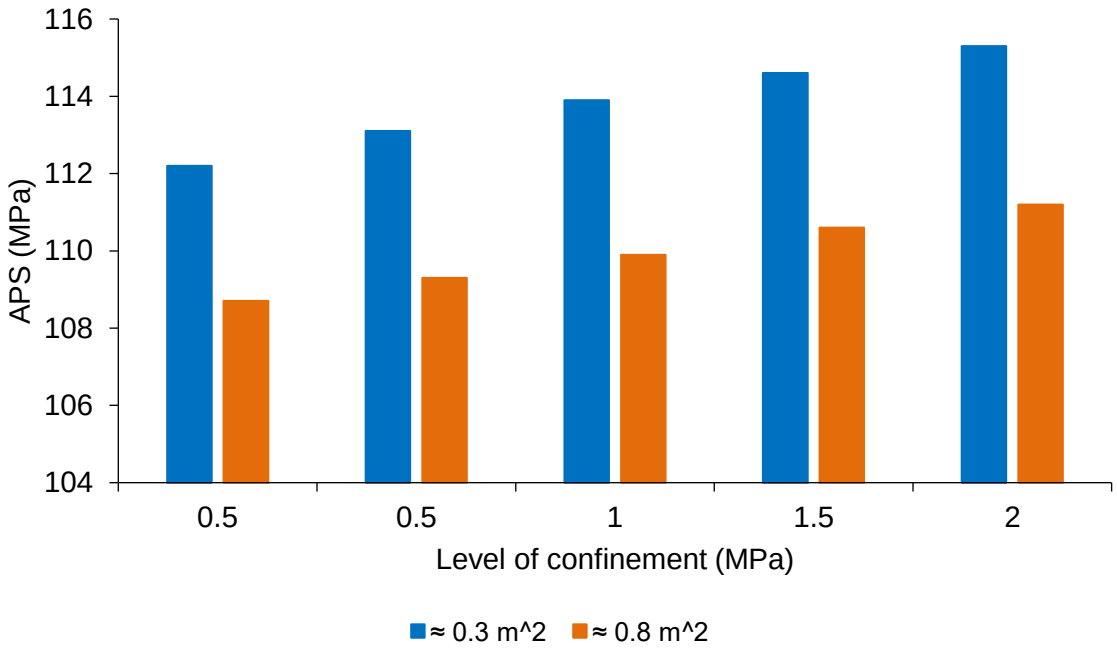

Figure 4-24. Simulated APS values for Pillar 46 using the LEM failure model for the two triangular element sizes.

4.5.2.2. Pillar failure for a square element simulation

The results obtained for the square element mesh illustrated a similar trend to the triangular element mesh simulations. The APS increases with confinement, and this is illustrated in Figure 4-25.

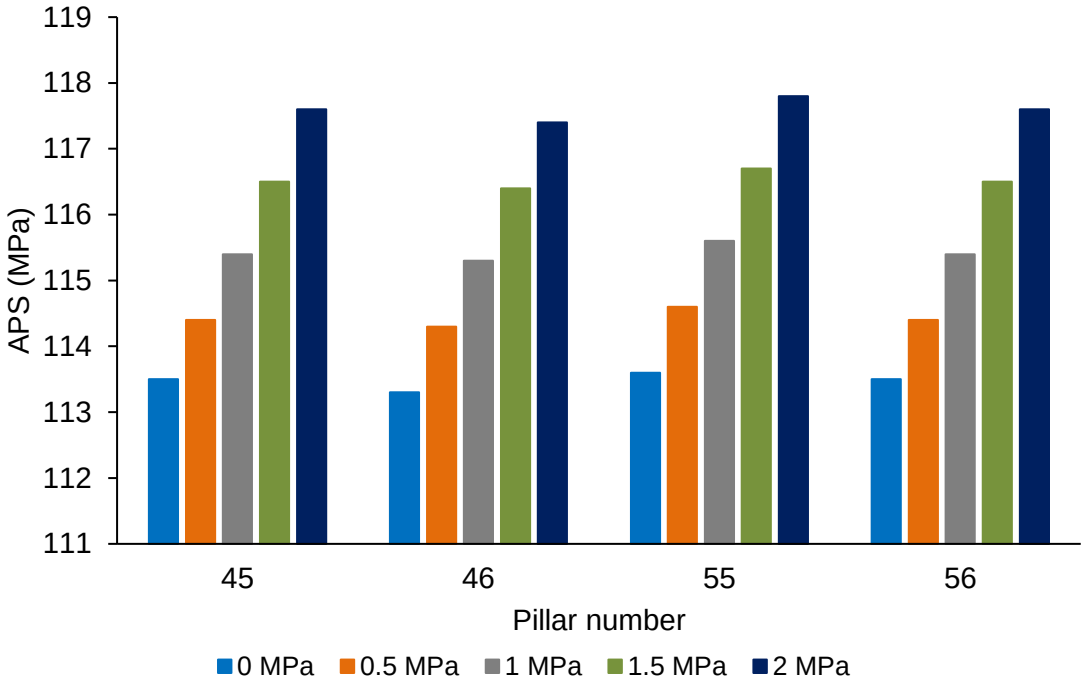

Figure 4-25. Simulated APS values by using a LEM failure model for the 0.25 m^2 square mesh.

Table 8-7 in APPENDIX B contains the LEM APS values that were obtained using each pillar's elements for the 0.25 m^2 element size. Figure 4-26 below illustrates the effect of element sizes on the simulated APS values.

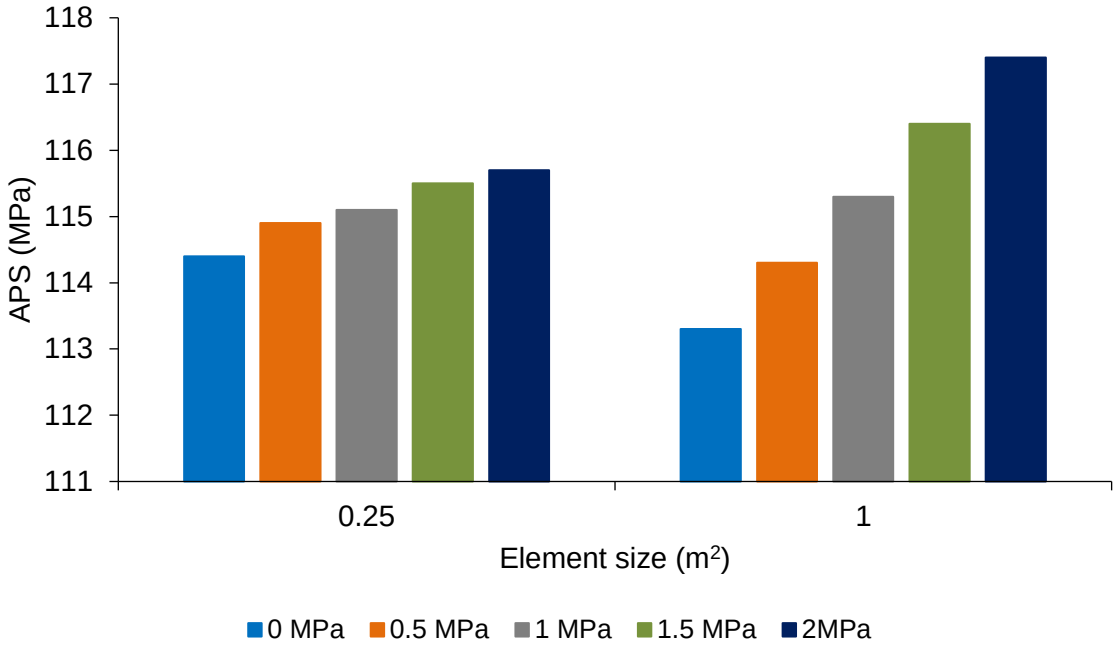

Figure 4-26. Simulated APS values for Pillar 46 using the LEM failure model for both square element sizes.

4.6. Simulating the effect of pillar extraction and sequence

A key aspect of studying the effect of backfill is to investigate whether some of the existing pillars can be extracted. In this section, a pillar mining sequence was studied. The 100-pillar idealised layout was used for this preliminary modelling to simulate how the pillars are affected by the extraction of adjacent pillars. The triangular element size of ≈ 0.8 m^2 was used.

To simulate a mining sequence in TEXAN, the constitutive code of the pillars being mined must be changed. Two mining options were studied. In the first sequence, the pillars were mined in quadrants in a sequence that resembles a checkerboard. This is shown in Figure 4-27. The pillars marked with crosses were first extracted and the remaining pillars in each quadrant were only then supported with backfill. The top left quadrant was mined first, with the other quadrants mined in a clockwise manner thereafter. Practical mining considerations, such as pumping the backfill and containing it in a particular quadrant, were not considered here and it is purely an academic exercise. In the second sequence, the entire area was first filled with backfill and then the same pillar extraction sequence followed as described above. This is not a practical sequence, but it was done as an academic study to illustrate the importance of the timing of backfill placement.

To clearly illustrate the value of pillar confinement, the properties of the LEM were downgraded compared to the simulations above. This made the pillars weaker. Table 4-6 illustrate the parameters used.

Table 4-6. Parameters used for the limit equilibrium model.

Parameter	Value
Intact strength intercept, σ_c^i (MPa)	20
Intact strength slope, m^i	5
Initial residual strength intercept, σ_c^f (MPa)	5
Initial residual strength slope, m^f	5
Seam height, H (m)	5.5
Depth (m)	1 000
Overburden density, ρ (kg/m^3)	3 000
Intact rock Young's Modulus, E (GPa)	70
Intact rock Poisson's ratio, v	0.25
Intact seam stiffness modulus, k_s (MPa/m)	12 727
Fracture zone interface friction angle (°)	30

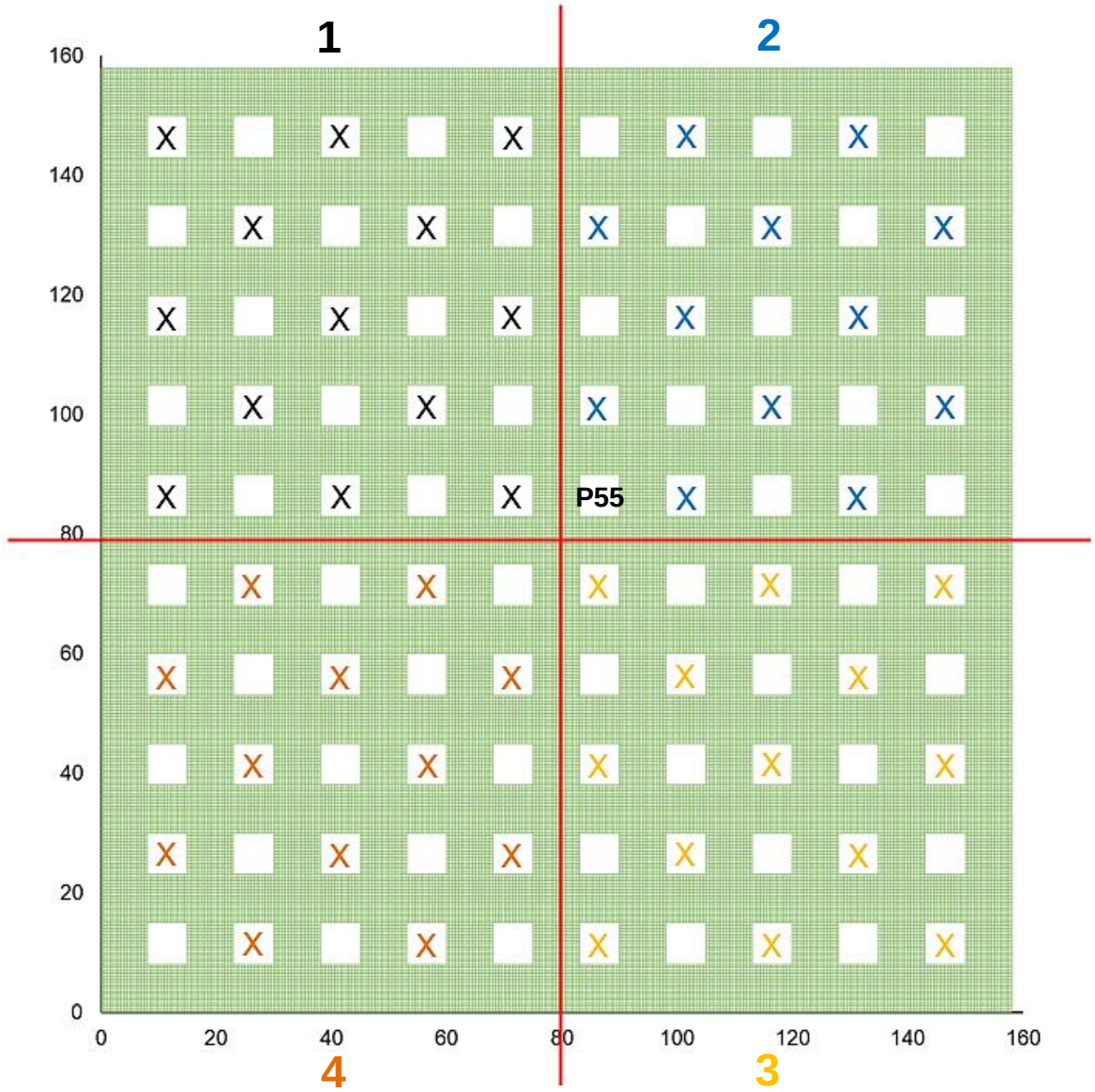

Figure 4-27. Mining sequence for the regular 100-pillar mining layout. The pillars marked with the crosses were mined out.

As described above, two sequences were simulated. The details of each are summarised below:

Sequence 1

1. Simulate and solve the rigid pillars (all four quadrants).
2. Allow pillar failure with a LEM simulation without any backfill (all four quadrants).
3. Extract the pillars in next quadrant (starting with first quadrant).
4. Place backfill of 0.5 MPa confinement in the quadrant that was mined.
5. Solve.
6. Repeat from step 3.

Sequence 2

1. Simulate and solve the rigid pillars (all four quadrants).
2. Allow pillar failure with a LEM simulation with backfill of 0.5 MPa (all four quadrants).
3. Extract the pillars of interest in quadrant 1 and solve.
4. Extract the pillars of interest in quadrant 2 and solve.
5. Extract the pillars of interest in quadrant 3 and solve.
6. Extract the pillars of interest in quadrant 4 and solve.

Sequence 2 is therefore placing backfill everywhere beforehand and Sequence 1 is only placing backfill in each quadrant in sequence and only after its pillars were mined.

4.6.1. Sequence 1

The table in APPENDIX C contains the APS values that were obtained for the initial elastic model with rigid pillars as well as from the LEM simulation following the pillar extraction and the confinement of the remaining pillars. The APS values for the outermost pillars were excluded from the table due to their proximity to the abutments.

The results correctly indicate that the APS values are highest for the pillars located in the quadrant where the pillar extraction has occurred. This occurs because of the higher extraction ratio. Additionally, the values for the confined pillars that remained at the end of the extraction are higher. Following the pillar extraction in each quadrant, the APS values of the remaining pillars increase owing to the gradually increasing overall extraction ratio.

Figure 4-28 to Figure 4-32 illustrate the pillar failure for the mining sequence.

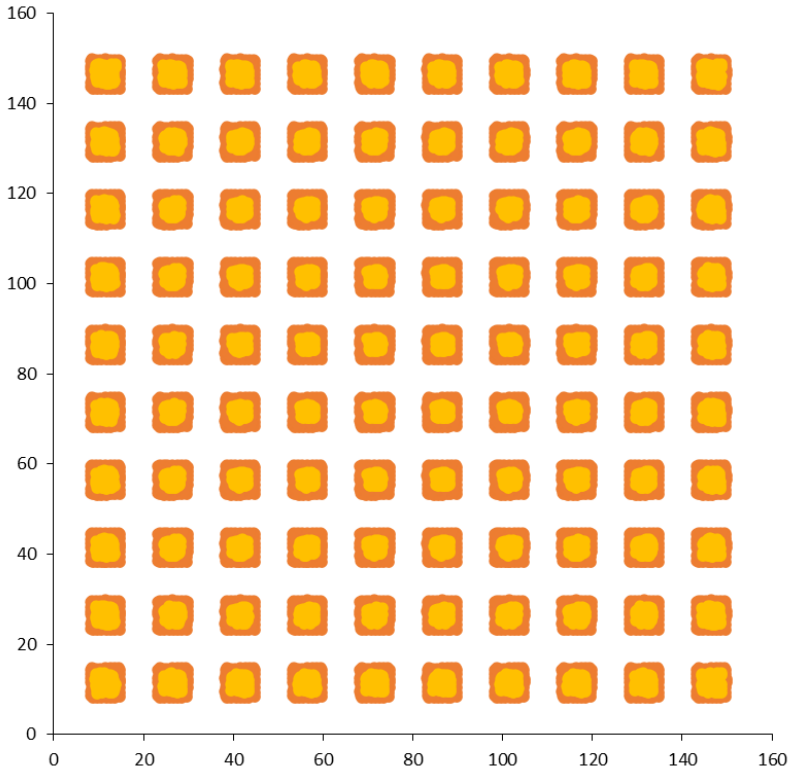

Figure 4-28. LEM plot of layout without backfill.

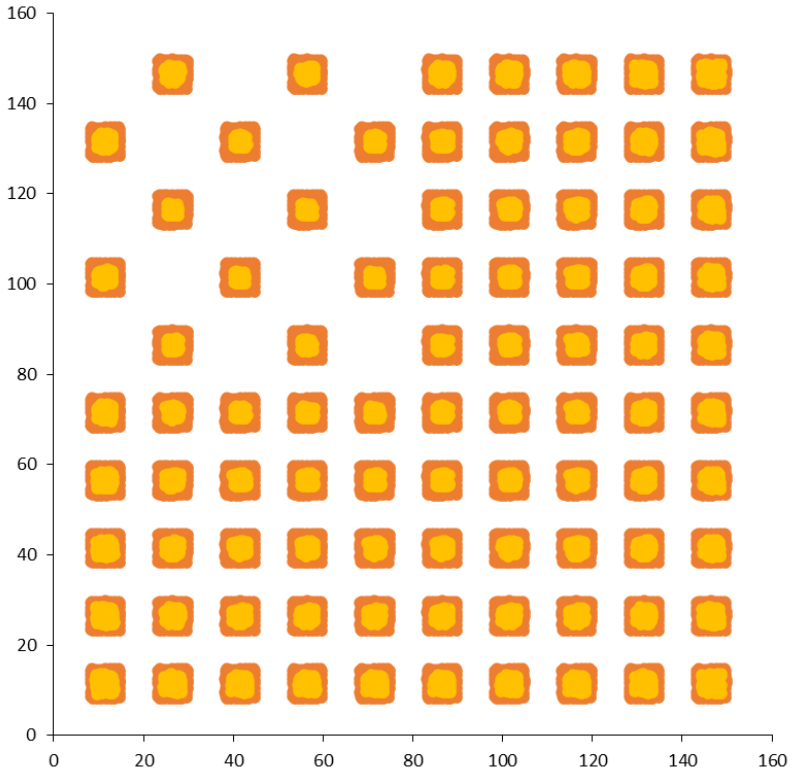

Figure 4-29. LEM plot following pillar confinement and pillar extraction in 1st Quadrant.

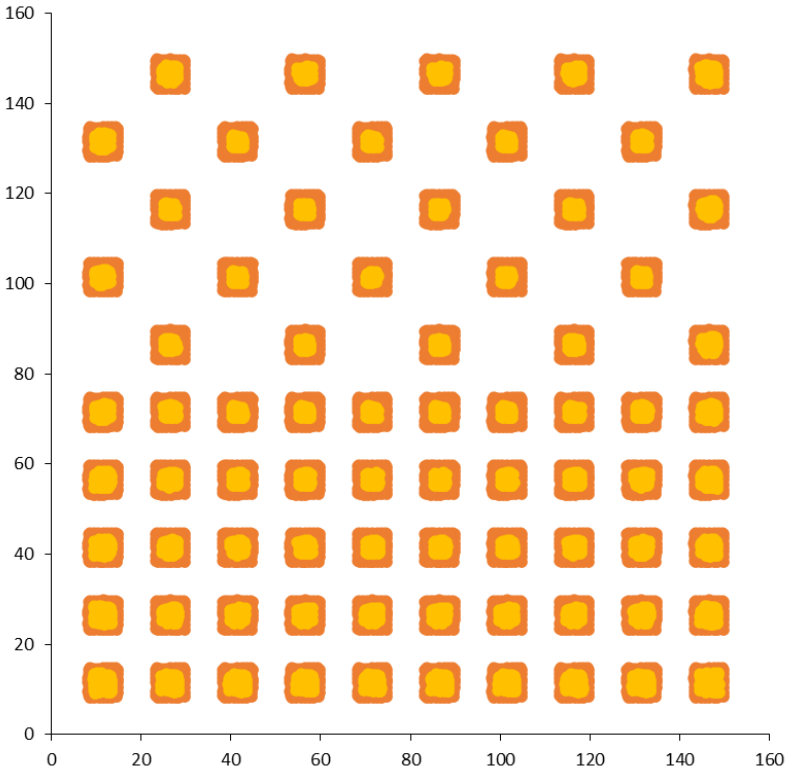

Figure 4-30. LEM plot following pillar confinement and pillar extraction in 2nd Quadrant.

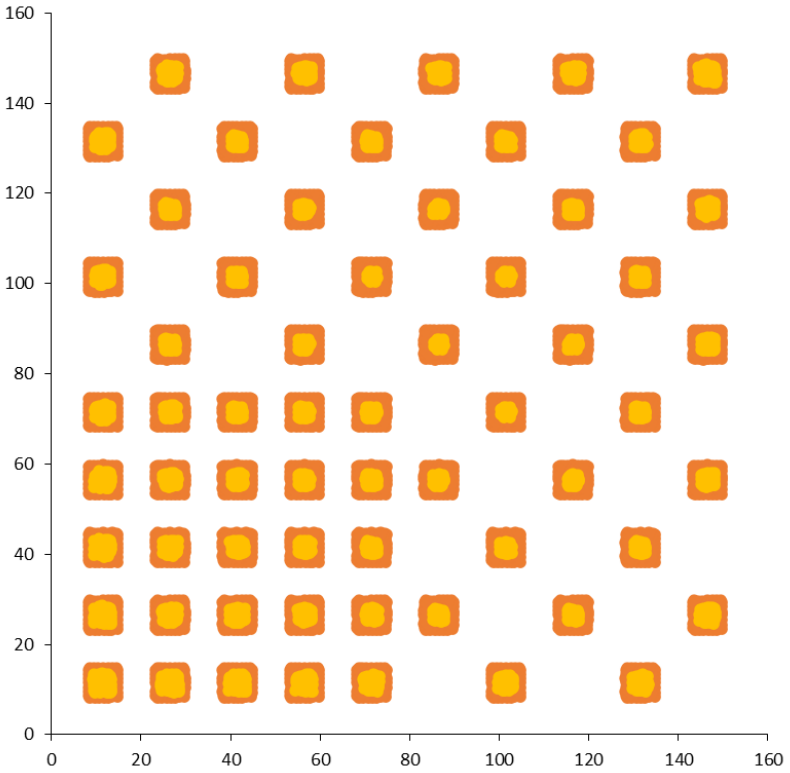

Figure 4-31. LEM plot following pillar confinement and pillar extraction in 3rd Quadrant.

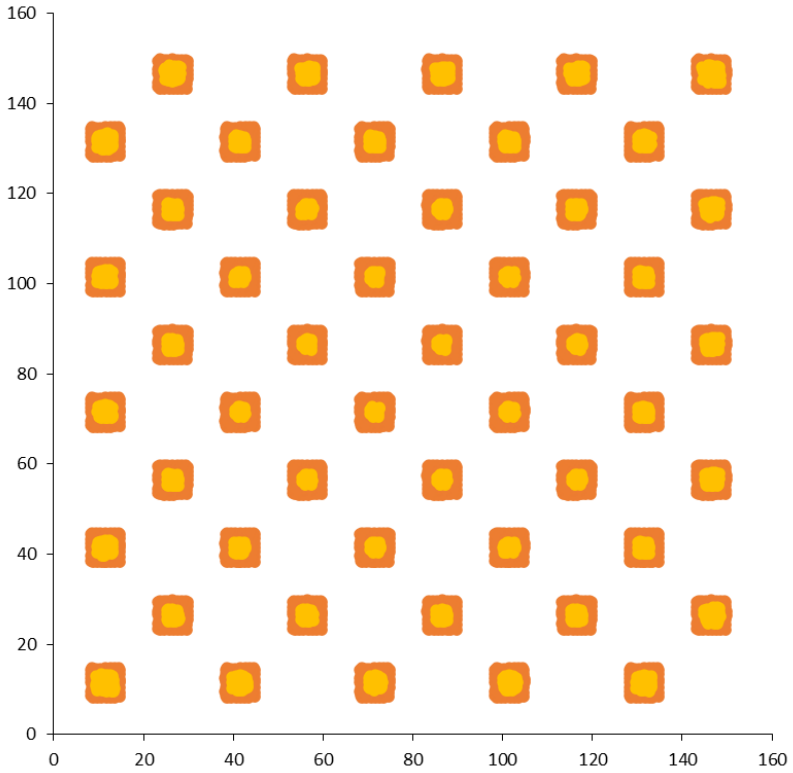

Figure 4-32. LEM plot following pillar confinement and pillar extraction in 4th Quadrant.

From the figures, the size of the intact core reduces considerably throughout the mining of the layout. This is particularly noticeable in the centremost pillars, which are highlighted in Figure 4-33 below. The reduced cores suggest that the amount of confinement was not sufficient to strengthen the pillars following the extraction. This sequence of backfill placement therefore does not seem of particular value in practice.

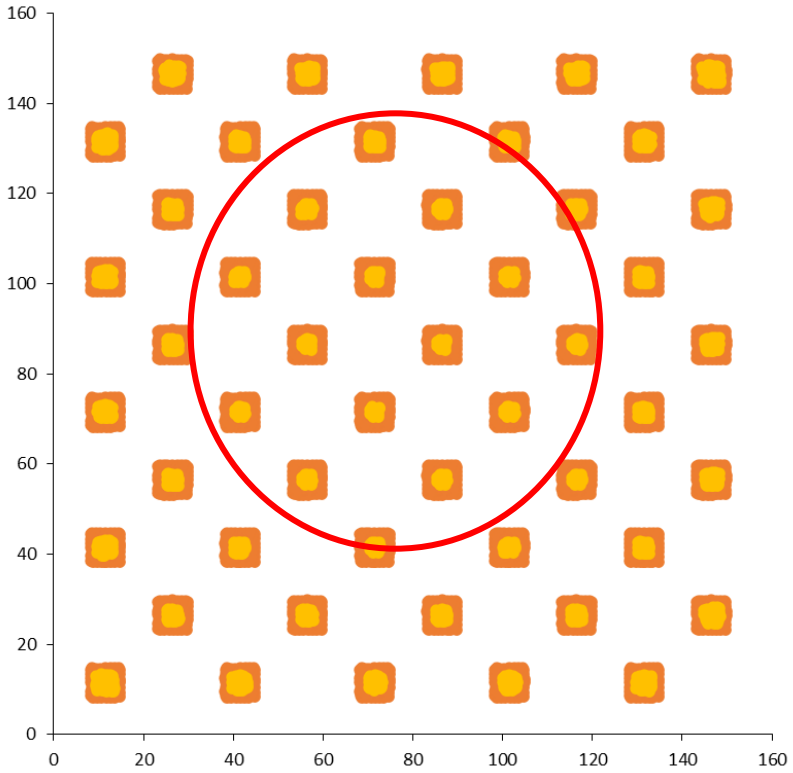

Figure 4-33. The pillars' intact core at the end of the mining sequence.

4.6.2. Sequence 2

The figures below illustrate the results for the mining for Sequence 2. The APS values that were obtained for the rigid pillars as well as for each step of the pillar extraction can be found in APPENDIX D.

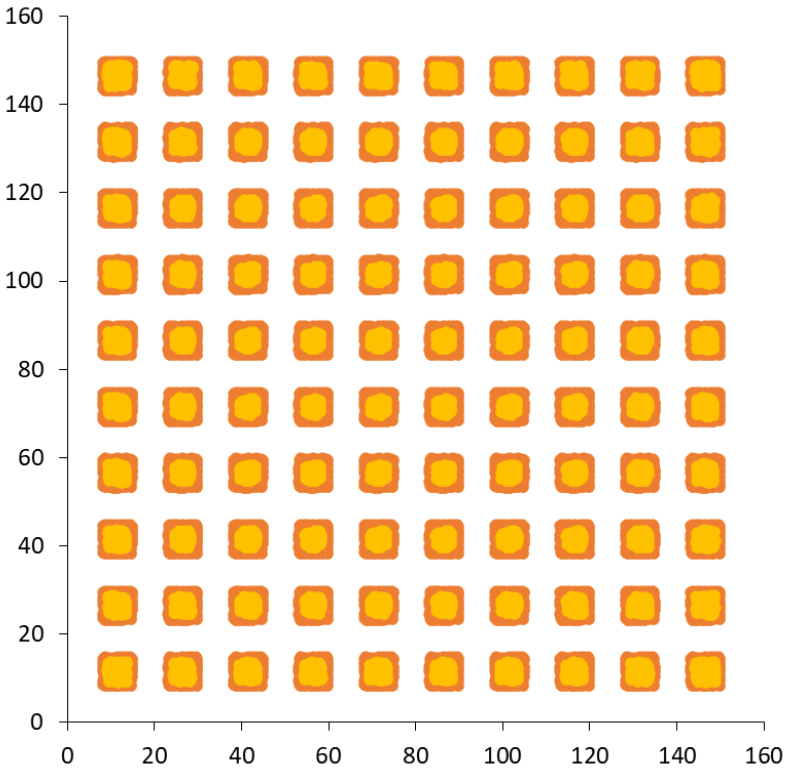

Figure 4-34. LEM plot of layout with backfill of 0.5 MPa prior to pillar extraction.

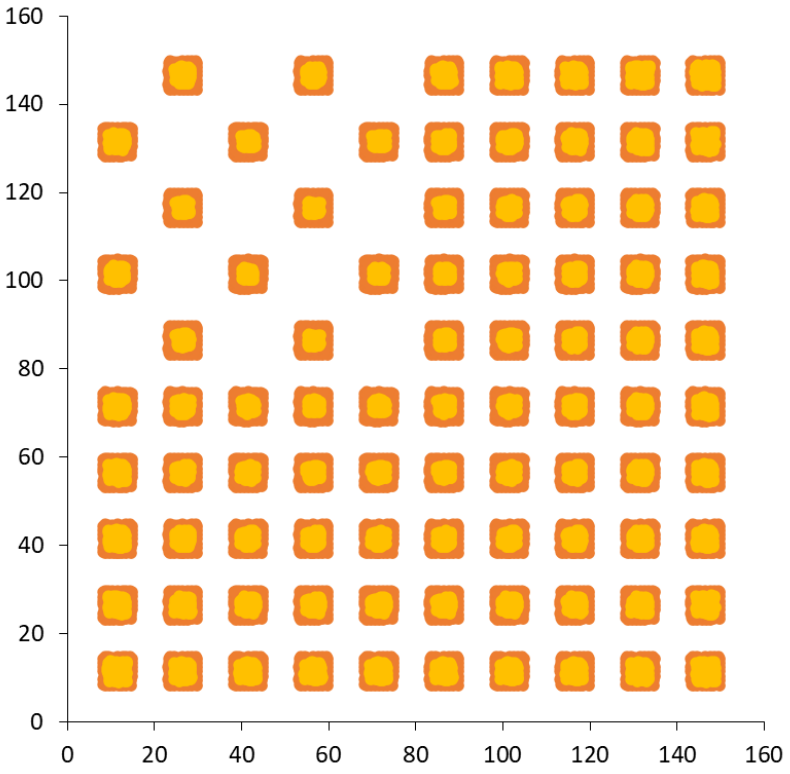

Figure 4-35. LEM plot of pillar extraction in 1st Quadrant with backfill of 0.5 MPa.

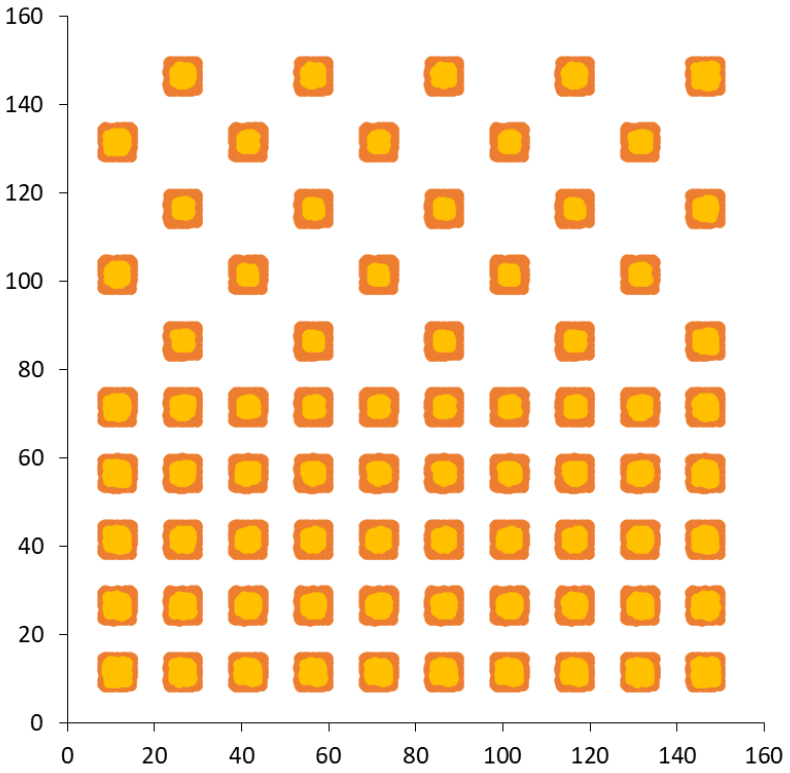

Figure 4-36. LEM plot of pillar extraction in 2nd Quadrant with backfill of 0.5 MPa.

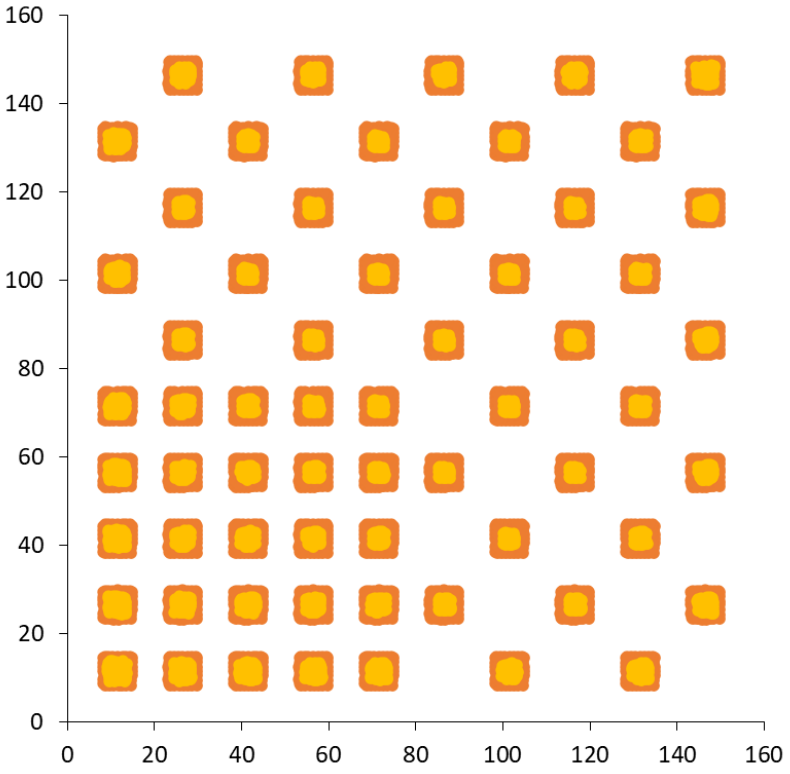

Figure 4-37. LEM plot of pillar extraction in 3rd Quadrant with backfill of 0.5 MPa.

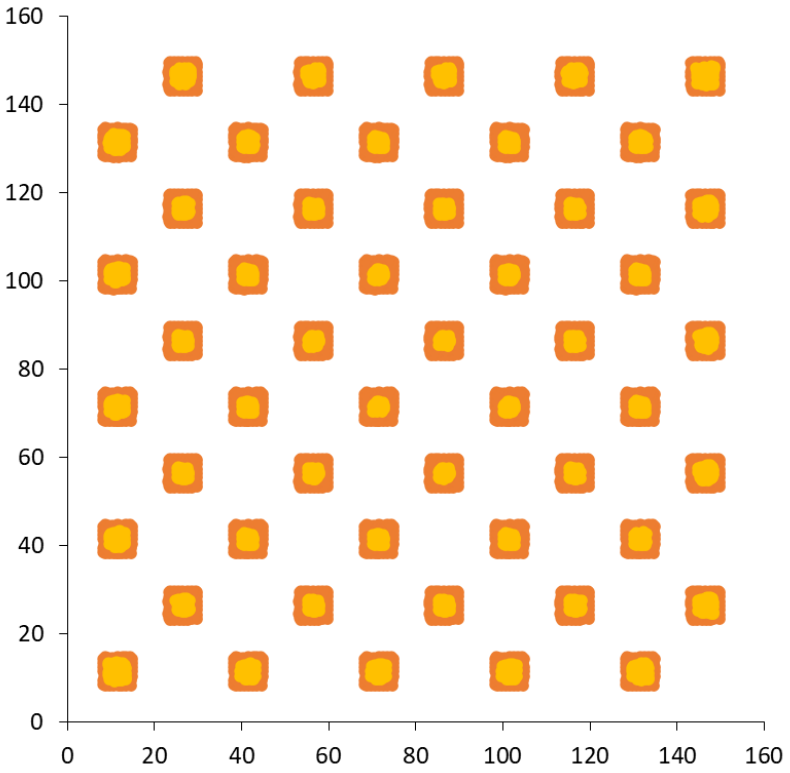

Figure 4-38. LEM plot of pillar extraction in 4th Quadrant with backfill of 0.5 MPa.

Table 4-7 illustrates the failure per pillar for both sequences after all pillar mining was completed. The pillar numbers refer to those shown in Figure 4-13. Of interest is that the percentage failed elements for Sequence 2 is less for many pillars. This is expected as the entire area was backfilled before any pillar mining was done and the pillars are confined from the start. The difference in pillar failure is not significant, however, and this is attributed to the small confinement of 0.5 MPa applied.

Table 4-7. The percentage of failure per pillar remaining after mining Quadrant 4 for both sequences.

Pillar number	Sequence 1 – Percentage of failed elements (%)	Sequence 2 – Percentage of failed elements (%)
13	81	78
15	81	81
17	81	81
19	80	77
22	81	78
24	85	81
26	87	82
28	82	81
33	85	81
35	88	84
37	87	82
29	81	81
42	81	81
44	88	84
46	88	85
48	86	82
53	86	82
55	88	85
57	87	84
59	82	81
62	81	81
64	87	82
66	87	84
68	85	81
73	82	81
75	86	82
77	86	81
79	81	79
82	78	77
84	81	81
86	82	81
88	81	79

Table 4-8 shows how the values increased for Pillar 55 in the layout, highlighted in Figure 4-27, throughout the mining sequences. The pillar was selected because of its central location relative to the mined-out pillars in the first three quadrants to demonstrate how the APS values increased with the mining of each quadrant.

Table 4-8. Simulated APS values for Pillar 55 throughout Sequence 1 and 2.

Sequence	No backfill confinement / no failure	1st Quadrant mining	2nd Quadrant mining	3rd Quadrant mining	4th Quadrant mining
Sequence 1	104.4	110.9	119.8	125.7	128.7
Sequence 2	106.7	113.8	123.5	130.4	134.2

The APS of this pillar increased as the first quadrant was mined. An even greater increase occurred thereafter as an additional two pillars were extracted adjacent to P55 in the second quadrant. The changes indicate that the values are highest for the pillars located in the quadrant where the pillar extraction has occurred.

The chart shown in Figure 4-39 compares the APS values for both sequences. The stresses for Sequence 2 are higher as the pillar is confined from the start and the smaller amount of failure in the pillars result in higher stress being carried.

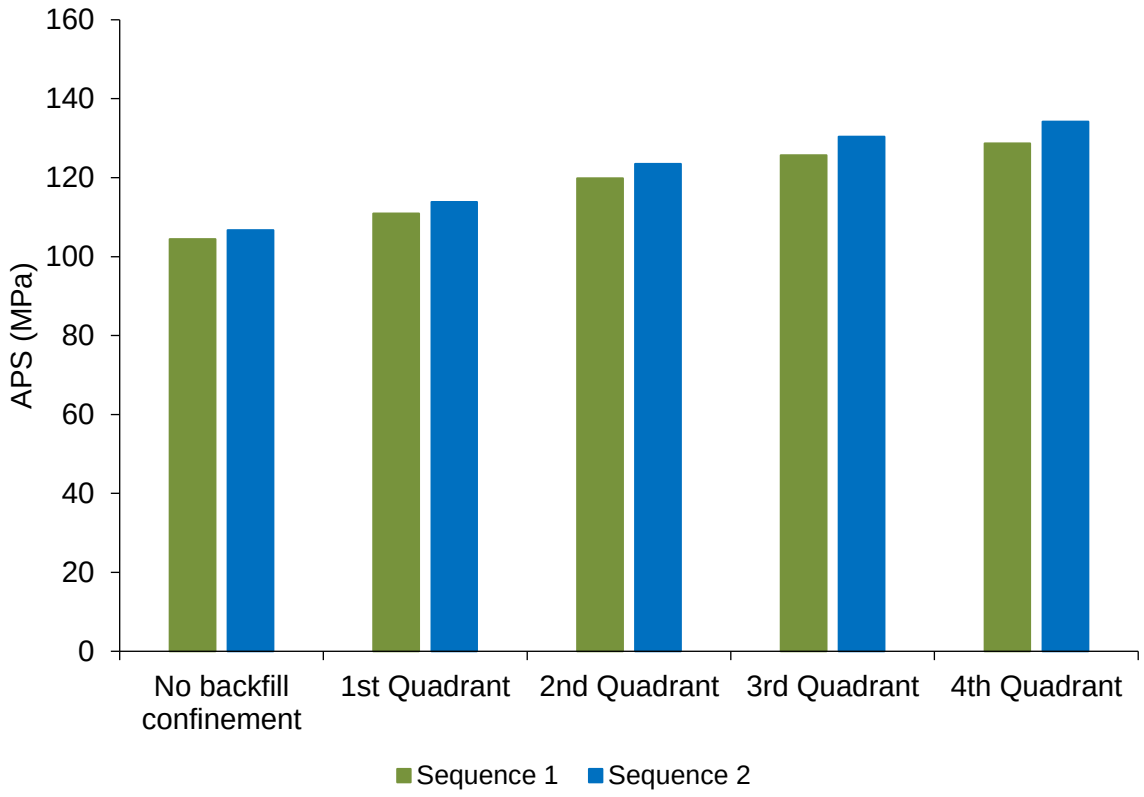

Figure 4-39. Comparison of simulated APS values for Sequence 1 and Sequence 2 for Pillar 55.

Although only a small difference in pillar behaviour was simulated for the two sequences above, the models are of value as they illustrate the potential of this constitutive model, implemented in a displacement discontinuity code, to simulate actual backfill placement problems in bord and pillar layouts. This can now be used in future to evaluate different sequences and the timing of backfill placement. Actual layouts with irregular pillars can also be simulated and this is illustrated in the next chapter.

5. NUMERICAL MODELLING OF AN UNDERGROUND LAYOUT

Backfilling is currently not used in the bord and pillar layouts of the Bushveld Complex and the numerical modelling is, therefore, a purely theoretical study to explore the potential benefits of backfill. In this chapter, numerical modelling of a shallow, mechanised platinum mine situated on the Eastern limb of the Bushveld Complex was conducted to illustrate the potential beneficial effects of backfill on pillar stability at greater depths. Decreasing extraction ratio at increasing depth is of concern to the mines and backfill may be a solution to mitigate this problem.

5.1. Pillar design methodology at the mine

Originally, a conservative approach was taken for the pillar design at the mine as a limited number of laboratory tests on the strength of the UG2 was available. The laboratory tests indicated an average UCS of 67.7 MPa and 94.1 MPa for the leader and main seam, respectively. The UCS of both the leader and main seams were higher for the point load tests that were conducted with values of 103 MPa and 100 MPa, respectively. All these tests were combined to give an average value of 91.4 MPa for the UG2. A K-value of 30 MPa was therefore assumed for the empirical pillar strength formula. This assumption of using a third of the UCS value ignores the complex composition of the pillar material and the weaker strength of the leader seam in some areas.

Regarding pillar design, a S_F of 1.5 was implemented, except for areas undermining a tailings dam which adopted a S_F of 2. Owing to the mountainous surface topography, the pillar width was kept constant in the design, but the length could be varied to increase pillar strength according to the overburden to be supported. If the equivalent width of the pillar exceeded 12, the squat pillar formula was used. The mining spans were kept constant at 10 m, and no allowance was made for future Merensky mining.

Owing to the low extraction ratio, a less conservative approach in terms of pillar strength was used by the mine and pillar sizes of 7 m × 7 m and 8 m bords were adopted. In September 2018, it was reported by the mine that pillar spalling was observed for fourteen pillars. The area of the mine that was simulated in TEXAN for this dissertation was specifically selected because of the minor pillar spalling observed in the area. It is shown in Figure 5-1.

To simplify the digitising of the outlines as well as the meshing procedure, the pillar outlines were approximated with straight line segments as illustrated in Figure 5-2. The figure also illustrates the pillar numbers used, with the pillars in the red outline being the pillars of interest. Although limited spalling was observed in this area, the pillars were rehabilitated with a line of resin tendon support

units all around the perimeters and the pillars were also covered with a 50-mm-thick, 35 MPa layer of shotcrete for additional confinement. The pillars appeared to be in a good condition, as shown in Figure 5-3.

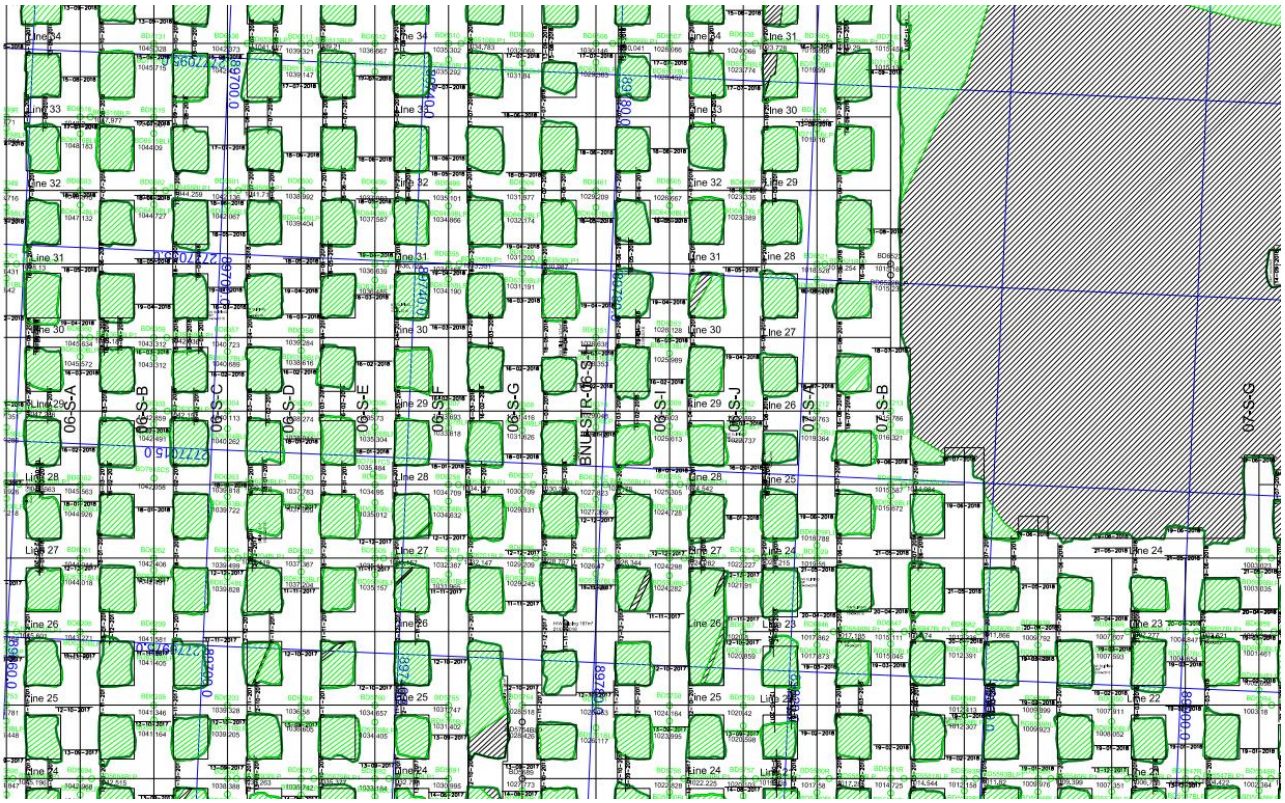

Figure 5-1. The area selected for the numerical modelling.

Figure 5-2. Simplified outlines of the pillars and the mining area.

Figure 5-3. Condition of a rehabilitated pillar (left) compared to most of the pillars in the area of interest (right) (courtesy of D. F. Malan).

For the modelling, the mined area was covered using a triangular mesh. As described in the previous chapter, it is known that when using displacement discontinuity boundary element modelling, the simulated APS is affected by element size. Small element sizes are therefore needed for these simulations to ensure an accurate LEM simulation. For the purposes of this study, the average element size was ≈ 0.4 m^2 and this was considered adequate for the APS calculations. This is significantly smaller than the typical 5 to 10 m^2 element sizes used in industry for the historic MINSIM simulations. Figure 5-4 and Figure 5-5 illustrate part of the mesh against the pothole and the mesh of pillar 73.

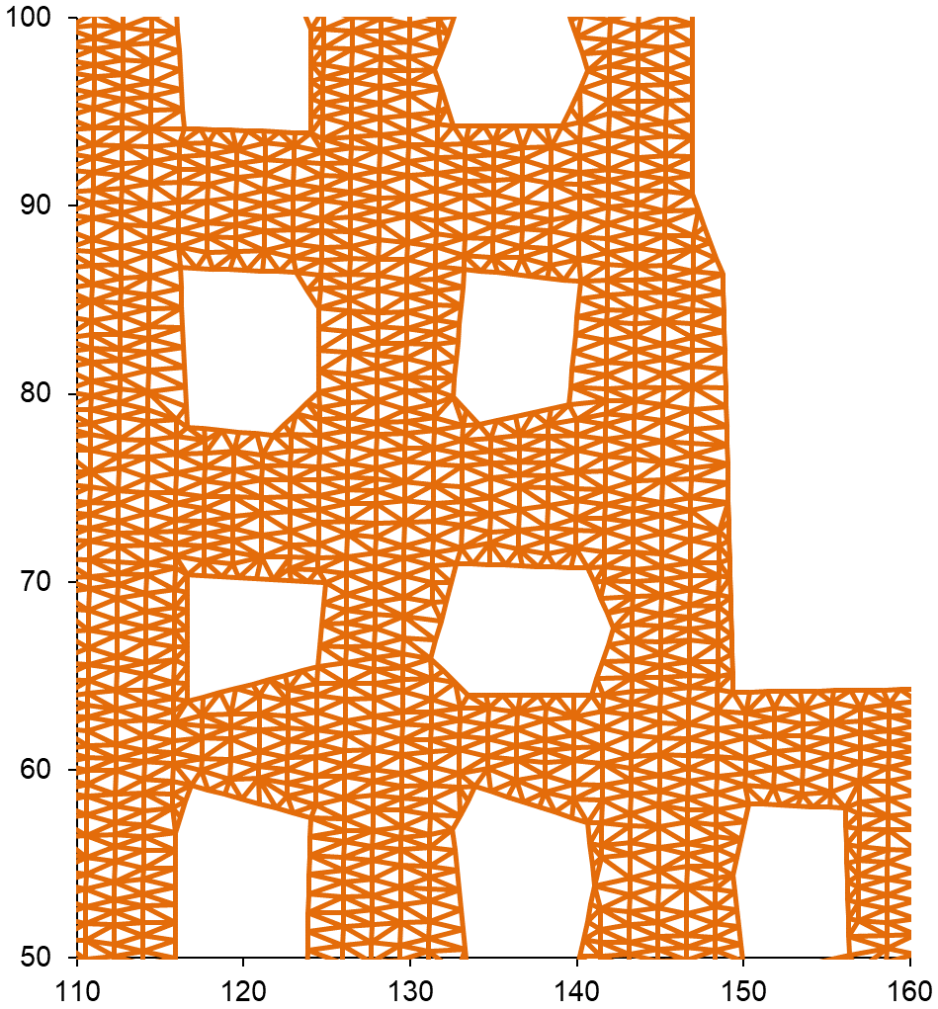

Figure 5-4. Example of the mesh generated to enable the simulation of the problem area for a portion of the area against the pothole.

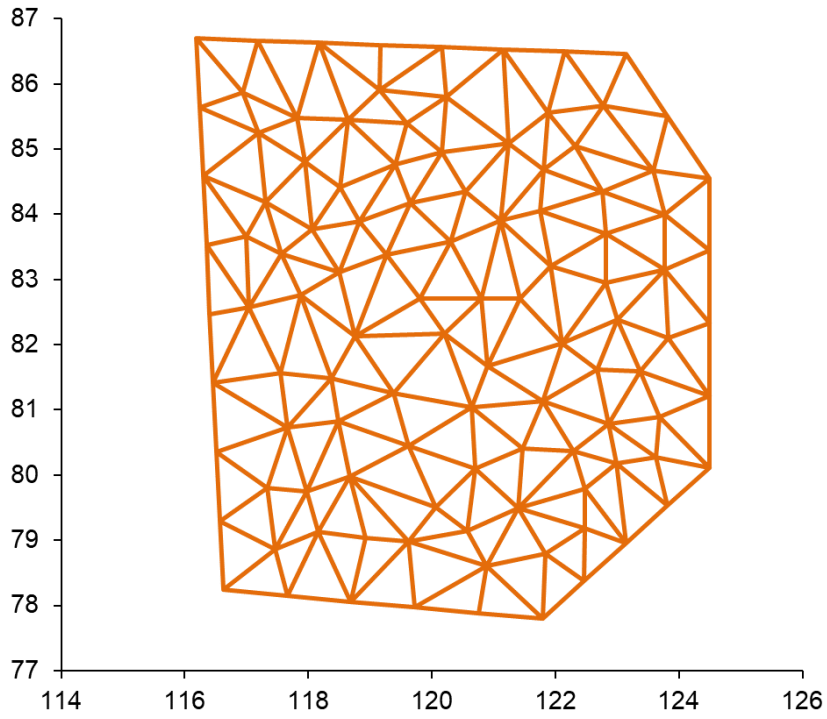

Figure 5-5. Example of the mesh generated for pillar 73.

5.2. Numerical modelling to simulate pillar spalling at increasing depths

The density of the overburden rock was assumed to be 3100 kg/m^3 and the depth of the excavation is approximately 290 m below surface. Although there are slight variations in depth in the area of interest, the excavation was assumed to be horizontal to simplify the model. The effect of shear stress on pillar strength is therefore not considered in this study. As described in previous chapters, the LEM as described above requires several parameters to be calibrated and these are listed in Table 5-1. The selected values were obtained from a back analysis of a pillar mining experiment at this particular mine (Napier and Malan, 2021). An extension of the model, not discussed in this paper, can allow for the time-dependent failure of the pillar material (Napier and Malan, 2014). This is typically not observed in shallow platinum mines and this effect was therefore ignored for this study. For the initial models, the effect of backfill was also ignored and no confinement was applied to the pillars.

Table 5-1. Parameters used to simulate the actual mining layout.

Parameter	Value
Intact strength intercept, σ_c^i (MPa)	60
Intact strength slope, m^i	7
Initial residual strength intercept, σ_c^f (MPa)	4
Initial residual strength slope, m^f	7
Seam height, H (m)	2.5
Intact rock Young's Modulus, E (GPa)	90
Intact rock Poisson's ratio, v	0.2
Intact seam stiffness modulus, k_s (MPa/m)	36 000
Fracture zone interface friction angle (°)	30

The selected parameters resulted in no spalling of the pillar edges at a depth of 290 m, and this agrees with the observations made in this area. To investigate the stability of the revised pillar design at increasing depths, the layout shown in Figure 5-2 was also simulated at 400 m, 600 m, and 800 m below surface. The parameters that predicted no pillar failure at 290 m below surface (Table 5-1), were also used for the simulations at increasing depths. The results are shown in Figure 5-6, Figure 5-7 and Figure 5-8, with the red dots indicating the areas of pillar spalling. It should be noted that the pillar spalling increases with depth until significant failure is observed at a depth of 800 m. The cores of the pillars remained intact at this depth, nonetheless. This deterioration in pillar condition with depth agrees qualitatively with the decrease in extraction ratio with depth that can be sustained if a reasonable pillar S_F needs to be maintained.

Table 5-2 contains the APS values obtained for the pillars of interest as well as the percentage of damage to each. The amount of damage was determined by dividing the number of elements that failed by the total elements for each pillar.

Table 5-2. Simulated pillar stresses for area of interest at different depths.

	290 m		400 m		600 m		800 m	
Pillar number	**APS (MPa)**	**Damage (%)**	**APS (MPa)**	**Damage (%)**	**APS (MPa)**	**Damage (%)**	**APS (MPa)**	**Damage (%)**
43	32.0	0%	40.9	18%	62.2	31%	82.3	37%
44	38.0	0%	42.9	35%	66.3	42%	86.7	48%
45	35.4	0%	43.9	25%	65.2	37%	85.5	45%
53	33.7	0%	44	15%	63.4	35%	84.1	39%
54	32.8	0%	42.7	20%	64	32%	84.2	39%
55	35.5	0%	43.5	24%	62.9	40%	82.2	48%
63	34.3	0%	41.1	26%	63.3	35%	82.7	43%
64	33.4	0%	43	18%	63.3	34%	83.2	41%
65	35.0	0%	41.6	28%	63.6	37%	83.3	44%

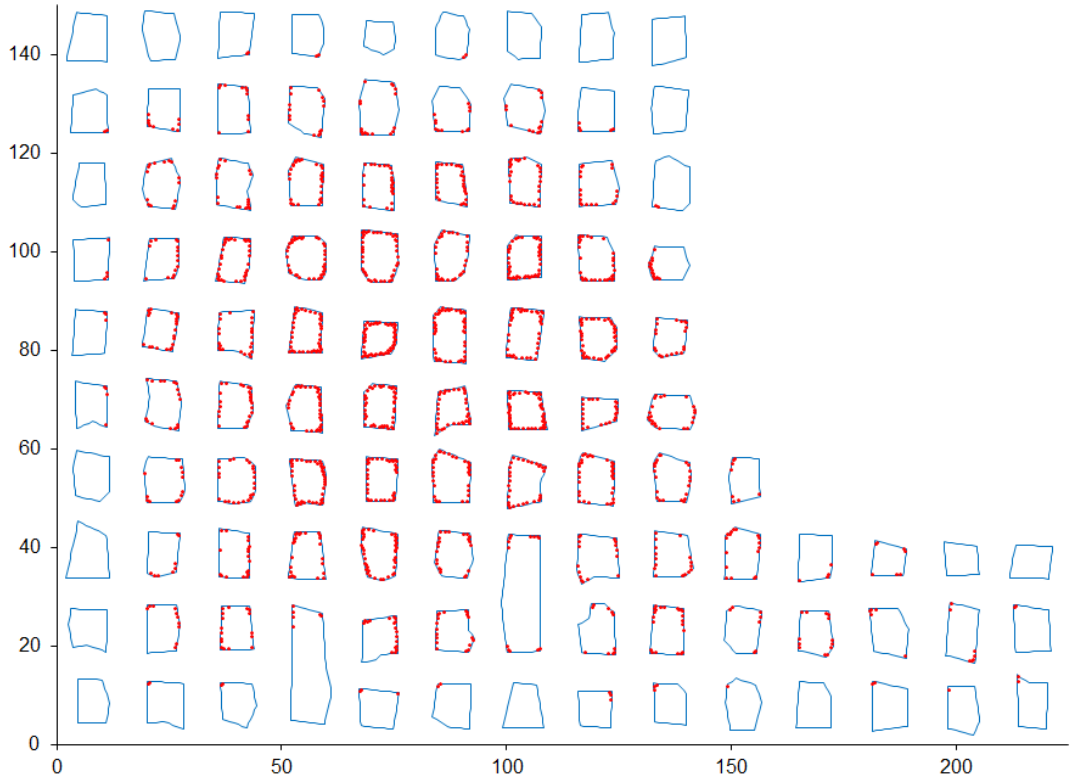

Figure 5-6. Predicted pillar spalling at 400 m below surface.

Figure 5-7. Predicted pillar spalling at 600 m below surface.

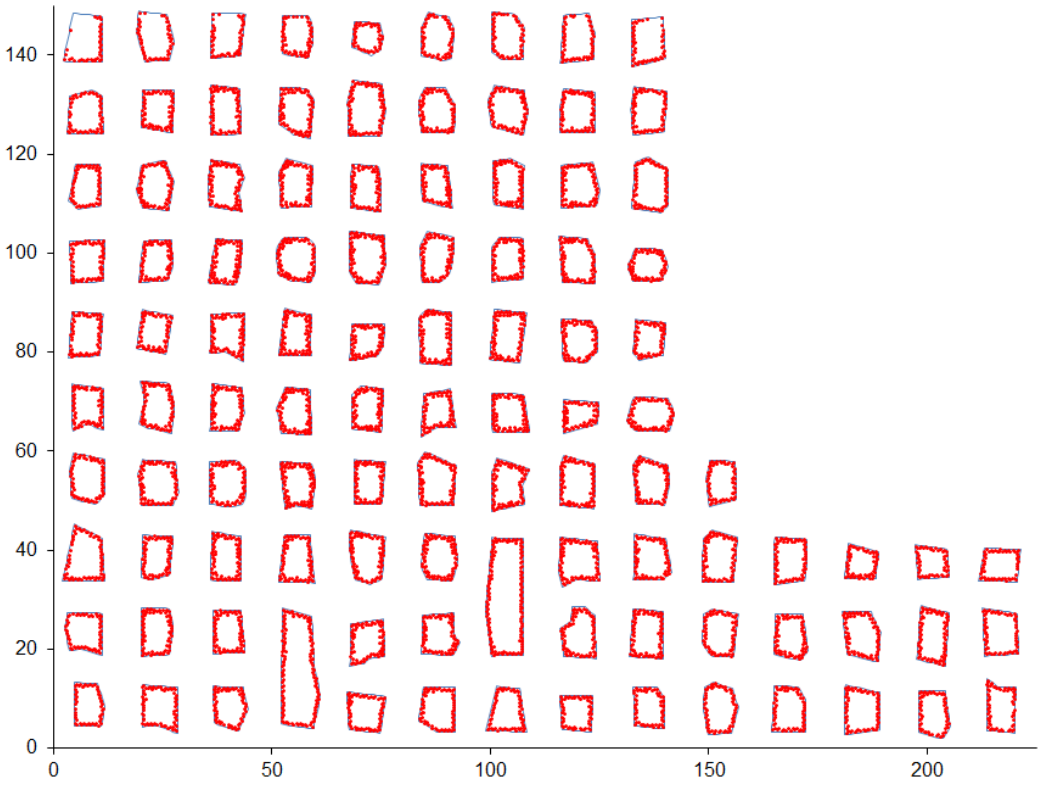

Figure 5-8. Predicted pillar spalling at 800 m below surface.

It should be noted that the pillar damage is substantial for the smaller pillars at a depth of 800 m. Pillar 44, for instance, has a simulated size of 50.7 m^2 and the increase in stress and damage of this pillar as a function of depth is shown in Figure 5-9. The fraction of the pillar that failed was once again calculated as the number of failed elements divided by the total number of pillar elements.

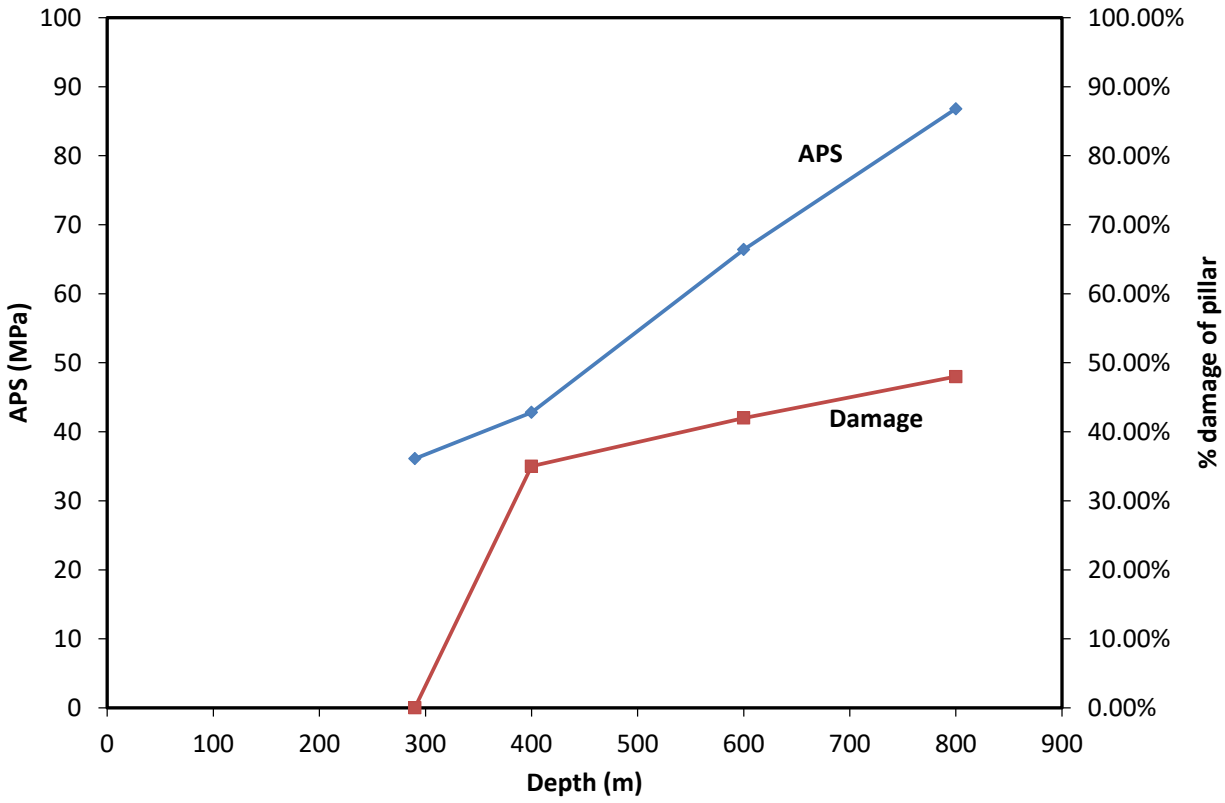

Figure 5-9. The increase in APS for Pillar 44 with increasing depth.

From the amount of damage simulated for the smaller pillars at greater depths, it appears that the current pillar sizes may be too small for the simulated deeper layouts. It should, however, be noted that this is based on the current calibration of the limit equilibrium parameters. A possible solution is to use backfill and this is explored in the next section.

5.3. Numerical modelling to simulate the effect of backfill confinement

To simulate the effect of backfill, the extended limit equilibrium model with confinement, as described in Section 4.3, was used. The same geometry as illustrated above was simulated at a hypothetical depth of 800 m. As there is uncertainty regarding the amount of confinement that the backfill will exert, different simulations with values of σ_h = 0.05 MPa, σ_h = 0.5 MPa, σ_h = 1 MPa, and σ_h = 2 MPa were conducted. Figure 5-10 illustrates the increase in APS for the pillars of interest with increasing backfill confinement.

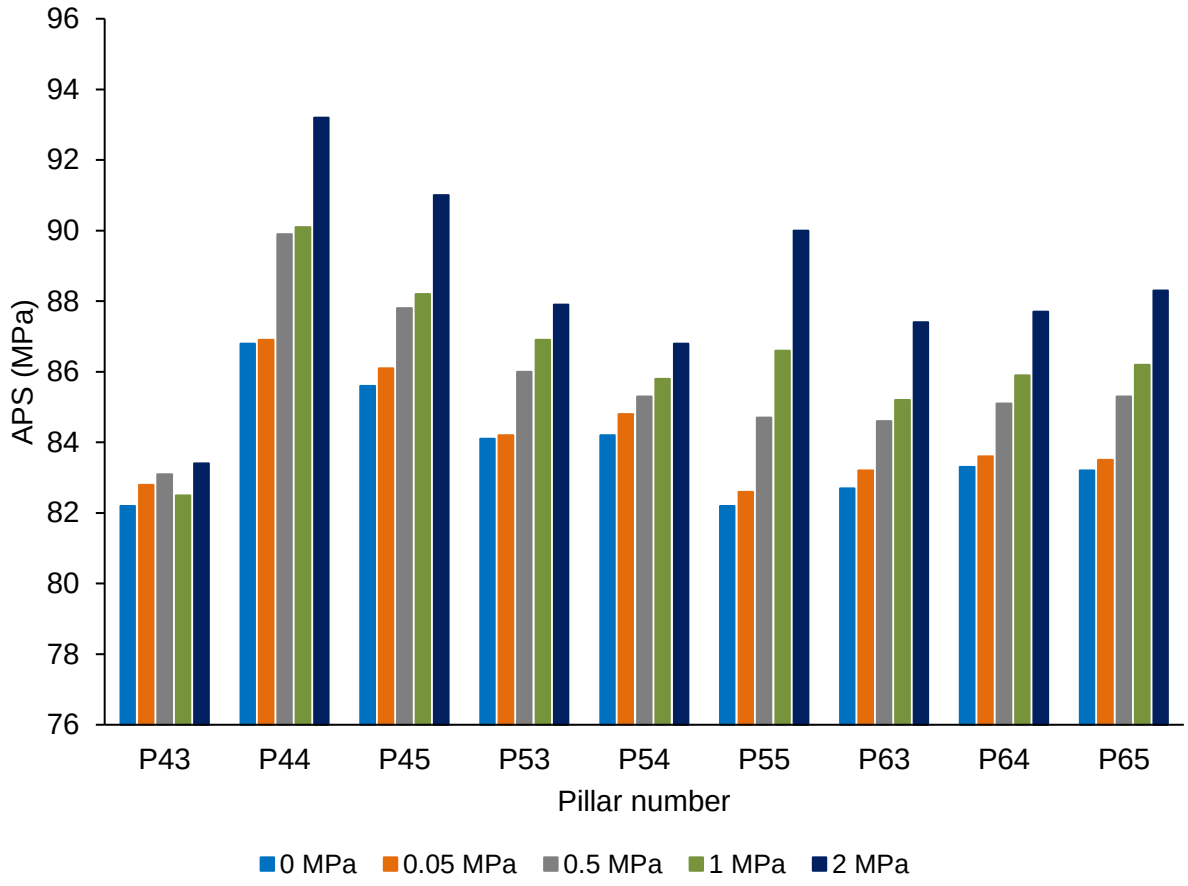

Figure 5-10. The effect of increasing confinement on the APS at a depth of 800 m.

As the confinement increased, the fraction of the pillar that failed decreased. The failure for 2 MPa confinement is illustrated in Figure 5-11 and can be compared to the same simulation without backfill confinement in Figure 5-8. It should be noted that there is significantly more failure for the simulation where no confinement is applied. This is also illustrated in Figure 5-12, where the fraction of the pillar that failed for a few select pillars in the centre of the focal area is shown. Note that the failure decreases as the amount of confinement increases, and there is a substantial

reduction for a value of 2 MPa. It is nevertheless doubtful whether such a magnitude of stress will be exerted by the backfill unless there is substantial pillar dilation.

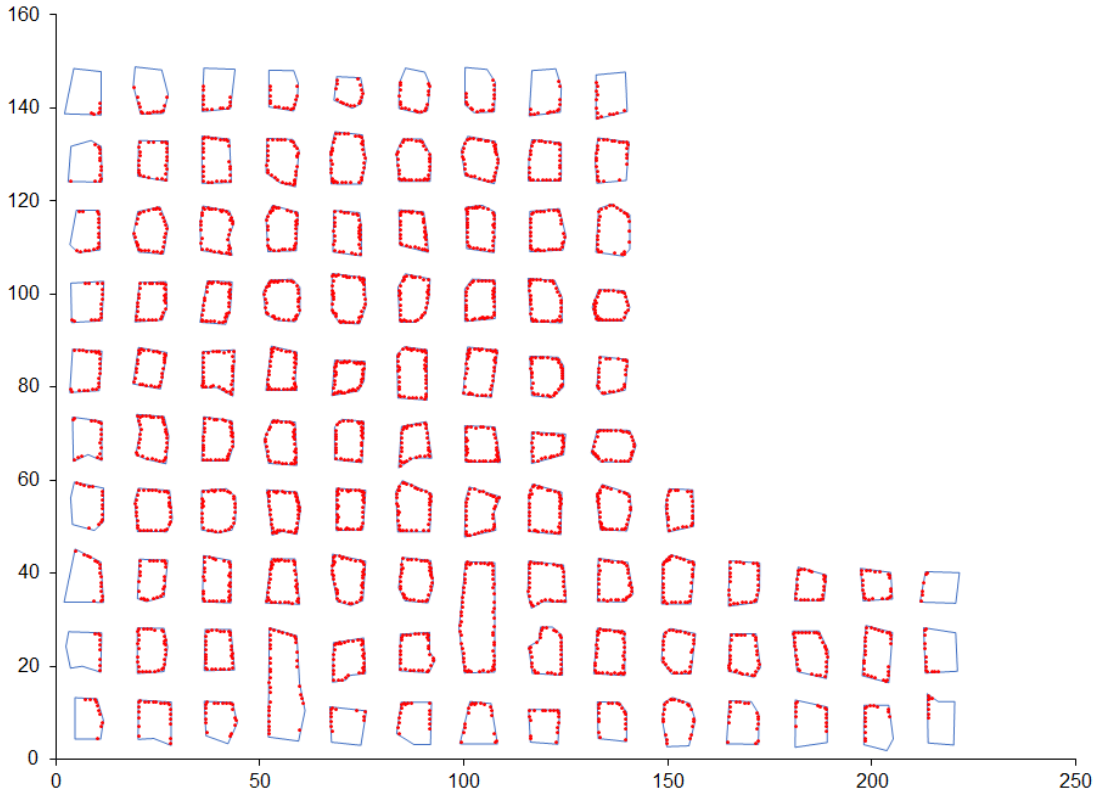

Figure 5-11. Predicted pillar spalling at a depth of 800 m if backfill exerts a confining stress of 2 MPa.

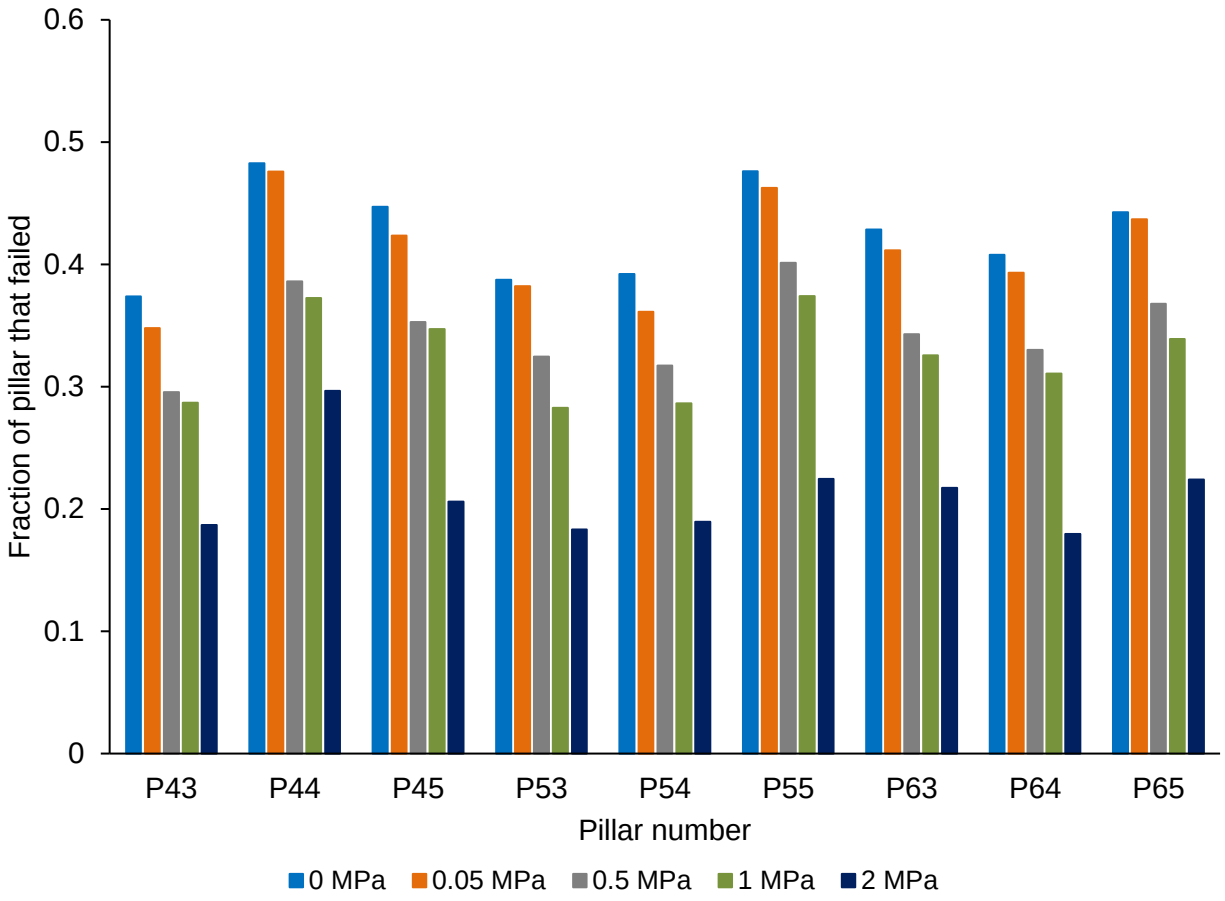

Figure 5-12. Fraction of the pillar that failed for some of the pillars with increasing backfill confinement at 800 m below surface.

The numerical modelling illustrated that the backfill confinement model is valuable to conduct studies of the effect of backfill on pillar strength. From the models, the amount of pillar spalling at depth is substantially decreased when confinement is applied to the pillar sidewalls. This is encouraging and an important result of this study.

The next step would be to quantify the confining effect of backfill using underground and laboratory experiments. Also critical is to devise a practical method to place the backfill in bord and pillar layouts. Containment in a particular area may be difficult as the construction of backfill paddocks similar to that used by the gold mines may not be feasible. An appropriate sequence of mining and backfill placement will also have to be developed. This work is outside the scope of this current study and needs to be conducted in future. A trial site was established by the mine described above to test the placement and containment of backfill and this work is still ongoing. No results were obtained from this site yet. The original intention was to use backfill bags to seal the holings between pillars. The trial site is shown in Figure 5-13 and the position of the bags is shown

by the blue hatched areas. Figure 5-14 and Figure 5-15 illustrate the partially-filled bags between the pillars. Filling the bags was problematic and the areas between the pillars could not be effectively sealed. In future, it is planned to build bulkheads using chains anchored into the pillars. These practical aspects are part of the proposed future work, and these aspects should be considered in a future research study as stated above.

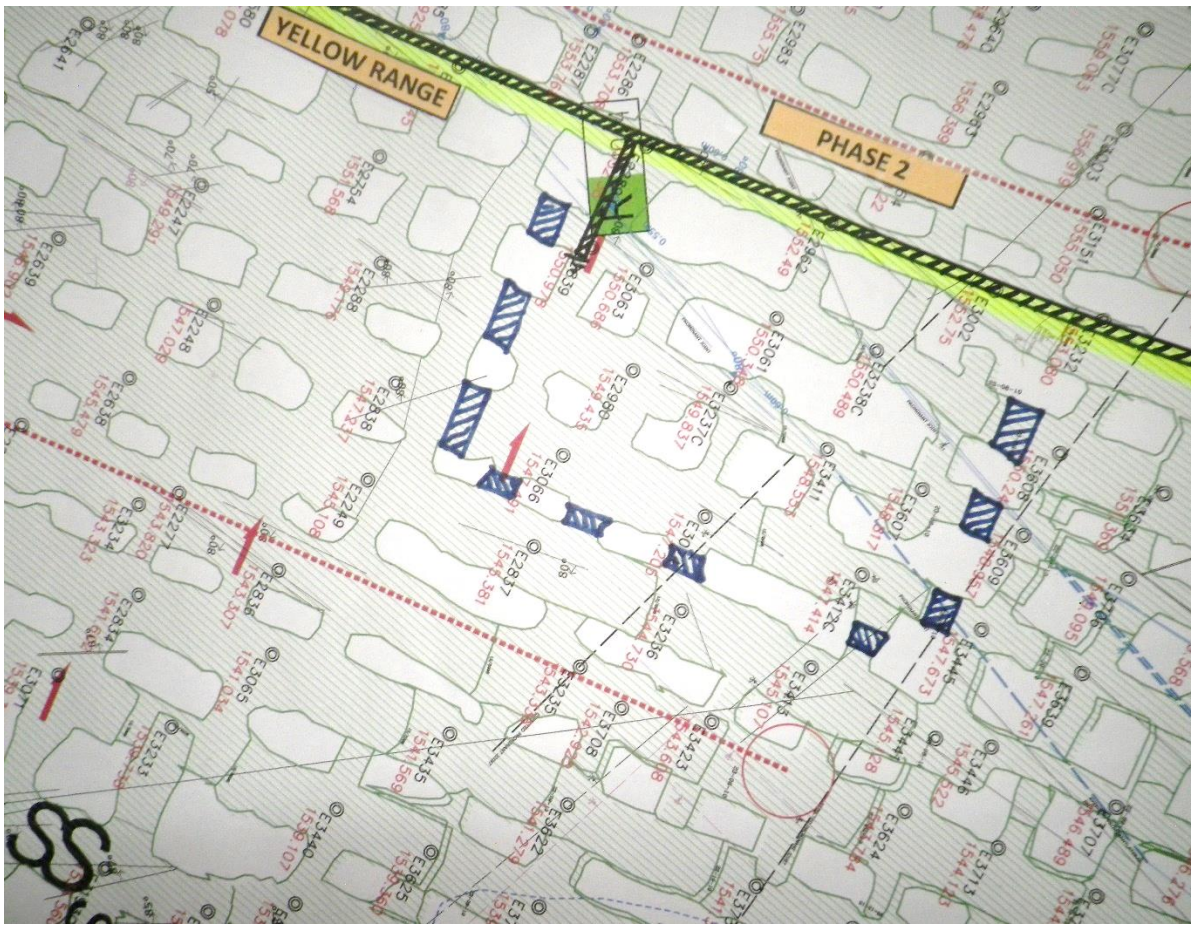

Figure 5-13. Planned trial site where the holings between pillars had to be sealed using backfill bags.

Figure 5-14. Use of backfill bags in an attempt to seal the holing between adjacent pillars (courtesy of D. F. Malan).

Figure 5-15. Use of backfill bags in an attempt to seal the holing between adjacent pillars (courtesy of D. F. Malan).

6. CONCLUSIONS AND RECOMMENDATIONS

As the global population increases, so does the demand for metals and minerals. This introduces the challenge of extracting greater value from low grade deposits, mining deeper ore bodies, and increased mineralogical complexity, all of which have the potential to lead to an even greater production of tailings. The occurrence of catastrophic tailings dam failures, such as those at Canada's Mount Polley in 2014 and Brazil's Brumadinho in 2019, illustrate that the storage of mining-generated waste on surface should be minimised to preserve the environment and prevent the loss of lives. This study was an investigation of the use of backfill in bord and pillar mines. This will potentially strengthen the pillars to enable the mining of historical pillars or enable the use of smaller pillars, thereby improving extraction ratios, and reduce the volume of tailings stored on surface.

The literature indicated that backfill is used extensively in Chinese coal mines in conjunction with high extraction mining methods, mostly for environmental considerations and to minimise the damage caused by subsidence. However, it is not commonly used in hard rock bord and pillar mines. The placement of backfill in sections of hard rock mines may be challenging as containment barriers will have to be built between adjacent pillars. The sequence and timing of mining a section and placing the backfill will have to be carefully managed. This is a challenging aspect that requires additional research in future. The Buick Mine case study, where the strength of the backfill was adequate to sustain time-dependent loading and remained stable for 16 years following its inception, was an example of successful pillar extraction in a hard rock mine using backfill.

As the pillars deform, the vertical and lateral compression of the backfill restrict their lateral deformation and increase the pillar strength. The amount of lateral compression, which is dependent on the backfill's density, enables the design of smaller pillars which improves extraction ratios (Donovan, 1999). Although higher extraction ratios are attainable, the cost of backfilling must be considered as it may offset the increase in profit. The increase in recovery must, therefore, be sufficient to balance the backfill costs.

The instruments used to conduct historical measurements of horizontal stress in backfill in the South African gold mines were not sensitive enough to determine the magnitude of the stress at small strains. This study used a combination of literature sources and classical earth pressure theory to estimate the level of confinement that can be expected when placing backfill. Lateral earth pressure refers to the pressure that soil exerts in the horizontal direction, and it is an important parameter for the design of geotechnical engineering structures such as retaining walls. Pillar design is typically based on ultimate strength, which implies that pillar failure will occur when

the acting load exceeds its strength. A confining pressure, which can be introduced through backfill, increases the pillar strength. A relationship between the initial strength, confining pressure, and the new pillar strength is therefore necessary to incorporate backfill confinement into pillar design (Donovan and Karfakis, 2004). The analysis and historic studies indicated that a value of 0.05 MPa is a viable realistic value of the confinement that will be exerted by backfill.

TEXAN was used for the numerical modelling in this study. The original version of the limit equilibrium model assumed there is no confinement on the pillar edges. A confinement component was recently added to the model to simulate pillar reinforcement. To explore this model, a simple plane strain model of the limit equilibrium model, with the confinement component, was derived in this study by the author. This was used to simulate the effect of the backfill confinement on the normal pillar stress in the failed zone of the pillar. The amount of confinement can be adjusted to simulate how pillars in an underground layout would behave for different types of backfill. When simulating a single pillar, the increasing confinement pressure resulted in a significant increase in the size of the pillar's intact core for both triangular and square meshes. This was also illustrated by conducting numerical modelling of an idealised 100-pillar bord and pillar layout geometry with increasing levels of confinement. The intact core of the pillars as well as their resulting APS increased in size for a higher value of confinement. These preliminary models indicated that the limit equilibrium model with the confinement component behaves as expected.

Regarding pillar mining and the sequence of backfill placement, a checkerboard mining method was simulated to test how two different mining sequences would affect the pillar stability. The models indicated that the timing of backfill placement is important, and less pillar failure occurs if the entire area is flooded with backfill before any pillar mining is done. This is not a practical mining sequence, however, and it indicates that further work is required in terms of the practical use of backfill. This will involve an in-depth study of practical methods to confine the backfill in a particular area and also the timing of backfill placement.

Numerical modelling of an actual platinum mine layout was conducted to illustrate the beneficial effect of backfill on pillar stability at greater depths. The limit equilibrium pillar models with no backfill confinement illustrated how the amount of pillar spalling increased with depth. In contrast, the models with backfill demonstrated how the application of adequate confinement to the pillar sidewalls substantially reduces the pillar failure. This effect was substantial for a 2 MPa confinement value. However, the confinement that will be induced by backfill in actual mining layouts is unknown and this needs to be quantified in future.

In summary, the most important contribution of this study was the illustration that a limit equilibrium model, with an edge confinement component, implemented in a displacement discontinuity code is a versatile method to simulate the effect of backfill placement in bord and pillar mines. This tool

can now be used in future studies to investigate the timing of backfill placement, the most appropriate pillar sizes to use, and whether some pillars can be reclaimed.

6.1. Recommendations

Although the numerical modelling conducted for this study revealed the positive effect that backfill has on pillar strength, it is not known how much confinement the backfill will exert in actual mining layouts. Trial backfill sections in the mines with sensitive instrumentation will be required in future to obtain calibrated model values.

Mining areas where the pillar strength is reduced due to the presence of weak layers may benefit significantly from the placement of backfill. In some areas, this may be the only method that will prevent large-scale collapses. The use of backfill in these areas, and whether it will be beneficial, require further study.

A further extension of the model in TEXAN is recommended. This will allow the coupling of the backfill lateral strain and resulting stress with the pillar dilation. A novel scheme to compute the lateral dilation in the pillar has already been implemented in the TEXAN code by Prof John Napier. The next step will be to include the effect of the placed backfill and its interaction with the pillar dilation.

Practical methods to use backfill in bord and pillar mines need to be developed. It is not clear what the best method is to seal the holings between adjacent pillars. Practical layouts and mining methods, which consider the timing of backfill placement as well as the areas of placement, need to be developed.

The financial aspects related to the use of backfill need to be considered. Backfilling methods are expensive, and this must be compared to the additional revenue that will be generated owing to higher extraction ratios. Of concern is that the backfill operations may slow down the rate of mining and this must be studied in detail.

7. REFERENCES

Alejano, L. R., Arzúa, J., Castro-Filgueira, U. and Malan, D. F., 2017. Strapping of Pillars with Cables to Enhance Pillar Stability. *The Journal of the Southern African Institute of Mining and Metallurgy,* 117(6), pp. 527-540.

Armstrong, M., Petter, R. and Petter, C., 2019. Why Have so Many Tailings Dams Failed in Recent Years?. *Elsevier,* 63(10), pp. 1-11.

Benton, D., 2013. *The Use of Paste Backfill to Increase Long-Term Mine Stability and Ore Extraction: A Theoretical Study for Illinois Basin Room and Pillar Coal Mines.* Carbondale: Southern Illinois University.

Bilght, G. E. and Spearing, A. J. S., 1996. The Properties of Cemented Silicated Backfill for Use in Narrow, Hard-rock, Tabular Mines. *The Journal of the Southern African Institute of Mining and Metallurgy,* 96(1), pp. 17-28.

Blight, G. E., 1984. Soil Mechanics Principles in Underground Mining. *Journal of Geotechnical Engineering,* 110(5), pp. 567-581.

Blight, G. E. and Clarke, L. E., 1983. *Design and Properties of Stiff Fill for Lateral Support of Pillars.* Proceedings of the International Symposium on Mining with Backfill, Lulea.

Boadle, A. and Nogueira, M., 2019. *Hundreds Missing after Vale Dam Burst at Brazil Mine, Seven Bodies Found.* [Online] Available at: https://www.reuters.com/article/us-brazil-vale-disaster/hundreds-missing-after-vale-dam-burst-at-brazil-mine-seven-bodies-found-idUSKCN1PJ1WT?edition-redirect=in [Accessed 23 May 2021].

Brady, B. H. G. and Bray, J. W., 1978. The Boundary Element Method for Elastic Analysis of Tabular Orebody Extraction, Assuming Complete Plane Strain. *International Journal of Rock Mechanics and Mining Science & Geomechanics Abstracts,* Volume 15, pp. 29–37.

Buddery, P. S., 1985. *The Hydraulic Placement of PFA in Underground Coal Mines for Waste Disposal and Environmental Control Purposes.* Pretoria, SANCOT Seminar, pp. 53-60.

Cai, S., 1983. *A Simple and Convenient Method for Design of Strength of Cemented Hydraulic Fill.* Proceedings of the International Symposium on Mining with Backfill, Rotterdam.

Cernica, J. N., 1995. *Geotechnical Engineering: Soil Mechanics.* New York: Wiley.

Cook, N. G. W., Hoek, E., Pretorious, J. P. G., Ortlepp, W. D. and Salamon, M. D. G., 1966. Rock Mechanics Applied to the Study of Rock Bursts. *The Journal of the Southern African Institute of Mining and Metallurgy,* Volume 66, pp. 436-528.

Cordova, M., Saw, H. and Villaescusa, E., 2016. *Laboratory Testing of Cemented Rock Fill for Open Stope Support.* Proceedings of the 7th International Conference and Exhibition on Mass Mining, Sydney.

Couto, P. M. and Malan, D. F., 2023. *A Limit Equilibrium Model to Simulate the Large-Scale Pillar Collapse at the Everest Platinum Mine.* [Online] Available at: https://doi.org/10.1007/s00603-022-03088-z [Accessed 2 November 2022].

Crouch, S. L. and Starfield, A. M., 1983. *Boundary Element Methods in Solid Mechanics: With Applications in Rock Mechanics and Geological Engineering.* London: George Allen and Unwin.

Decipher, 2020. *Lessons Learned from the Mount Polley Disaster.* [Online] Available at: https://www.decipher.com.au/blog/mining-resources/lessons-learned-from-the-mount-polley-disaster [Accessed 15 May 2021].

Do Carmo, F. F., Kamimo, L. H. Y., Junior, R. T., de Campos, I. C., do Carmo, F. F., Silvino, G., de Castro, K. J., Mauro, M. L., Rodrigues, N. U. A., de Souza Miranda, M. P. and Ferreira Pinto, C. E., 2017. Fundão Tailings Dam Failures: the Environment Tragedy of the Largest Technological Disaster of Brazilian Mining in Global Context. *Perspectives in Ecology and Conservation,* 15(3), pp. 145-151.

Donovan, J. G., 1999. *The Effects of Backfill on Ground Control and Recovery in Thin-Seam Coal Mining.* Blacksburg: Virginia Polytechnic Institute and State University.

Donovan, J. G. and Karfakis, M. G., 2001. *The Effects of Backfilling on Ground Control and Recovery in Thin-Seam Coal Mining.* Seattle, The 7th International Symposium on Mining with Backfill.

Donovan, J. G. and Karfakis, M. G., 2004. Design of Backfilled Thin-seam Coal Pillars Using Earth Pressure Theory. *Geotechnical and Geological Engineering,* 22(1), pp. 627-642.

Durrheim, R., 2010. Mitigating the Risk of Rockbursts in the Deep Hard Rock Mines of South Africa: 10 Years of Research. In: J. Brune, ed. *Extracting the Science: A Century of Mining Research.* Englewood: Society for Mining, Metallurgy and Exploration, pp. 156-171.

Esterhuizen, G. S., Dolinar, D. R. and Ellenberger, J. L., 2008. *Pillar Strength and Design Methodology for Stone Mines.* Morgantown, West Virginia, 27th International Conference on Ground Control in Mining.

Franke, K., 2017. *CEEN 341 - Lecture 24 - Lateral Earth Pressures, Part I.* [Online] Available at: https://www.youtube.com/watch?v=gxsKH5zRWVI [Accessed 14 September 2022].

Galvin, J. M., 2016. *Ground Engineering - Principles and Practices for Underground Coal Mining.* New York: Springer.

Galvin, J. M., Hebblewhite, B. K. and Salamon, M. D. G., 1999. *University of New South Wales Coal Pillar Strength Determinations for Australian and South African Mining Conditions.* Proceedings of the 37th US Rock Mechanics Symposium, Vale.

Galvin, J. M. and Wagner, H., 1981. Use of Ash to Improve Strata Control in Bord and Pillar Workings. *Developments in Geotechnical Engineering,* Volume 32, pp. 264-270.

Gcasamba, S., Ramasenya, K., Diop, S., Vadapalli, V. R. K. and Ekolu, S., 2019. *Comparative Study of Two Biggest Mineral Wastes in South Africa for Mine Reclamation: A Geotechnical Study.* Perm, IMWA 2019 Conference – Mine Water: Technological and Ecological Challenges.

Gurjar, R., 2018. *Earth Pressure.* [Online] Available at: https://medium.com/@rohitgurjar009/earth-pressure-9d41e83a164c [Accessed 14 September 2022].

Haldar, S. K., 2018. Elements of Mining. In: *Mineral Exploration: Principles and Applications.* s.l.:Elsevier, pp. 229-258.

Hatch, 2022. *Hatch Analysis on the Effectiveness of Technologies to Reduce Mine Waste.* [Online] Available at: https://www.hatch.com/Hatch-Tailings-Report [Accessed 06 November 2022].

Hedley, D. G. F. and Grant, F., 1972. Stope-and-Pillar Design for the Elliot Lake Uranium Mines. *Canadian Institute of Mining, Metallurgy and Petroleum,* Volume 65, pp. 37-44.

Hoek, E. and Wood, D. F., 1987. Support in Underground Hard Rock Mines. *Underground Support Systems,* Volume 35, pp. 1-6.

Hu, B., Zhao, Q., Fan, S. and Hao, J., 2001. *Study on Subsidence and Interaction Between Backfill and Pillar in Coal Mining.* Seattle, The 7th International Symposium on Mining with Backfill.

Hume, R. G. and Searle, G. K., 1998. Improved Recovery in Highwall Mining Using Backfill. *Australasian Institute of Mining and Metallurgy,* Volume 98, pp. 197-205.

International Council on Mining and Metals (ICMM), 2022. *Tailings Reduction Roadmap.* [Online] Available at: https://www.icmm.com/en-gb/guidance/innovation/2022/tailings-reduction-roadmap [Accessed 26 October 2022].

Jager, A. J. and Ryder, J. A., 1999. *A Handbook on Rock Engineering Practice for Tabular Hard Rock Mines.* Johannesburg: The Safety in Mines Research Advisory Committee.

Jamal, H., 2017. *Earth Pressure Coefficients - Types, Concept and Theory.* [Online] Available at: https://www.aboutcivil.org/earth-pressure.html [Accessed 14 September 2022].

Jamal, H., 2017. *Rankine's Assumptions for Earth Pressure Theory for Active/Passive Pressure.* [Online]
Available at: https://www.aboutcivil.org/theories-of-earth-pressure.html [Accessed 20 July 2022].

Jiang, N., Zhao, J., Sun, X., Bai, L. and Wang, C., 2017. Use of Fly Ash Slurry in Backfill Grouting in Coal Mines. *Heliyon,* 3(11).

Jjuuko, S. and Kalumba, D., 2014. *A Review of Application and Benefits of Thin Spray-on Liners for Underground Rock Support in South African Mines.* Stellenbosch, The 8th South African Young Geotechnical Engineers Conference.

Jooste, Y. and Malan, D. F., 2015. Rock Engineering Aspects of a Modified Mining Sequence in a Dip Pillar Layout at a Deep Gold Mine. *The Journal of the Southern African Institute of Mining and Metallurgy,* 115(11), pp. 1097-1112.

Kolapo, P., Onifade, M., Said, K. O., Amwaama, M., Aladejare, A. E. Lawal, A. I. and Akinseye, P. O., 2021. On the Application of the Novel Thin Spray-on Liner (TSL): A Progress Report in Mining Operations. *Geotechnical and Geological Engineering,* 39(5), p. 5445–5477.

Kossoff, D., Dubbin, W. E., Alfredsson, M., Edwards, S. J., Macklin, M. G. and Hudson-Edwards, K. A., 2014. Mine Tailings Dams: Characteristics, Failure, Environmental Impacts, and Remediation. *Applied Geochemistry,* Volume 51, p. 229–245.

Kostecki, T. and Spearing, A. J. S., 2015. Influence of Backfill on Coal Pillar Strength and Floor Bearing Capacity in Weak Floor Conditions in the Illinois Basin. *International Journal of Rock Mechanics and Mining Sciences,* 76(3), pp. 55-67.

Kuijpers, J., Milev, A., Jager, A. and Acheampong, E., 2002. *Performance of Various Types of Containment Support Under Quasi-Static and Dynamic Loading Conditions, Part 1,* s.l.: Miningtek.

Li, C., 2011. Rock Support for Underground Excavations Subjected to Dynamic Loads and Failure. In: *Advances in Rock Dynamics and Applications.* Boca Raton: CRC Press, pp. 483-506.

Lunder, P. J. and Pakalnis, R. C., 1997. Determination of the Strength of Hard-Rock Mine Pillars. *CIM Bulletin,* Volume 90, pp. 51-55.

Malan, D. F. and Esterhuyse, J. C., 2021. *Work Package 4.3.1: Rock Engineering Criteria for Mechanised Mining,* Pretoria: SAMERDI.

Malan, D. F. and Napier, J. A. L., 2006. *Practical Application of the TEXAN Code to Solve Pillar Design Problems in Tabular Excavations.* Rustenburg, South African National Institute of Rock Engineering Symposium, pp. 1-20.

Malan, D. F. and Napier, J. A. L., 2011. The Design of Stable Pillars in the Bushveld Complex Mines: A Problem Solved?. *The Journal of the Southern African Institute of Mining and Metallurgy,* 111(12), pp. 821-836.

Malan, D. F. and Napier, J. A. L., 2018. Reassessing Continuous Stope Closure Data Using a Limit Equilibrium Displacement Discontinuity Model. *The Journal of the Southern African Institute of Mining and Metallurgy,* 118(3), pp. 227-234.

Maritz, J. A., 2015. *The Effect of Shear Stresses on Pillar Strength.* Pretoria: University of Pretoria.

Martin, C. D. and Maybee, W. G., 2000. The Strength of Hard Rock Pillars. *International Journal of Rock Mechanics and Mining Science*, Volume 37, pp. 1239-1246.

McCrae, M. A., 2016. *Why Samarco Tailings Dam Failed.* [Online] Available at: https://www.mining.com/why-samarco-tailings-dam-failed/ [Accessed 22 May 2021].

Minerals Council South Africa, 2020. *We Care and We Remember Merriespruit, 22 February 1994.* [Online]
Available at: https://www.mineralscouncil.org.za/industry-news/we-care-we-remember/324-we-remember-merriespruit
[Accessed 15 May 2021].

Mo, S., Canbulat, I., Zhang, C., Oh, J., Shen, B. and Hagan, P., 2018. Numerical Investigation into the Effect of Backfilling on Coal Pillar Strength in Highwall Mining. *International Journal of Mining Science and Technology,* Volume 28, pp. 281-286.

Mulenga, P. A., 2018. *Designing a Feasible Methodology for Selecting Permanent Areal Support for Varying Environments in Underground Mines.* Johannesburg: University of the Witwatersrand.

Napier, J. A. L. and Malan, D. F., 2007. The Computational Analysis of Shallow Depth Tabular Mining Problems. *The Journal of the Southern African Institute of Mining and Metallurgy,* Volume 107, pp. 725-742.

Napier, J. A. L. and Malan, D. F., 2011. Numerical Computation of Average Pillar Stress and Implications for Pillar Design. *The Journal of the Southern African Institute of Mining and Metallurgy,* Volume 111, pp. 837-846.

Napier, J. A. L. and Malan, D. F., 2014. *A Simplified Model of Local Fracture Processes to Investigate the Structural Stability and Design of Large-Scale Tabular Mine Layouts.* 48th US Rock Mechanics / Geomechanics Symposium, Minneapolis, pp. 1928-1936.

Napier, J. A. L. and Malan, D. F., 2021. A Limit Equilibrium Model of Tabular Mine Pillar Failure. *Rock Mechanics and Rock Engineering,* Volume 54, pp. 71-89.

Owen, J. R., Kemp, D., Lèbre, É., Svobodova, K. and Pérez Murillo, G., 2020. Catastrophic Tailings Dam Failures and Disaster Risk Disclosure. *International Journal of Disaster Risk Reduction,* 42(1), pp. 1-10.

Palarski, J., 1993. The Use of Fly Ash, Tailings, Rock and Binding Agents as Consolidated Backfill for Coal Mines. *Minefill 93, SAIMM,* pp. 403-408.

Piper, P. S., Gürtunca, R. G. and Maritz, R. J., 1993. Instrumentation to Quantify the in-Situ Stress–Strain Behaviour of Mine Backfill. *The Journal of the Southern African Institute of Mining and Metallurgy,* pp. 109-120.

Piper, P. S. and Ryder, J. A. 1988. *An Assessment of Backfill for Regional Support in Deep Mines*. Backfill in South African Mines, Johannesburg, SAIMM, pp. 111-136.

Plewman, R. P., Deist, F. H. and Ortlepp, W. D., 1969. The Development and Application of a Digital Computer Method for the Solution of Strata Control Problems. *The Journal of the Southern African Institute of Mining and Metallurgy*, Volume 70, pp. 33-44.

Rankine, R. M., 2004. *The Geotechnical Characterisation and Stability Analysis of BHP Billiton's Cannington Mine Paste Fill.* Queensland: James Cook University.

Rankine, R. M., Pacheco, M. and Sivakugan, N., 2007. *Underground Mining with Backfills.* [Online] Available at: https://www.researchgate.net/publication/279586585_Underground_mining_with_backfills [Accessed 08 June 2021].

Rotta, L. H. S., Alcântara, E., Park, E., Negri, R. G., Lin, Y. N. Bernardo, N., Mendes, T. S. G. and Filho, C. R. S., 2020. The 2019 Brumadinho Tailings Dam Collapse: Possible Cause and Impacts of the Worst Human and Environmental Disaster in Brazil. *International Journal of Applied Earth Observation and Geoinformation,* 90(8).

Ryder, J. A. and Jager, A. J., 2002. *A Textbook on Rock Mechanics for Tabular Hard Rock Mines.* Johannesburg: Safety in Mines Research Advisory Committee (SIMRAC).

Ryder, J. A. and Officer, N. C., 1964. An Elastic Analysis of Strata Movement Observed in the Vicinity of Inclined Excavations. *The Journal of the Southern African Institute of Mining and Metallurgy*, Volume 64, pp. 219-244.

Salamon, M. D. G. 1964. Elastic Analysis of Displacements and Stresses Induced by the Mining of Seam or Reef Deposits - Part II: Practical Methods of Determining Displacement, Strain and Stress Components from a Given Mining Geometry. *The Journal of the Southern African Institute of Mining and Metallurgy,* Volume 64, pp. 197-218.

Salamon, M. D. G. and Munro, A. H., 1967. A Study of the Strength of Coal Pillars. *The Journal of the Southern African Institute of Mining and Metallurgy,* 4(9), pp. 55-67.

Salamon, M. D. G. and Oravecz, K., 1976. *Rock Mechanics in Coal Mining.* Johannesburg: Chamber of Mines of South Africa.

Shamsabadi, A., Dasmeh, A. and Taciroglu, E., 2017. *Guidelines for Analysis and LRFD-Based Design of Earth Retaining Structures ,* Los Angeles: University of California, Los Angeles (UCLA).

Shen, B., Poulsen, B., Luo, X., Qin, J., Thiruvenkatachari, R. and Duan, Y., 2017. Remediation and monitoring of abandoned mines. *International Journal of Mining Science and Technology,* 27(5), pp. 803-811.

South African National Institute of Rock Engineering (SANIRE), 2021. *Rock Talk.* [Online] Available at: https://www.sanire.co.za/news/newsletters/817-sanire-newsletter-volume7-issue1-april-2021/file
[Accessed 24 March 2023].

Spencer, D., 1999 *A Case Study of a Pillar System Failure at Shallow Depth in a Chrome Mine*. Proceedings of the 2nd Southern African Rock Engineering Symposium, Johannesburg.

Squelch, A. P. 1990. *Horizontal Stresses in the Face Area Hangingwall of Backfilled and Conventional Stopes at Vaal Reefs*. Internal Note No. R16/90, Johannesburg, Chamber of Mines Research Organization.

Squelch, A. P., 1993. A Methodology for the Selection of Backfill as Local Support for Tabular Stopes in South African Gold Mines. *The Journal of the Southern African Institute of Mining and Metallurgy,* pp. 9-15.

Squelch, A. P., Milev, A. M., Acheampong, E., Dlokweni, T., Janse van Rensburg, A. and Watson, B. P. 2001. *Influence of Regional Support Systems (Pillars and Backfill) on Local Areas and Internal Support Requirements Adjacent to That Regional Support*. Safety in Mines Research Advisory Committee, GAP 615, pp. 1-130.

Stacey, T. R. and Ortlepp, W. D., 2001. Tunnel Surface Support - Capabilities of Various Types of Wire Mesh and Shotcrete Under Dynamic Loading. *The Journal of the Southern African Institute of Mining and Metallurgy,* 101(7), pp. 337-342.

Stacey, T. R. and Page, C. H., 1986. *Practical Handbook for Underground Rock Mechanics.* s.l.:Trans Tech.

Stradling, A. W. 1988. Backfill in South Africa: Developments to Classification Systems for Plant Residues. *Minerals Engineering*, 1(1), pp. 31-40.

Sun, Q., Zhang, J. and Zhou, N., 2018. Study and Discussion of Short-Strip Coal Pillar Recovery with Cemented Paste Backfill. *International Journal of Rock Mechanics and Mining Sciences,* 104(3), pp. 147-155.

Tesarik, D. R., Seymour, J. B. and Yanske, T. R., 2009. Long-Term Stability of a Backfilled Room-and-Pillar Test Section at the Buick Mine Missouri, USA. *International Journal of Rock Mechanics and Mining Sciences,* Volume 46, pp. 1182-1196.

Tesarik, D. R., Seymour, J. B., Yanske, T. R. and McKibbin, R. W., 1995. *Stability Analysis of a Backfilled Room-and-Pillar Mine.* [Online] Available at: https://www.cdc.gov/niosh/mining%5C/UserFiles/works/pdfs/ri9565.pdf [Accessed 17 July 2021].

Thomas, E. G., 1973. *A Review of Cementing Agents for Hydraulic Fill.* Proceedings of the Jubilee Symposium on Mine Filling, Queensland.

Van der Merwe, N., 2006. Beyond Coalbrook: What Did we Really Learn?. *The Journal of the Southern African Institute of Mining and Metallurgy,* 106(12), pp. 857-868.

Van der Merwe, N. and Mathey, M., 2013. Update of Coal Pillar Strength Formulae for South African Coal Using Two Methods of Analysis. *The Journal of the Southern African Institute of Mining and Metallurgy,* 113(11), pp. 841-847.

Van der Spuy, B. 2021. Determining the Required Underground Grout Pack Production Profile for Narrow Tabular Mining Operations. *Minefill 2020-2021*. London: Taylor & Francis Group, pp. 153-167.

Wagner, H., 1974. Determination of the Complete Load-Deformation Characteristics of Coal Pillars. 3rd International Congress on Rock Mechanics. Denver, Colorado. *International Society for Rock Mechanics*. Volume 2B, pp. 1076-1082.

Wang, H., Poulsen, B. A., Shen, B., Xue, S. and Jiang, Y., 2011. The Influence of Roadway Backfill on the Coal Pillar Strength by Numerical Investigation. *International Journal of Rock Mechanics and Mining Sciences,* 48(3), pp. 443-450.

Watson, B. P., Theron, W., Fernandes, N., Kekana, W. O., Mahlangu, M. P., Betz, G. and Carpede, A., 2021. UG2 Pillar Strength: Verification of the PlatMine Formula. *The Journal of the Southern African Institute of Mining and Metallurgy,* 121(8), pp. 449-456.

Wei, C., Zhang, C., Canbulat, I., Song, Z. and Dai, L., 2022. A Review of Investigations on Ground Support Requirements in Coal Burst-prone Mines. *International Journal of Coal Science and Technology,* Volume 13, pp. 1-20.

Yu, X., Kemeny, J., Tan, Y., Song, W. and Huang, K., 2021. Mechanical Properties and Fracturing of Rock-backfill Composite Specimens Under Triaxial Compression. *Construction and Building Materials,* Volume 304, pp. 1-17.

Zhang, J.-X., Li, M., Taheri, A., Zhang, W., Wu, Z. and Song, W., 2019. Properties and Application of Backfill Materials in Coal Mines in China. *Minerals,* 53(9), pp. 1-21.

Zipf, R. K., 2001. *Toward Pillar Design to Prevent Collpase in Room-and-Pillar Mines.* Denver, 108th Annual Exhibit and Meeting, Society for Mining, Metallurgy and Exploration.

Zur, K. J. and Apel, D., 2004. *Use of Cemented Rock Fill for Enhanced Pillar Recovery in Area 1 of the Doe Run Company.* Proceedings of the International Conference on Case Histories in Geotechnical Engineering, New York.

Zvarivadza, T., 2012. *Evaluation of Pillar Design Systems for Low Reef Platinum Mining.* Johannesburg: University of the Witwatersrand.

8. APPENDICES

APPENDIX A – Tables of simulated APS values for the 10×10 layout using rigid pillars

Table 8-1. Simulated pillar stresses for the ≈ 0.3 m² triangular mesh of the regular layout.

Pillar number	Simulated APS (MPa)
23	130.7
24	132.6
25	132.8
26	133.8
27	133.2
28	130.7
33	132.7
34	133.9
35	134.6
36	133.9
37	130.8
38	128.0
43	128.7
44	134.2
45	136.1
46	136.0
47	133.6
48	132.4
53	134.1
54	134.8
55	136.0
56	134.8
57	134.9
58	129.3

63	129.0
64	130.3
65	132.3
66	135.6
67	134.9
68	131.8
73	131.5
74	133.2
75	134.2
76	134.1
77	134.0
78	130.9

Table 8-2. Simulated pillar stresses for the ≈ 0.8 m² triangular mesh of the regular layout.

Pillar number	Simulated APS (MPa)
23	122.7
24	123.3
25	124.9
26	124.4
27	124.1
28	122.7
33	123.8
34	125.0
35	125.8
36	126.3
37	128.8
38	124.1
43	126.0
44	125.8
45	125.9
46	126.6
47	125.8
48	124.1
53	124.8
54	125.7
55	125.7
56	126.5
57	126.1
58	126.0
63	124.0
64	127.9
65	126.1
66	127.0
67	124.6
68	123.7

73	122.9
74	124.6
75	124.5
76	125.1
77	124.1
78	123.4

Table 8-3. Simulated pillar stresses for the 0.25 m^2 square mesh of the regular layout.

Pillar number	Simulated APS (MPa)
23	125.3
24	126.2
25	126.8
26	126.4
27	126.4
28	125.0
33	126.8
34	127.7
35	128.4
36	128.0
37	128.0
38	126.4
43	126.8
44	127.8
45	128.5
46	128.1
47	128.0
48	126.5
53	127.2
54	128.1
55	128.9
56	128.3
57	128.4
58	126.8
63	126.5
64	127.5
65	128.1
66	127.8
67	127.7
68	126.2

73	125.7
74	126.5
75	127.2
76	126.8
77	126.8
78	125.3

Table 8-4. Simulated pillar stresses for the 1 m² square mesh of the regular layout.

Pillar number	Simulated APS (MPa)
23	124.4
24	125.3
25	126.0
26	125.6
27	125.5
28	124.0
33	126.0
34	126.9
35	127.7
36	127.3
37	127.2
38	125.5
43	126.0
44	127.0
45	127.8
46	127.4
47	127.3
48	125.6
53	126.4
54	127.4
55	128.2
56	127.8
57	127.7
58	126.0
63	125.7
64	126.7
65	127.4
66	127.0
67	126.9
68	125.3

73	124.8
74	125.7
75	126.4
76	126.0
77	126.0
78	124.4

APPENDIX B – Tables of simulated APS values for the 10×10 layout using a limit equilibrium model

Table 8-5. LEM and confinement model pillar stresses for the ≈ 0.3 m² triangular mesh of the regular layout.

Pillar number	0 MPa confinement	0.5 MPa confinement	1 MPa confinement	1.5 MPa confinement	2 MPa confinement
23	97.2	98.1	99.0	99.7	100.3
24	102.2	103.1	103.9	104.7	105.3
25	103.6	104.5	105.4	106.1	106.4
26	103.6	104.5	105.3	106.1	106.7
27	102.3	103.3	104.1	104.9	105.5
28	97.2	98.2	99.0	99.7	100.2
33	102.3	103.3	104.1	104.9	105.5
34	108.5	109.4	110.3	111.0	111.7
35	110.5	111.4	112.2	112.9	113.6
36	110.1	111.0	111.8	112.5	113.2
37	107.8	108.7	109.5	110.2	110.8
38	101.2	102.1	102.9	103.6	104.1
43	102.7	103.6	104.4	105.1	105.6
44	1100.1	111.1	111.9	112.6	113.3
45	112.6	113.5	114.4	115.0	115.7
46	112.2	113.1	113.9	114.6	115.3
47	110.0	111.0	111.8	112.4	113.1
48	103.4	104.3	105.1	105.9	106.5
53	103.9	104.9	105.7	106.5	107.1
54	110.4	111.4	112.2	112.9	113.6
55	112.7	113.6	114.4	115.1	115.8

56	112.3	113.2	114.0	114.6	115.3
57	110.5	111.4	112.1	113.0	113.7
58	102.9	103.7	104.6	105.2	105.8
63	101.5	102.4	103.2	103.9	104.4
64	107.6	108.5	109.3	110.0	110.6
65	109.9	110.8	111.6	112.2	113.0
66	110.3	111.2	112.0	112.7	113.4
67	108.7	109.7	110.5	111.3	111.9
68	102.0	103.0	103.8	104.5	105.1
73	97.5	98.5	99.3	100.0	100.6
74	102.4	103.4	104.2	105.0	105.6
75	104.0	105.0	105.8	106.6	107.2
76	103.8	104.8	105.6	106.4	107.0
77	102.7	103.7	104.6	105.3	106.0
78	97.4	98.3	99.2	99.9	100.4

Table 8-6. LEM and confinement model pillar stresses for the ≈ 0.8 m² triangular mesh of the regular layout.

Pillar number	0 MPa confinement	0.5 MPa confinement	1 MPa confinement	1.5 MPa confinement	2 MPa confinement
23	95.6	96.6	97.6	98.3	98.8
24	99.7	100.6	101.4	102.2	102.8
25	101.4	102.2	103.0	103.8	105.5
26	100.9	101.8	102.6	103.4	104.0
27	100.0	100.9	101.8	102.6	103.2
28	95.6	96.6	97.5	98.2	98.6
33	99.8	100.7	101.6	102.4	103.0
34	105.4	106.1	106.8	107.6	108.2
35	107.3	107.9	108.6	109.2	109.9
36	107.2	107.9	108.6	109.2	109.9
37	106.7	107.4	108.2	108.9	109.7
38	100.1	100.9	101.8	102.6	103.2
43	101.5	102.4	103.3	104.1	104.8
44	107.2	107.8	108.5	109.2	109.8
45	108.9	109.5	110.1	110.7	111.3
46	108.7	109.3	109.9	110.6	111.2
47	107.4	108.0	108.7	109.4	110.0
48	101.2	102.0	102.8	103.6	104.2
53	101.3	102.1	103.0	103.8	104.4
54	107.2	107.9	108.5	109.2	109.9
55	108.9	109.5	110.1	110.7	111.4
56	108.8	109.5	110.1	110.7	111.3
57	107.4	108.1	108.7	109.4	110.1
58	101.7	102.5	103.4	104.2	104.8
63	99.8	100.7	101.6	102.4	103.0

64	106.3	107.0	107.8	108.5	109.3
65	107.3	108.0	108.7	109.3	110.0
66	107.1	107.8	108.4	109.1	109.8
67	105.4	106.0	106.7	107.5	108.1
68	99.8	100.7	101.6	102.3	102.9
73	95.7	96.7	97.6	98.3	98.8
74	100.1	101.0	101.9	102.6	103.2
75	101.2	102.1	102.9	103.7	104.2
76	101.0	101.9	102.7	103.5	104.0
77	100.0	100.8	101.7	102.5	103.0
78	95.8	96.8	97.8	98.4	98.8

Table 8-7. LEM and confinement model pillar stresses for the 0.25 m^2 square mesh of the regular layout.

Pillar number	0 MPa confinement	0.5 MPa confinement	1 MPa confinement	1.5 MPa confinement	2 MPa confinement
23	108.1	109.3	110.6	111.9	112.2
24	109.8	110.9	112.1	113.5	114.0
25	110.6	111.7	112.8	114.1	114.8
26	110.4	111.5	112.7	114.0	114.6
27	109.8	110.0	112.2	113.5	114.1
28	107.9	109.1	110.5	111.7	110.6
33	110.0	111.2	112.3	113.7	114.4
34	111.9	112.9	114.0	115.2	116.1
35	112.8	113.8	114.8	116.0	117.0
36	112.6	113.6	114.6	115.8	116.8
37	112.0	113.0	114.1	115.3	116.2
38	109.8	111.0	112.2	113.5	112.8
43	110.6	111.7	112.8	114.2	114.9
44	112.5	113.5	114.6	115.7	116.7
45	113.5	114.4	115.4	116.5	117.6
46	113.3	114.3	115.3	116.4	117.4
47	112.6	113.6	114.6	115.8	116.8
48	110.4	111.5	112.7	114.0	113.3
53	110.8	111.8	113.0	114.3	115.1
54	112.7	113.7	114.7	115.9	116.9
55	113.6	114.6	115.6	116.7	117.8
56	113.5	114.4	115.4	116.5	117.6
57	112.8	113.8	114.8	116.0	117.0
58	110.6	111.7	112.8	114.1	113.5
63	109..9	111.1	112.3	113.6	114.2

64	111.8	112.8	113.9	115.1	116.0
65	112.7	113.7	114.7	115.9	116.9
66	112.5	113.5	114.6	115.7	116.7
67	111.9	112.9	114.0	115.2	116.1
68	109.8	110.9	112.1	113.5	112.7
73	108.3	109.5	110.8	112.1	112.5
74	109.9	111.1	112.3	113.6	114.2
75	110.8	111.8	113.0	114.3	115.1
76	110.6	111.7	112.8	114.2	114.9
77	110.0	111.2	112.3	113.7	114.4
78	108.1	109.3	110.6	111.9	110.9

Table 8-8. LEM and confinement model pillar stresses for the 1 m² square mesh of the regular layout.

Pillar number	0 MPa confinement	0.5 MPa confinement	1 MPa confinement	1.5 MPa confinement	2 MPa confinement
23	108.7	109.0	109.4	109.7	110.0
24	110.6	110.9	111.3	111.6	111.9
25	111.4	111.8	112.2	112.5	112.8
26	111.3	111.6	112.0	112.3	112.6
27	110.6	111.0	111.4	111.7	112.0
28	108.5	108.8	109.2	109.5	109.8
33	110.9	111.2	111.6	111.9	112.2
34	112.9	113.3	113.6	114.0	114.2
35	113.9	114.3	114.6	115.0	115.2
36	113.7	114.1	114.4	114.7	115.0
37	113.0	113.4	113.7	114.1	114.4
38	110.6	111.0	111.4	111.7	112.0
43	111.5	111.8	112.2	112.5	112.8
44	113.6	114.0	114.3	114.6	114.9
45	114.6	115.0	115.3	115.6	115.9
46	114.4	114.9	115.1	115.5	115.7
47	113.7	114.1	114.4	114.7	115.0
48	111.3	111.6	112.0	112.3	112.6
53	111.7	112.1	112.4	112.7	113.0
54	113.8	114.2	114.5	114.8	115.1
55	114.8	115.2	115.5	115.8	116.1
56	114.6	115.0	115.3	115.6	115.9
57	113.9	114.3	114.6	115.0	115.2
58	111.4	111.8	112.2	112.5	112.8
63	110.8	111.1	111.5	111.8	112.1
64	112.8	113.2	113.5	113.9	114.1

65	113.8	114.2	114.5	114.8	115.1
66	113.6	114.0	114.3	114.6	114.9
67	112.9	113.3	113.6	114.0	114.2
68	110.6	110.9	111.3	111.6	111.9
73	108.9	109.2	109.6	110.0	110.3
74	110.8	111.1	111.5	111.8	112.1
75	111.7	112.1	112.4	112.7	113.0
76	111.5	111.8	112.2	112.5	112.8
77	110.9	111.2	111.6	111.9	112.2
78	108.7	109.0	109.4	109.7	110.0

APPENDIX C – Tables of simulated APS values for the 10×10 layout following pillar extraction (Sequence 1)

Table 8-9. Simulated pillar stresses for the regular layout's pillar extraction (Sequence 1).

Pillar number	No backfill confinement / no failure	1st Quadrant mining	2nd Quadrant mining	3rd Quadrant mining	4th Quadrant mining
12	91.1	*	*	*	*
13	94.8	110.3	111.7	112.5	114.7
14	96.3	*	*	*	*
15	96.8	108.9	110.2	111.4	118.2
16	96.7	103.5	104.7	106.2	*
17	96.4	100.1	101.1	102.7	117.2
18	94.8	96.9	97.7	99.4	*
19	91.1	92.7	93.3	94.8	109.7
22	94.3	110.0	112.0	112.9	114.5
23	98.6	*	*	*	*
24	100.6	115.9	118.2	119.7	123.6
25	101.3	*	*	*	*
26	101.3	108.8	110.5	112.6	124.7
27	100.6	104.5	105.9	108.3	*
28	98.6	100.9	102.0	104.4	120.6
29	94.7	96.2	97.0	99.3	*
32	96.3	*	*	*	*
33	100.6	116.0	119.8	121.3	123.6
34	102.6	*	*	*	*
35	103.5	115.4	118.5	121.3	127.5
36	103.3	110.2	112.5	116.0	*
37	102.4	106.2	108.0	111.9	126.2

38	100.2	102.5	103.9	107.9	*
39	96.4	97.9	98.9	102.8	117.3
42	96.6	108.8	115.4	116.7	118.3
43	101.0	*	*	*	*
44	103.4	115.4	122.2	124.8	127.5
45	104.4	*	*	*	*
46	104.2	110.7	114.1	120.6	238.6
47	103.3	106.7	109.2	116.0	*
48	101.2	103.3	105.0	112.5	124.7
49	97.0	98.4	99.6	106.5	*
52	97.1	103.8	*	*	*
53	101.5	109.0	121.0	123.2	124.8
54	103.5	110.4	*	*	*
55	104.4	110.9	119.8	125.7	128.7
56	104.3	108.6	113.7	*	*
57	103.5	106.1	109.3	121.3	127.5
58	101.0	102.8	104.8	*	*
59	96.7	97.9	99.3	111.4	118.1
62	96.4	100.1	114.8	116.4	117.6
63	100.4	104.2	*	*	*
64	102.3	106.1	120.9	124.5	126.2
65	103.3	106.7	*	*	*
66	103.4	106.1	113.1	124.8	127.5
67	102.7	104.6	108.3	*	*
68	100.5	101.9	104.1	119.7	123.5
69	96.3	97.3	98.8	*	*
72	94.8	96.9	*	*	*
73	98.8	101.1	117.1	119.6	120.8
74	100.7	103.0	*	*	*

75	101.5	103.6	115.9	123.2	124.8
76	101.4	103.2	110.2	*	*
77	100.8	102.2	106.0	121.5	123.7
78	98.6	99.7	102.0	*	*
79	94.5	95.3	96.8	112.4	114.5
82	91.2	92.6	107.5	109.0	109.8
83	94.8	96.3	*	*	*
84	96.4	97.9	112.8	116.4	117.5
85	96.8	98.2	*	*	*
86	96.8	98.0	105.2	116.9	118.5
87	96.5	97.5	101.1	*	*
88	94.8	95.6	97.7	113.3	114.9
89	91.2	91.8	93.2	*	*

* Mined out

APPENDIX D – Tables of simulated APS values for the 10×10 layout following pillar extraction (Sequence 2)

Table 8-10. Simulated pillar stresses for the regular layout's pillar extraction (Sequence 2).

Pillar number	No backfill confinement / no failure	1st Quadrant mining	2nd Quadrant mining	3rd Quadrant mining	4th Quadrant mining
12	93.0	*	*	*	*
13	96.7	114.0	115.5	116.4	118.8
14	98.3	*	*	*	*
15	98.7	112.2	113.7	115.0	122.2
16	98.6	106.1	107.4	109.1	*
17	98.3	102.3	103.4	105.1	121.3
18	96.7	99.0	99.8	101.6	*
19	93.1	94.5	95.2	96.8	113.5
22	96.2	113.6	115.8	116.8	118.5
23	100.6	*	*	*	*
24	102.6	119.9	122.1	123.6	127.8
25	103.4	*	*	*	*
26	103.4	111.8	113.7	116.0	129.1
27	102.7	107.0	108.5	111.1	*
28	100.6	103.1	104.2	106.9	124.6
29	96.6	98.2	99.0	101.5	*
32	98.3	*	*	*	*
33	102.7	119.9	123.7	125.3	127.9
34	104.8	*	*	*	*
35	105.7	119.0	122.2	125.1	132.7
36	105.5	113.1	115.8	119.5	*
37	104.5	108.8	110.7	115.0	131.0

38	102.3	104.7	106.2	110.7	*
39	98.4	99.9	101.0	105.2	121.4
42	98.5	112.1	119.4	120.8	122.3
43	103.1	*	*	*	*
44	105.6	119.0	126.2	129.2	132.7
45	106.6	*	*	*	*
46	106.5	113.6	117.4	124.2	134.0
47	105.5	109.3	111.9	119.5	*
48	103.3	105.6	107.4	115.9	129.1
49	98.9	100.4	101.7	109.4	*
52	99.0	106.6	*	*	*
53	103.6	112.0	125.0	127.4	129.3
54	105.7	113.3	*	*	*
55	106.7	113.8	123.5	130.4	134.2
56	106.5	111.3	117.0	*	*
57	105.7	108.7	112.1	125.1	132.7
58	103.1	105.0	107.2	*	*
59	98.6	99.9	101.4	115.0	122.2
62	98.3	102.4	118.7	120.5	121.6
63	102.4	106.8	*	*	*
64	104.5	108.7	124.8	129.0	131.2
65	105.5	109.3	*	*	*
66	105.6	108.6	116.4	129.2	132.7
67	104.9	107.0	111.1	*	*
68	102.6	104.0	106.5	123.6	127.8
69	98.2	99.2	100.8	*	*
72	96.7	98.9	*	*	*
73	100.8	103.3	121.1	123.6	124.8
74	102.8	105.3	*	*	*

75	103.7	105.9	119.6	127.5	129.4
76	103.6	105.4	113.2	*	*
77	102.9	104.4	108.7	125.5	128.1
78	100.6	101.8	104.3	*	*
79	96.3	97.1	98.7	116.2	118.6
82	93.1	94.5	111.1	112.7	113.4
83	96.7	98.3	*	*	*
84	98.3	99.8	116.5	120.4	121.6
85	98.6	100.1	*	*	*
86	98.6	99.9	108.1	121.0	122.5
87	98.4	99.4	103.4	*	*
88	96.7	97.5	99.7	117.2	118.9
89	93.0	93.7	95.1	*	*

* Mined out